Sustainable Recycling Technologies for Lithium-ion Batteries

A THESIS
SUBMITTED TO THE CHEMICAL AND PROCESS
ENGINEERING FACULTY
OF THE UNIVERSITY OF CANTERBURY
BY

Zain Abdool Kader

IN PARTIAL FULFILMENT OF THE REQUIREMENTS
FOR THE DEGREE OF
MASTER OF ENGINEERING

ASSOCIATE PROFESSOR AARON MARSHALL and JOHN KENNEDY

FEBRUARY 2021

Acknowledgements

During my time at the University of Canterbury, it is undeniable that my achievements, especially this thesis, would not have been possible without the many contributions from knowledgeable mentors, unwavering friends, and supportive family members. Although I cannot hope to repay this debt within a page, I would like to humbly acknowledge those that have contributed to my personal and academic growth.

I would like to acknowledge my supervisors, Associate Professor Aaron Marshall and John Kennedy. I cannot imagine a more encouraging research environment than that which is cultivated through your collaboration. I thank you for allowing me to foster diversity in my research and your patience that you maintained while I navigated through this unfamiliar terrain. Furthermore, I thank you both for being excellent teachers that generously shared your time and advice throughout.

The Chemical and Process Engineering faculty at the University of Canterbury has guided me through my undergraduate and now postgraduate studies. I wish to thank all the lecturers, tutors and staff who have enabled this development.

My family has acted as the stabilising force during these hard times, that being of the Covid-19 global pandemic. I thank my parents and brother, Abed, Shamla and Tariq for their unwavering love and confidence in me seeing it through.

Finally, I am profoundly grateful to my partner, Petra for remaining a grounded pillar of support throughout the entirety of my studies. Whether reassuring me of my capabilities or reminding me to maintain a balanced life, I thank you sincerely.

Nomenclature

BMS	Battery Management System
CAN	Acetonitrile
CAPE	Chemical and Processing Engineering
CED	Cumulative Energy Demand
CMR	Carcinogenic, Mutagenic and Reprotoxic
CO_2e	Carbon Dioxide Equivalent
DMC	Dimethyl Carbonate
DMG	Dimethylglyoxime
DoD	Depth of Discharge
DRC	Democratic Republic of Congo
EC	Ethylene Carbonate
EIS	Electrochemical Impedance Spectroscopy
EoL	End of Life
ESR	Equivalent Series Resistance
EV	Electric Vehicle
GNS	Geological and Nuclear Sciences
H&S	Health and Safety
HF	Hydrogen Fluoride
HSNOA	Hazardous Substances and New Organisms Act
IEA	International Energy Agency
IFRI	French Institute of International Relations
LCA	Life Cycle Analysis
LCO	Lithium Cobalt Oxide, $LiCoO_2$
LFP	Lithium Iron Phosphate, $LiFePO_4$
LGA	Local Government Act
LiB	Lithium-ion Battery
$LiPF_6$	Lithium Hexafluorophosphate
LMO	Lithium Manganese Oxide, $LiMn_2O_4$
MFA	Material Flow Analysis
MP-AES	Microwave Plasma Atomic Emission Spectroscopy

NCA	Lithium Nickel Cobalt Aluminium Oxide, $LiNi_{0.8}Co_{0.15}Al_{0.05}O_2$
NMC	Lithium Nickel Manganese Cobalt Oxide, $LiNi_{1/3}Mn_{1/3}Co_{1/3}O_2$
NMP	N-Methyl-2-Pyrrolidone
NZ ETS	New Zealand Emissions Trading Scheme
NZD	New Zealand Dollar, 2020 (unless otherwise specified)
PhEV	Plug-in Hybrid Electric Vehicle
PPE	Personal Protective Equipment
PVDF	Polyvinylidene Fluoride
RMA	Resource Management Act
SEI	Solid Electrolyte Interface
SoC	State of Charge
UC	University of Canterbury
UN	United Nations
US	United States of America
USD	United States Dollar
USEPA	United States Environmental Protection Agency
UWR	Universal Waste Rule
WMA	Waste Minimisation Act
WMINZ	Waste Management Institute of New Zealand

Executive Summary

The urgency to meet our climate obligations under the Paris Agreement has prompted a surge in the production and consumption of electric vehicles and with it, a growing waste-stream of end-of-life lithium-ion batteries. The environmental consequences of this growth are profound. Insofar as, the depletion of natural resources, and when lithium-ion batteries are incorrectly landfilled, pollution to groundwater and soil. Sustainable recycling technologies must be implemented to construct a cyclic-economy for the lithium-ion battery market and help alleviate the severity of these environmental consequences. Here we evaluate the opportunities in lithium-ion battery recycling and outline areas for future progress. Literature review found several methods of processing spent lithium-ion batteries to extract the metals within. However, current industrial recovery-methods involve high temperature pyrometallurgy, which emit toxic flue gases and produce poor-quality metal alloys. Hydrometallurgy techniques pose a viable alternative and were examined at lab-scale with the results used to conduct a preliminary design for commercial lithium-ion recycling in New Zealand. Second-use options, such as stationary storage to supplement grid power, were identified as feasible in extending the end-of-life of lithium-ion batteries. Therefore, the design and build of a 1.2 kWh proof-of-concept battery pack was achieved using spent 18650 cells.

Table of Contents

List of Tables

List of Figures

1 Literature Review

1.1 Introduction

The lithium-ion battery market is increasing exponentially, going from $12 billion USD in 2011 to $50 billion USD in 2020 (Hu et al., 2020). Estimates now forecast an increase to $77 billion USD by 2024 (Hu et al., 2020). Data from the International Energy Agency (IEA) shows a six-fold increase in lithium-ion battery production between 2016 – 2022. Therefore, combined with estimates from Winslow *et al.*, 5.9 Mt of lithium-ion batteries are expected to be produced in the year of 2022 alone (Winslow et al., 2018). This growth is unprecedented and will continue to grow in the future, largely attributed to the rapid propagation of electric vehicles (Harper et al., 2019). The environmental consequences of this growth is profound, with the depletion of natural resources, and the pollution to groundwater and soil when incorrectly landfilled.

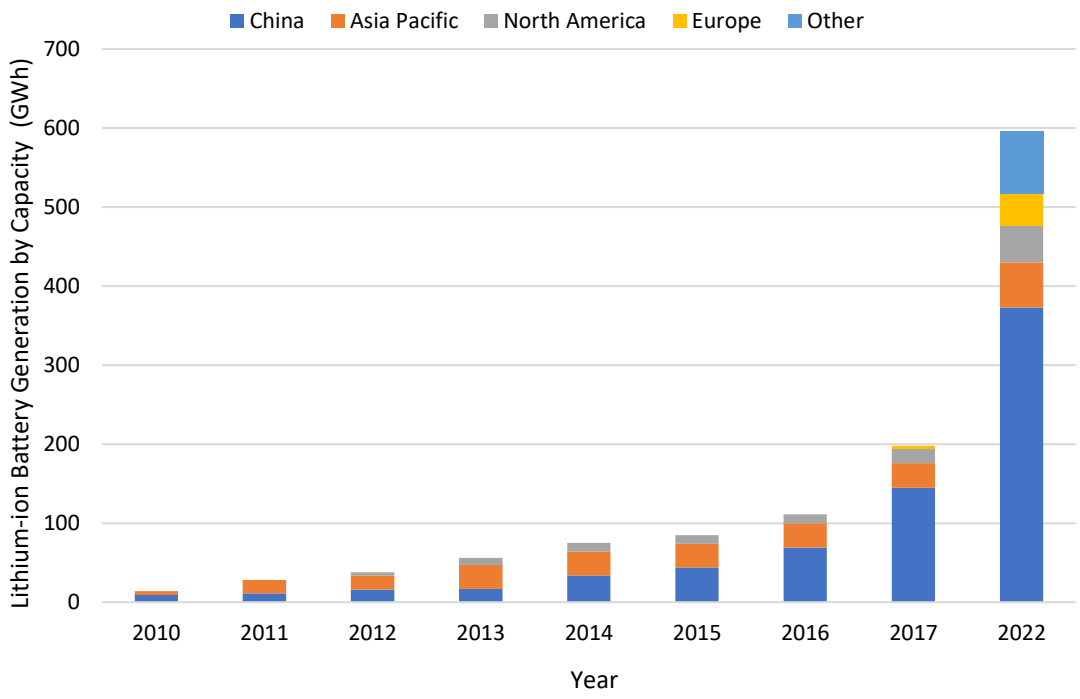

Figure 1: Global lithium-ion battery production by capacity (IEA, 2020).

Sustainable recycling technologies must be implemented to construct a circular economy for the lithium-ion battery market, thereby alleviating the severity of these environmental consequences. However, global recycling rates are less than 4% (Shi et al., 2018), with the

majority of these recycling processes using energy intensive, polluting processes that fail to recover the environmentally harmful and valuable metals contained within.

1.2 Background

1.2.1 Primary Consumers of Lithium-ion Batteries

Lithium-ion batteries are used in a wide range of applications including electric vehicles, electronic devices and electric micro-mobility. Electric vehicles utilise an increasing market share of lithium-ion batteries and offer a sustainable option within the automotive industry; with zero exhaust emissions, better efficiency than vehicles with internal-combustion engines and a potential for reduced embodied energy when coupled with renewable electricity infrastructure – as in New Zealand, where 82% of electricity generated is from renewable resources (MBIE, 2020). Globally, electric vehicles avoided the consumption of over 600,000 barrels of oil products per day or approximately 35 GL in 2019 (IEA, 2020). Similarly, the electricity generation to supply the global electric vehicle fleet in 2019 emitted 51 Mt CO_2-e, thereby avoiding 53 Mt CO_2-e of emissions for an equivalent fleet of internal-combustion engine vehicles (IEA, 2020). Although beneficial to meeting global climate obligations, electric vehicles are the primary consumers of lithium-ion batteries globally (Harper et al., 2019) and pose a serious problem in the generation of lithium-ion battery waste. In so much as, the rapid increase in electric vehicle sales, reaching 2.1 million globally in 2019 (IEA, 2020), with estimates of 11 million in 2025, and expanding to 30 million in 2030 (Vector, 2019). Significantly, the cathode chemistry, shape and packaging used in electric vehicles vary between manufacturers. For example, the 85 kWh Tesla Model S battery modules contain 444 NCA cells with 6 series and 74 in parallel. These cells are cylindrical, 18650 cells, at 3.6 V and 3.2Ah. Contrastingly, the Audi Q5 PhEV (Plug-in Hybrid Electric Vehicle) possesses 4 modules that contain 18 pouch NMC cells at 3.7 V and 5 Ah. These are all connected in series, yielding a total of 72 cells thereby requiring different pre-treatment methods. (Buchmann, 2020; Harper et al., 2019; Or et al., 2020). Table 1 summarises the performance of three key battery types used in current EVs. Consumer adoption of EVs since market inception has been significant, although expected to increase this up-take cannot be accurately predicted. Similarly, the rapid development of cathodic composition prevents efficient recovery techniques being implemented at an industrial

scale. This makes the processing aspect of lithium-ion battery recycling difficult. A life cycle analysis conducted by Gaines *et al.*, found that up to 4 Mt of spent lithium-ion batteries from electric vehicles could be generated between 2015 – 2040 (Gaines et al., 2018), with a commodity value of approximately $8 billion USD assuming complete recovery (Gaines et al., 2018; Harper et al., 2019).

Table 1: Examples of three different battery packs and modules currently in use in EVs (Harper et al., 2019).

Cell Shape	Cylindrical	Prismatic	Pouch
Vehicle	Tesla model S	BMW i3	Nissan Leaf
Manufacturer	Panasonic	Samsung/SDI	AESC
Cathode Type	NCA	NMC	LMO/NMC
Power			
Battery Pack (kWh)	85	22	22
Battery Pack (V)	375	355.2	360
Cell - Cathode (V)	3.6	3.7	3.75
Weight (kg)			
Battery Pack	530	235	294
Module	25	24.5	3.8
Cell - Anode	0.0485	2	0.914
Inventory			
Total Modules	16	8	48
Cells/Module	444	12	4
Total Cells	7104	96	192
Battery Pack	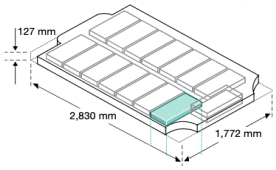	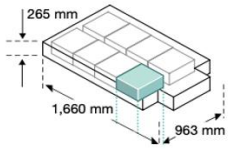	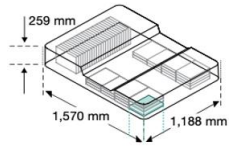
Module	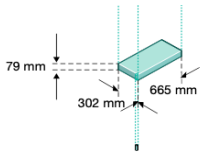	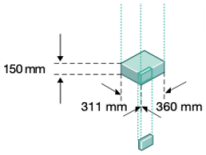	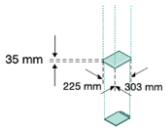
Cell	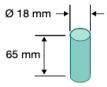	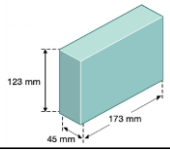	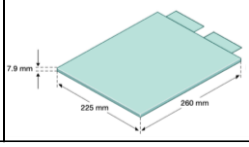

1.2.2 Structure and Composition of Lithium-ion Batteries

LiBs consist of a positive and negative electrode, an electrolyte, and a separator (Aaltonen et al., 2017). The cathode during discharge is the anode during charging, but for descriptive purposes the cathode is stated as the positive terminal as per convention. The composition of LiBs, for 10 kg of mixed LiB scrap is given in Table 2. During discharge, the negative and positive electrodes correspond to the anode and cathode respectively. Fabrication of the electrodes occur by combining conductive additives such as carbon black and a polymer binder such as PVDF (Polyvinylidene Fluoride) to form greater than 80 wt% aggregates bound to metal current collectors, usually graphite deposited on copper, and metal oxides on aluminium for the anode and cathode respectively (Aaltonen et al., 2017; Or et al., 2020).

Table 2: Bill of Materials for Li-ion Batteries Assessed – Total Mass: 10-12 kg (Amarakoon et al., 2013).

Component	**Mass of Total (%)**
Anode	15-24
Cathode	29-39
Separator	2-3
Cell Casing Aluminium casing and polymer pouch	3-20 3-20
Electrolyte Carbonate solvents $LiPF_6$ (Lithium Hexafluorophosphate)	8-15 7-13 1-2
BMS (Battery Management System) Copper wiring Steel Printed wire board	2 1 1 <1
Battery Pack Casing/Housing Polypropylene/polyethylene terephthalate/steel	17-23 17-23
Passive Cooling System Steel and aluminium	17-20 17-20
Total	100

LiBs rely on the intercalation and deintercalation mechanism of lithium ions between the electrodes. During charging, a flow of lithium ions oxidises the transition metals in the cathode, thus causing a release of a lithium ions into the electrolyte – deintercalation, and simultaneously a flow of electrons into the system (Or et al., 2020). Electrons are

intercalated with lithium ions at the anode. During discharge – when a load is drawn on the system, the reverse reaction occurs, both electrons and lithium ions are released from the negative electrode, and the flow of electrons generates a current.

A variety of compositions for the cathode are available: LFP (Lithium Iron Phosphate), LMO (Lithium Manganese Oxide), NMC (Lithium Nickel Manganese Cobalt Oxide), NCA (Lithium Nickel Cobalt Aluminium Oxide), LCO (Lithium Cobalt Oxide), with LCO being the most common due to their use in EVs (Electric Vehicles). The percentage composition of LiB constituents for the range of cathode chemistries are given in Table 3. These varieties of LiBs have different operational characteristics which are both advantageous and detrimental with respect to energy density, power density, cost, safety, and lifespan as given in Table 4. LCO batteries are commonly favoured due to their high energy density and ease of manufacturing. However, are limited by a high associated cost and limited cobalt resources. The chemical reaction for LCO LiBs for the cathode and anode is given in the chemical equations below. Where the forward direction is the charge reaction and the reverse is the discharge reaction (Xu et al., 2008).

$$6C + xLi^+ + xe^- \Leftrightarrow C_6Li_x$$

$$LiCoO_2 \Leftrightarrow Li_{(1-x)}CoO_2 + xLi^+ + xe^-$$

Overall, energy in the battery is stored by the lithium intercalation cycle according to (3).

$$LiCoO_2 + 6C \Leftrightarrow Li_{1-x}\,CoO_2 + C_6\,Li_x$$

Table 3: Concentration of LiB constituents by mass percentage of total (Winslow et al., 2018).

Materials	**NCA (Gaines et al., 2012)**	**LMO (Gaines et al., 2012)**	**NMC (Richa et al., 2016)**	**LCO (H. Wang et al., 2015)**	**LFP (X. Wang et al., 2016)**
Aluminium	21.9	21.7	22.72	5.2	6.5
Cobalt	2.3	0	8.45	17.3	0
Copper	13.3	13.5	16.6	7.3	8.2
Iron/Steel	0.1	0.1	8.79	16.5	43.2
Lithium	1.9	1.4	1.28	2	1.2
Manganese	0	10.7	5.86	0	0
Nickel	12.1	0	14.84	1.2	0
Binder	3.8	3.7	1.39	2.4	0.9
Carbon (non-graphite)	2.4	2.3	3.47	6	2.3
Electrolyte and Solvent	11.7	11.8	1.66	14	14.9
Fluoride	-	-	4.99	-	-
Graphite	16.5	16.3	-	23.1	13
Thermal Insulation	1.2	1.2	-	-	-
Oxygen	8.3	12.4	4.52	-	-
Phosphorous	-	-	2.04	0	5.4
Plastics	4.2	4.5	3.29	4.8	4.4

Table 4: LIB cathode chemistries and performance, modified from (Harper et al., 2019; Or et al., 2020; Ordoñez et al., 2016).

Cathode Types	**LCO**	**LFP**	**LMO**	**NCA**	**NMC**	**LTO**
Chemical Formula	$LiCoO_2$	$LiFePo_4$	$LiMn_2O_4$	$LiNi_{0.8}Co_{0.15}Al_{0.05}O_2$	$LiNi_{1/3}Mn_{1/3}Co_{1/3}O_2$ (NMC111) $LiNi_{0.5}Mn_{0.3}Co_{0.2}O_2$ (NMC532) $LiNi_{0.6}Mn_{0.2}Co_{0.2}O_2$ (NMC622) $LiNi_{0.8}Mn_{0.1}Co_{0.1}O_2$ (NMC811)	Li_2TiO_3
Structure	Layered	Olivine	Spinel	Layered	Layered	Spinel
Year Introduced	1991	1996	1996	1999	2008	2008
Market Share (Global)	Consumer devices	large vehicles, storage	Power tools, EVs,	EVs	NMC111 > NMC532 > NMC622 > NMC811 > no-cobalt	Electric powertrain and storage
2008 (Gaines et al., 2012)	61%	4%	11%	7%	19%	-
2012 (Gaines et al., 2012)	37%	5%	21%	7%	29%	-
2014 (Christophe et al., 2015)	40%	9%	16%	5%	31%	-
2018 (King et al., 2018)	37%	5%	21%	7%	29%	-
Excellent / Good / Moderate / Poor — Safety						
Energy Density						
Power Density						
Calendar Lifespan						
Cycle Lifespan						
Performance						
Cost						
Nominal Voltage (V)	3.6	3.3	4	3.7	3.7	2.4
Gravimetric Capacity (mAh/g)	145	165	120	200	170	-
Specific Energy (Wh/kg)	175	100	125	230	180	65
Volumetric Capacity (mAh/cm^3)	550	589	496	700	600	-

1.2.2.1 Cathode

The cathode materials used in LiBs can incorporate a variety of metal oxides that are capable of oxidation to higher valence states (Whittingham, 2004). The specific composition of the cathode is approximately 85% metal oxide powder, 10% PVDF and 5% acetylene black (Chagnes et al., 2013). LFP and LMO cathodes cost significantly less to produce than LCO cathodes because of the lower value metals used (Thackeray et al., 2005). However, the intrinsic value of LCO is the highest among LiB chemistries due to the valuable cobalt they contain (Amarakoon et al., 2013; H. Wang et al., 2015). A generalised bill of materials is shown below in Table 5.

Table 5: Bill of Materials for Li-ion Batteries Assessed - Total Mass: 10-12 kg (Amarakoon et al., 2013).

Component	**Mass of Total (%)**
Cathode	29-39
Aluminium (collector)	4-9
Lithium-ion material	22-31
Polymer/other	<1-3
Auxiliary solvent	<1-11

1.2.2.2 Anode

The anode comprises of graphite – hexagonally-bonded carbon atoms arranged in adjacent sheets. The bill of materials for the anode is given in Table 6. During charging, lithium ions are stored within the graphite lattice (De las Casas et al., 2012). Therefore, the capacity of a LiB is determined by the number of lithium ions that can be stored in a given amount of anodic material. The theoretical storage capacity of graphite is fairly low, at 372 mAh/g (De las Casas et al., 2012; Moradi et al., 2016).

Developments in anodic technology, such as nanotubes, metal compounds, and nanoparticles have increased the performance of LiBs (De las Casas et al., 2012). These new anodic chemistries have the potential to increase the recycling value of the anode, which is currently recycled for the copper current collector (Moradi et al., 2016; Winslow et al., 2018).

Table 6: Materials for Li-ion Batteries Assessed - Total Mass: 10-12 kg (Amarakoon et al., 2013).

Component	Mass of Total (%)
Anode	15-24
Copper Foil (Collector)	1-12
Battery grade graphite/carbon	8-13
Polymer	<1-0
Auxiliary solvent	<1-6

1.2.2.3 Electrolyte

The electrolyte consists of a lithium salt dissolved in organic solvent, usually a mixture of ethylene carbonate and dimethyl carbonate as shown in Table 7. The solvent containing the electrolyte typically has a high permittivity and low viscosity (Aravindan et al., 2011). This provides high electrochemical stability, thus the LiB is able to operate on a wider voltage range (Heelan et al., 2016).

Table 7: Materials for Li-ion Batteries Assessed - Total Mass: 10-12 kg (Amarakoon et al., 2013).

Component	Mass of Total (%)
Electrolyte	8-15
Carbonate solvents	7-13
Lithium hexafluorophosphate ($LiPF_6$)	1-2

1.2.2.4 Separator

The separator is a porous polypropylene, semi-permeable, insulating membrane, that prevents electrical short circuiting and provides an ionic conduction pathway for the electrolyte (Chagnes et al., 2013; Heelan et al., 2016). Table 8 summarises the percentage composition of the separator in 10 kg of spent LiBs.

Table 8: Materials for Li-ion Batteries Assessed - Total Mass: 10-12 kg (Amarakoon et al., 2013).

Component	Mass of Total (%)
Separator	2-3
Polymer	2-3

1.2.3 Mechanisms Responsible for Lithium-ion Battery Capacity Loss

Over time, the capacity of lithium-ion batteries decrease, and eventually do not hold enough charge for their intended applications, thereby reaching their end-of-life. The three main processes responsible for this capacity loss and the eventual end-of-life of lithium-ion

batteries are: mechanical degradation, formation of a solid electrolyte interface, electrolyte oxidation, and lithium plating.

A solid electrolyte interface forms during charging, wherein both lithium oxide and lithium carbonate atoms form a film on the negative electrode – anode. The formation of this barrier of lithium ions prevents successful intercalation, thus increasing the internal resistance (Aaltonen et al., 2017; Or et al., 2020). Solid electrolyte interface formation is the leading contributor to capacity loss in most graphite-based LiBs below 3.9V (Gaines et al., 2018). Correct addition of electrolyte additives can mitigate the formation of the solid electrolyte interface in the short-term. Research associated with the prevention of the solid-electrolyte interface is well established, but ongoing.

Mechanical degradation of electrodes or loss of stack pressure in pouch-type cells are one of the ways lithium-ion batteries lose capacity. The chemical and physical changes that lithium-ion batteries undergo can cause immense strain on the internal materials resulting in minute fractures in the electrodes (Or et al., 2020). Mechanical degradation does not often hinder lithium-ion battery performance but has the potential to reduce capacity and in some cases cause complete failure of the cell. Cell design and correct electrolyte additives can minimise these effects.

Electrolyte oxidation, can form on the positive electrode – cathode, if the lithium-ion battery is operated in temperatures exceeding 40˚C (Horn et al., 2019), which is often achieved under normal operating conditions. Electrolyte oxidation also induces self-discharge and is exacerbated when the lithium-ion battery is at full charge. The film caused by electrolyte oxidation is thickened over several charge and discharge cycles. Each time the film thickens it reduces the mobility of lithium ions between the plates, thereby reducing battery capacity (Ordoñez et al., 2016).

Lithium-plating typically occurs on the surface of the negative electrode (anode during discharge) and is induced by high charging rates and cold temperatures (Ramoni et al., 2013). When lithium-ion batteries are rapidly charged the rate of lithium ions leaving the positive electrode exceeds the rate at which the negative electrode can effectively absorb

the ions. Therefore, excess lithium ions become deposited on the electrode surface. The reduction in available lithium ions hinders battery capacity and, in some cases, can cause a short circuit.

1.2.4 Policy and Regulation for Lithium-ion Battery Disposal

Specialised recycling companies have begun to grow in response to the increasing waste stream of lithium-ion batteries. Most of these companies still use traditional, energy intensive methods such as pyrometallurgy.

New Zealand has a growing recognition of the indigenous Māori people and their values. The concept of ōhanga āmiomio, the circular economy, is reflected in regulation(Vector, 2018). New Zealand's Resource Management Act and the Waste Minimisation Act provides definitions for sustainable management and encourages a reduction in the amount of waste generated and disposed of (MFE, 2020). However, end-of-life lithium-ion batteries are yet to be specifically integrated in New Zealand's legislation.

China has recently issued regulatory measures on the recycling and reuse of batteries from electric vehicles – specifically including lithium-ion batteries. This was introduced in August 2018; it mandated strict guidelines on maintenance, collection and transport, as well as, reuse and recycling technologies (Gaines et al., 2018; J. Zhang et al., 2018). The progressive policy ensures electric vehicle manufacturers are responsible for the collection, sorting, storage, and transportation of lithium-ion batteries. It is also stipulated that lithium-ion batteries must have a means of tracking for future recycling purposes. The regulation also promotes initial design forethought for disassembly and recycling with open-source information across the supply chain (Gaines et al., 2018).

The European Union mandates that battery manufacturers are responsible for the collection and recycling of spent lithium-ion batteries (Gaines et al., 2018). As discussed above, this mandate encourages the planning for lithium-ion battery disposal in the design stages. The mandate required 45% of battery production – inclusive of lithium-ion batteries, to be recovered by 2016, which the majority of members have achieved (Dahllöf et al., 2019).

At the national level, no policy exists in the United States to address the recycling of lithium-ion batteries. lithium-ion batteries are not considered dangerous under the United States Environmental Protection Agency Universal Waste Rules, and therefore are not covered under the Battery Act, even though they are classified as hazardous substances by the Department of Transportation because of their fire risk (Gaines et al., 2018). Eight states, in the United States, have waste management regulations and mechanisms for battery disposal, only three of which explicitly incorporate lithium-ion batteries.

In general, recycling has positive repercussions, creating a cyclic, sustainable society. However, recycling technologies for LiBs have become stagnated due to:

- A lack of economic incentive; currently, it is more economical to mine LiB constituents than attempt to recycle them (Heelan et al., 2016; Or et al., 2020).
- The constant development of cathode chemistries makes advancements in recycling technologies difficult.
- Although LiBs are physically and environmentally hazardous, government regulation often fails to enforce the recycling of LiBs and these batteries often end up in landfills.

A potential recovery process must be capable of industrial scale-up, and economically viable both now and in the future. The metal oxides that often make up the cathode are the most costly component of LiBs (Ramoni et al., 2013). An ideal recycling method could process the many variations of LiBs and recover or regenerate cathodes directly instead of secondary raw materials that require further processing (Or et al., 2020).

Currently, LiB recycling is not being addressed during their design and manufacturing. However, manufacturers also hold responsibility in the EoL (End of Life) of LiBs, which must be considered in the design stages. A more robust recycling system would provide the means to identify specific battery compositions and efficiently recover LiB constituents (Heelan et al., 2016).

The European Union mandates that battery manufacturers are responsible for the collection and recycling of spent LiBs (Gaines et al., 2018). As discussed above, this mandate encourages the planning for LiB EoL in the design stages. The mandate required 45% of

battery production – inclusive of LiBs, to be recovered by 2016, which the majority of members have achieved (Dahllöf et al., 2019).

China has recently issued regulatory measures on the recycling and reuse of batteries from EVs – specifically including LiBs. This was introduced in August 2018; it mandated strict guidelines on maintenance, collection and transport, as well as, reuse and recycling technologies (Gaines et al., 2018; X. Zhang et al., 2018). The progressive policy ensures EV manufacturers are responsible for the collection, sorting, storage, and transportation of LiBs. It is also stipulated that LiBs must have a means of tracking for future recycling purposes. The regulation also promotes initial design forethought for disassembly and recycling with open-source information across the supply chain (Gaines et al., 2018).

Overall, no policy exists in the US to address the recycling of LiBs. LIBs are not considered dangerous under the USEPA (United States Environmental Protection Agency) UWR (Universal Waste Rule) and therefore are not covered under the Battery Act, even though they are classified as hazardous substances by the Department of Transportation because of their fire risk (Gaines et al., 2018). Eight US states have waste management regulations and mechanisms for LiBs, only three of which explicitly incorporate LiBs.

1.3 Environmental Impacts of Lithium-ion Batteries

A life cycle analysis conducted by Peters *et al.*, found that it took 330 kWh and 110 kg CO_2-e (Or et al., 2020; Peters et al., 2017) to produce 1 kWh of lithium-ion battery storage. Comparatively, 1 kWh of energy from bituminous coal, resulted in an approximate cumulative energy demand of 0.2 kWh (Mann et al., 2000) and 1.1 kg CO_2-e (Agrawal et al., 2014), but can only be used once. Sustainable recycling technologies have the potential to significantly reduce these emissions, especially if pyrometallurgical methods are avoided, which release toxic flue gases (Or et al., 2020).

A LCA (Life Cycle Analysis) conducted by Peters et al., found that producing 1 kWh of LiB storage, resulted in a CED (Cumulative Energy Demand) of 328 kWh and 110 kg of CO_2e (Carbon Dioxide Equivalent) (Or et al., 2020; Peters et al., 2017). Sustainable recycling

technologies have the potential to significantly reduce these emissions, especially if pyrometallurgical methods are avoided, which release toxic flue gases (Or et al., 2020).

When LiBs are disposed to landfill, and water passes through, toxic metals are leached from the LiBs causing adverse effects on the wider environment: compromising the water table, polluting the soils and often causing explosions leading to fires. Acid producing anaerobic microorganisms often corrode the casing exacerbating these repercussions (L. Li et al., 2010; Nan et al., 2005; Or et al., 2020; Vector, 2018).

1.3.1 Natural Resource Extraction

Resource extraction is a serious environmental issue and is responsible for the majority of global greenhouse gas emissions and more than 80% of biodiversity loss according to the United Nations Global Resources Outlook for 2019 (Oberle et al., 2019). Within the lithium-ion battery context the estimated material demand for the 2.1 million electric vehicles sold in 2019 was approximately 19 kt for cobalt, 17 kt for lithium, 22 kt for manganese and 65 kt for nickel (IEA, 2020). By 2030, the resource demand for LiBs is set to increase to 180 kt per year for cobalt, lithium to approximately 185 kt per year, manganese to 180 kt per year and nickel to 930 kt per year (IEA, 2020).

Lithium carbonate is used in the manufacturing of lithium-ion batteries. Chile is the largest supplier, followed by China and Russia (Castillo et al., 2002; Chagnes et al., 2013). The environmental implications of lithium extraction are profound, insomuch as 750 t of brine and 1.9 kt of water is needed, to produce one ton of lithium (Castillo et al., 2002; Harper et al., 2019). Thereby, the process of lithium production consumes as much as 65% of Salar de Atacama's water supply (Harper et al., 2019). In comparison, 1 t of lithium can be recovered from 28 t of spent lithium-ion batteries or 260 electric vehicle battery packs(Harper et al., 2019; Heelan et al., 2016). Therefore, the net environmental impact attributed to lithium in lithium-ion batteries can be greatly reduced if constituents of lithium-ion batteries can be sustainably recycled. Although the global lithium reserves are estimated at 62 Mt (Bernhardt et al., 2019; Fan et al., 2020) – based on current lithium consumption, this should be able to meet long-term projected demands up to 2100 (Or et al., 2020); other

metal constituents, such as cobalt, do not have a continuous supply chain due to geopolitical and social implications.

Cobalt is a strategic metal, with global identified reserves estimated in the order of 25 Mt, with estimates of 120 Mt of unidentified reserves (Bernhardt et al., 2019; Fan et al., 2020). While the annual extraction of cobalt is approximately 100 kt (Chagnes et al., 2013; Heelan et al., 2016), the demand for cobalt is expected to increase in the future associated with the increase in electric vehicles (Fan et al., 2020). Therefore, recycling materials containing cobalt are particularly important from an environmental and health standpoint as cobalt is classified as a carcinogen, mutagen and reproductive impacting substance (Chagnes et al., 2013). Cobalt reserves are geographically concentrated in the Democratic Republic of Congo and these reserves have experienced significant price variations attributed to their geopolitics. In addition, cobalt from the Democratic Republic of Congo raise both ethical and environmental concerns around their extraction (Chagnes et al., 2013; Harper et al., 2019). According to UNICEF, around 40,000 children are involved in cobalt mining in Democratic Republic of Congo where they make less than $2 USD per day (Vector, 2018).

Current lithium-ion battery recycling often centres around the recovery of cobalt, due to older LCO batteries nearing their end-of-life, and the high value of cobalt. This economic incentive is expected to decline over time due to a shifting market; from LCO batteries towards cathodes with reduced cobalt content, such as NMC and NCA (Or et al., 2020; Winslow et al., 2018). Therefore, this review covers reuse, recovery and recycling strategies for a range of varying cathode compositions.

The reserves of other transition metals, such as manganese, nickel, cobalt, copper and aluminium, used in the construction of lithium-ion batteries are better established. Although, the increasing popularity of NMC and NCA in the LiB market, will result in a net increase in mined nickel. This increase is largely attributed to manufacturers attempting to reduce their reliance on cobalt. However, global identified reserves of nickel are estimated to be only 89 million tons (Bernhardt et al., 2019; Fan et al., 2020). Magnesium compounds are globally widespread and can be extracted from a wide range of sources, the global resource of magnesite is estimated in excess of 12 Gt (Bernhardt et al., 2019; Fan et al.,

2020). Manganese reserves are estimated as large and dispersed and recycling is crucial to prevent leaching if landfilled incorrectly. However, it was shown that the sole recycling of manganese is not profitable (X. Wang et al., 2016).

There are currently 2.1 Gt of identified copper resources, with an estimate of 3.5 Gt of unidentified copper resources available (Bernhardt et al., 2019). Similarly, The worlds aluminium resources are estimated to be large, in the order of 55 – 75 Gt (Bernhardt et al., 2019). Geopolitical issues surround the access to graphite, which has large global reserves of approximately 800 Mt, but in the year of 2018, 70% of this was produced in China (Bernhardt et al., 2019; Fan et al., 2020), synthetic graphite offers an alternative, but remains expensive.

1.3.2 Disposal Consequences

The repercussions of landfilling spent lithium-ion batteries are dire. When lithium-ion batteries are disposed to landfill, acid producing microorganisms can corrode the aluminium casing. Therefore, when water passes through, toxic metals – such as, cobalt, nickel and manganese are leached from the lithium-ion batteries, which compromise the water table, pollute the soils and often cause major safety hazards (L. Li et al., 2010; Nan et al., 2006; Or et al., 2020; Vector, 2018). When the lithium-ion battery casing is corroded the electrolyte within can also react with water, which can release harmful gases such as hydrogen fluoride into the atmosphere. Similarly, when lithium-ion batteries with significant lithium plating are disposed to landfill, the deposited lithium reacts violently with water causing serious explosions and fires (Weiguang et al., 2018).

1.4 Lithium-ion Battery Recycling Options

LiB recycling covers reuse, second life and metal recovery. The objective of these recycling technologies is to create a cyclic system in which new LiBs can be manufactured from recycled materials. By way of this, the strain on the environment can be mitigated and such recycling processes can provide an economically viable pathway for future LiB manufacturing.

1.4.1 Reuse

For this paper, reuse is defined as LiBs being reused for their intended purpose. This extends to direct recycling methods, which recovers cathode materials as reusable cathode mixtures instead of as individual metals, thus reducing the need for downstream processing (Or et al., 2020).

1.4.1.1 Regeneration

Shi et al., examined two different cathode regeneration methods: Combined hydrothermal treatment and short annealing. The hydrothermal method involved, LCO powders heated inside a Teflon-lined autoclave filled with 80 mL of 4 M lithium hydroxide solution. The powders were then washed with deionised water before being annealed (Shi et al., 2018). The work optimised the annealing rate over a range of temperatures. Furthermore, it was found that full recovery of the specific capacity and cycling stability was attainable without changing the original morphology and size distribution (Shi et al., 2018).

1.4.1.2 Second Life

Second life, in the LiB context, is defined as repurposing for an alternate use, with the original product remaining intact. Second life applications can prolong the life of spent EV batteries. However, the differing shapes, capacities and chemistries restrict applications for second use.

1.4.1.2.1 Stationary Storage

Repurposed batteries can be adopted in grid power applications. New Zealand's largely renewable infrastructure can be complemented with stationary storage to absorb peak loading. Second life, stationary storage systems have been adopted internationally as per Table 9. However, economic uncertainty surrounds the supply chain of LiBs, such as raw materials, which are heavily influenced by market prices. LiBs have great potential in the secondary storage sector largely due to their energy density – approximately 200 Wh/kg; power output, and cycle stability of approximately 2000 cycles. In addition, the global cost of LiBs is rapidly reducing as global production increases (Or et al., 2020).

Table 9: Second life demonstration projects with car manufactures as partners (Martinez-Laserna et al., 2018).

Project Name	Year	Second-life Application
Bosch, BMW, Vattenfall	2015	Smart-grid
Daimler AG, Getec Energie	2016	Wholesale energy market
BMW, UC Sand Diego Second Life	2016	Micro-grid with PV system
General Motors	-	Micro-grid with PV and wind system
UPC, SEAT	2015	Energy management strategies
Mitsubishi, PSA, EDF Forsee Power	2015	Optimisation of electricity storage
Nissan Eaton, The Mobility House	-	Energy from the grid

1.4.2 Recovery

Recovery of LiBs is defined as the process of recycling componentry and extracting metal constituents. There is a plethora of recovery processes in current use; these differ in economic cost, environmental cost and extraction efficiencies a range of these recovery processes are given in Table 11 and 12.

Wang et al. estimated that, based on recycling efficiencies given in literature, one ton of LCO batteries could yield up to $13,000 NZD, whereas one ton of LMO batteries would only yield $1,300 NZD (Or et al., 2020; X. Wang et al., 2016). For LMO and LFP batteries, the copper foil was the most valuable component. Therefore, under current market rates, LCO LiBs must comprise at least 20% of the total LiB scrap in order for current recycling plants to be profitable (X. Wang et al., 2016). A summary of the recoverable value from mixed LiB scrap is given in Table 10.

Table 10: Recoverable value from mixed spent LiBs, converted from AUD TO NZD (1SF) (Vector, 2018) .

Component	Composition (%)	Value (NZD 2018/ton)	Potential Recoverable Value Minimum (NZD 2018/ton)
Aluminium	4-24	$ 3,000	$ 60
Cobalt	5-20	$ 100,000	$ 3000
Copper	1-5	$ 9,000	$ 300
Iron	5-25	$ 70	$ 2
Lithium	1-7	$ 20,000	$ 100
Manganese	10-15	$ 300,000	$ 200
Nickel	5-15	$ 17,000	$ 500

Currently, recovery processes can be divided into four main types: pre-treatment; physical, chemical and biological processes. Often in current practice a combination of these processes are used. Physical processes consist of the physical separation of the battery components by methods such as crushing and heating. While the chemical process involves leaching and separation of metal ions from the electrode materials. Biological methods are still under development, but this is a rapidly advancing field (Barik et al., 2017).

Table 11: Comparison of metal extraction techniques modified from (Dahllöf et al., 2019; Zheng et al., 2018).

Recovery Method	Description	Advantages	Disadvantages
Pyrometallurgy	LiBs are heated at high temperatures. Electrolytes and plastics are burned. Metal alloys remain in the slag. Leaching usually proceeds. Lithium carbonate can be reduced to a pure metal by a carbothermal reduction.	Minimal disassembly required. Flexible, able to recycle different chemistries at the same time. Relatively cheap on an industrial scale.	Loss of quality material. Hard to separate the alloys from the slag. Energy intensive and high CO_2 and harmful gas emissions. Low metal recovery rate. Process must be continuous.
Hydrometallurgy	Use of acids or bases to dissolve metals. Most metal can be recycled.	Very high recovery rate and most metals can be recovered. Not energy intensive.	Need for sorting and disassembly. Toxic gases released. Large number of reagents used. Expensive
Mechanical	Crushing and shredding. Then either low yield, which targets copper and aluminium or high yield methods to keep the cathode powder intact.	No chemicals needed.	Risk for violent reactions. Oxygen free environment needed or freezing of batteries before shredding.
Biometallurgy	Bacteria produce both organic and inorganic acids which promotes metal leaching.	Low energy consumption. Mild conditions. High metal recovery rate.	Long reaction period. Difficult to cultivate bacteria.

Mechanochemical	Grinding together with solvents such as polyvinyl chloride to produce lithium and cobalt chlorides that are extracted with solutes such as water.	Simple, lower energy use, less chemical reagents, lower environmental pollution.	Higher energy use than hydrometallurgy processes. Large equipment costs and long processing times.

Table 12: Comparison of metal extraction techniques modified from a range of sources.

Reference	Process	Battery Type	Objective	Major Findings
(Paulino et al., 2008)	Calcination at 500˚C for 5 hours, Fusion with potassium bisulphate at 500 ˚C for 5 hours.	LMO	Recovery of metals with low waste generation	Objectives met.
(Bertuol et al., 2015)	Pre-treatment separation based on brands and models from a range of EVs. Subsequent grinding, sieving and elutriation.	LiBs	A sample of LiBs were shredded, and the materials separated by spouted bed elutriation.	Simple and inexpensive way for separation.
(L. Li et al., 2010)	Citric acid and hydrogen peroxide were introduced as leaching reagents. Subsequent leaching of cobalt and lithium.	LCO	Recovery of metals by novel hydrometallurgy methods that are environmentally friendly.	≈100% Li and 90% Co were extracted using 1.25 M citric acid, 1.0 vol% hydrogen peroxide at 90 ˚C and a S:L of 20 g/L and a time interval of 30 minutes.
(Dorella et al., 2007)	Manual pre-treatment. Subsequent acid leaching, precipitation with ammonium hydroxide, liquid-liquid extraction using Cyanex 272.	LiBs	To modify the route proposed by (Zhang et al., 1998) through the introduction of selective precipitation after leaching.	Objective was to reduce the amount of aluminium in the leach liquor, approximately 50% of the cobalt was recovered from the LiB dust.
(Garcia et al., 2008)	Electrochemistry quartz crystal microbalance technique.	LiBs	To clarify the cobalt electrodeposition mechanism as a function of pH.	Electro dissolution of cobalt occurs directly to Co^{2+} in pH 2.7 through the intermediary Co^{+} that is oxidised to Co^{2+} in pH.5.4.
(Zhou et al., 2010)	Mechanical pulverisation and sieving process.	LiBs	To recycle most valuable components from spent LiBs.	95.9% of Cu was recovered after shredding and sieving to ≈0.20 mm after pulverisation. The organic solvent DMF successfully dissolved the adhesive between the electrodes.
(Bahgat et al., 2007)	Separation of the main cathode electrode material LCO from the anode. Chemical grade iron oxide was added for the synthesis of ferrite.	LCO	To synthesise Li/Co ferrite composite form spent LiBs. To test structural and magnetic properties under different reaction conditions.	Objective met.
(Nayl et al., 2015)	Acid leaching for mixed LiBs. Carried out after alkali decomposition using ammonium hydroxide, followed by sulfuric acid and hydrogen peroxide leaching.	LiBs	To establish a procedure for dissolving and recovering Al, Cu, Mn, Co, Ni and Li present in the powder obtained from crushing and mixing different types of spent LiBs	Objective met.
(Mishra et al., 2008)	Elemental sulfur and ferrous iron used as energy source to create leaching medium made up of metabolites. Application of chemolithotrophs and acidophilic bacteria.	LCO	To attempt bioleaching of spent LCO LiBs.	Objective met.
(Zeng et al., 2015)	LCO can be leached using oxalic acid without assistance from hydrogen peroxide solution.	LiBs	To develop a recovery method with only acid leaching and filtering.	Objective met.
(B. Xin et al., 2009)	The bioleaching mechanisms of Co and Li from spent LiBs by sulfur-oxidising and iron oxidising bacteria.	LiBs	Investigate bioleaching mechanisms of Co and Li from spent LiBs applying a mixed culture of sulphur oxidising and iron oxidising bacteria.	Objective met

1.4.2.1 Pre-treatment

Manufacturers have varying LiB designs. This poses a serious issue for pre-treatment prior to recycling (Harper et al., 2019). Throughout LiB manufacturing there is no standardisation of LiBs. This lack of standardisation is expected to remain in the future when compared to other LiB products, such as mobile phones, which have varying shapes, size and chemistry. A range of current pre-treatment processes are given in Table 13.

Table 13: Comparison of pre-treatment processes modified from (Dahllöf et al., 2019; Zheng et al., 2018).

Pre-treatment Process	**Description**	**Advantages**	**Disadvantages**
Further dismantling	The cathode, anode and separator are separated and dried under inert conditions (liquid nitrogen or argon). Limited to lab scale.		
Dissolution with solvent	Organic solvent used to weaken binder. Cathode materials are then removed from aluminium foil.	Efficient and recovers the aluminium foil.	Expensive and serious environmental implications.
Dissolution with NaOH	Dissolution with solvent, NaOH.	Simple operation and high efficiency.	Difficult to recover the aluminium foil, alkaline wastewater.
Ultrasonic-assisted separation	Ultrasonic cleaning in combination with mechanical agitation. Used for stripping cathode material from aluminium foil. A cleaning solution is needed.	Simple operation and very low exhaust emissions	Expensive equipment and noisy.
Thermal treatment (smelting or pyrolysis)	High temperature decomposes binder to reduce bonding in cathode material.	Simple operation and high throughput. Can discharge and remove electrolyte.	High energy consumption, expensive equipment and poisonous gas emissions.
Mechanical treatment	Effective method of crushing, sieving and magnetic separation. Dismantling is not always necessary. The magnetic parts can also be recovered with magnetic separation	Simple and convenient operation.	The separation is not complete for all materials. Poisonous gas emissions occur.

1.4.2.1.1 Discharge

LiBs must first be discharged to reduce the metallic lithium present, which reacts violently under atmospheric conditions. A common method involves the use of salt-saturated solutions such as sodium chloride. However, it releases HF (Hydrogen Fluoride) caused by the reaction of electrolyte in water (Weiguang et al., 2018). Discharging is not necessary if the atmosphere for the recycling process is inert, this can be achieved through argon. Alternatively, disassembly can be done under passivation, through cooling, which lowers the reactivity of lithium ions and thereby, reduces the risk associated with explosions, fires, and toxic emissions (Or et al., 2020).

1.4.2.1.2 Disassembly

Automation, in the processing of waste LiBs, offers a solution to the broad range of designs. Automation of the disassembly process would significantly reduce the risk to human workers, and would reduce cost, potentially making recycling economically viable (Or et al., 2020). However. there are major challenges in automating the disassembly line; namely, various designs of LiBs; environmental damage, such as corrosion; and lack of labelling systems to identify varying cathodic compositions. Hermann et al., investigated the state of automation in the industry and proposed a multifaceted process based on industry-specified, technical difficulties. It was found that some aspects were well suited for automation— such as, dismantling of the individual cells by a prototype jaw-system, which monitored cell health before dismantling (Herrmann et al., 2012; Or et al., 2020).

1.4.2.1.3 Electrolyte Recovery

Electrolyte recovery from LiBs has been established at both the lab and industrial scale. Often in recycling processes the electrolyte and other organic compounds are discarded, although electrolyte recovery has been shown to be profitable in literature. One method of electrolyte recovery involves condensation, whereby organic solvent can be recovered by distillation due to its high boiling point relative to water (He et al., 2019). Some electrolyte may remain captured within the pores of the electrode material, which could be removed by super-critical CO_2 from the processed LiB powder (Grützke et al., 2015; Nowak et al., 2017; Or et al., 2020).

Hazardous gases can be released if the electrolyte and solvent are exposed to atmosphere (Nan et al., 2006; Ribière et al., 2012; Sonoc et al., 2015). The electrolyte and separator are often placed in an alkaline solution after dismantling to prevent the release of toxic fluoride-based gases (Archuleta, 1995; Nan et al., 2005).

1.4.2.1.4 Graphite

Graphite recovery has been investigated at lab scale. Anodes are separated from LiBs. Subsequently, graphite can be separated from the copper current collector by NMP (N-Methyl-2-Pyrrolidone) dissolution, acid dissolution or mechanical scraping (Y. He et al., 2017; F. Wang et al., 2018; Yu et al., 2018). Although, NMP remains too expensive for scale-up processes, and alternative dissolution compounds must be evaluated (Xu et al., 2008). Pre-treated LiBs powder, contains electrode materials wherein separation of graphite and metals can be achieved through flotation or magnetic separation (Or et al., 2020). The main challenge found in the recovery of graphite is in separating the SEI layer, binder and additives away from the graphite. High temperature thermal treatment is likely necessary to remove carbon-based components, whilst electrolyte can be removed by super-critical CO_2 extraction (Grützke et al., 2015; Nowak et al., 2017; Or et al., 2020).

1.4.2.2 Physical Processes

1.4.2.2.1 Pyrometallurgy

Pyrometallurgy involves high-temperature processing to recover metals and other materials. Although used widely in industry, this method generates toxic flue gas, which requires downstream treatment to meet environmental regulations. However, pyrometallurgy is adaptable, simplistic and capable of a high processing capacity. Furthermore, it is able to facilitate a mixed LiB feed. Minimal pre-treatment is needed for this process. Spent LiBs including plastic, electrolyte and other components are decomposed in high-temperature, oxygen-rich furnaces, with temperatures exceeding 1200 ˚C (Amarakoon et al., 2013). Metallic oxides are formed through the furnace, thereby creating a metal alloy. The metal alloy requires further processing before it can be used in further LiB manufacturing (Amarakoon et al., 2013). Due to the significant power consumption attributed to heating to such high temperatures, lab-scale research is limited (M. Chen et al., 2019). However, this process is constrained by its immense power usage, and failure to

recover lithium, which is often lost as slag. Pyrometallurgical recycling has been proven to result in a net increase of GHG emissions and energy consumption compared to raw material extraction largely attribute to the combustion of non-metallic based LiB componentry (Or et al., 2020).

1.4.2.2.2 Mechanical Separation

Mechanical separation is a form of pre-treatment that uses processing techniques to concentrate the metallic-fraction; according to properties such as density, conductivity and magnetic behaviour (L. Li et al., 2017). The disadvantage of mechanical separation is that not all components of LiBs are separated since they are composed of several metals alongside organic and inorganic substances which are imbedded in each other (Ordoñez et al., 2016).

1.4.2.2.3 Thermal Treatment

Thermal treatment involves the separation of insoluble organic additives and adhesives. This is achieved by heating to approximately 150 ˚C in a controlled atmosphere. Thermal treatment is appealing, as it is effective in removing LiB impurities before further processing. However, like pyrometallurgic processes, thermal treatment has been linked to high dioxin emissions and chloride compounds. Therefore, downstream air purification is necessary (Ordoñez et al., 2016).

1.4.2.3 Chemical Processes

1.4.2.3.1 Hydrometallurgy

Hydrometallurgy encompasses leaching, solvent extraction and precipitation, utilising a broad range of reagents. A summary of these processes and subsequent reagents are given in Table 14. Compared with pyrometallurgy and bio-metallurgy processes hydrometallurgy can achieve higher purity, lower energy consumption and lower gas emissions (Joulié et al., 2014; Y. Xin et al., 2016). The hydrometallurgical recycling process given in Figure 2 is appealing because it can be applied to a range of LiB chemistries.

Table 14: List of hydrometallurgical technologies development in the literature.

Reference	Process	Reagents	Efficiency (%)				
			Li	Co	Ni	Mn	Cu
(Zheng et al., 2017)	Alkali Leaching	NH_3, $(NH_4)_2SO_4$, Na_2SO_3	>98	>98	>98		
(Barik et al., 2017)	Inorganic Acid Leaching	HCl		>99		>99	
(L. Li et al., 2017)	Organic Acid Leaching	Lactic Acid	>97	>97	>97	>97	
(Bahaloo-Horeh et al., 2017)	Bioleaching	Organic Acid (Aspergillus Niger)	100				100
(Virolainen et al., 2017)	Solvent Extraction	Cyanex 272 & PC-88A	99.9	99.6	99.7		
(Yang et al., 2017)	Solvent Extraction	D2EHPA in Kerosene	99				
(Pinna et al., 2017)	Chemical Precipitation	H_3PO, Li_3PO_4, $H_2C_2O_4$, CoC_2O_4	88	99			
(X. Chen et al., 2016)	Chemical Precipitation	H_3PO, Li_3PO_4, $H_2C_2O_4$, CoC_2O_4, $C_4H_8N_2O_2$, $Ni(C_4H_6N_2O_2)_2$	93	97	96		

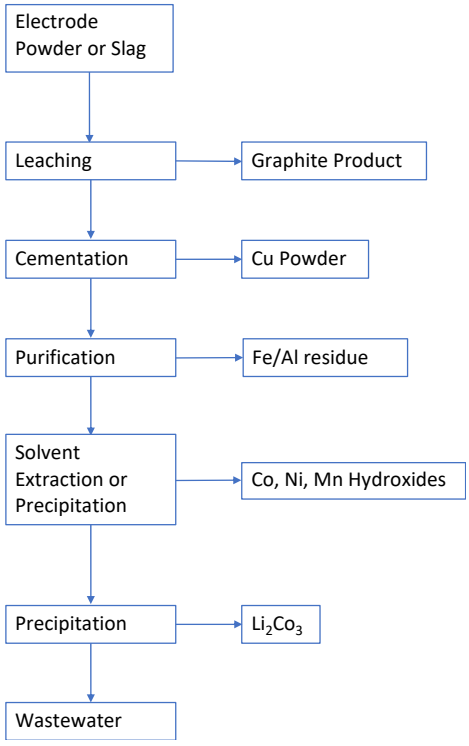

Figure 2: General hydrometallurgy process modified from (Friedrich et al., 2017).

After pre-treatment, batteries are shredded and powdered by ball mill and undergo further reduction by dosing of lithium brine. Four streams result from this process which are summarised in Figure 3. The final step, metal separation, often uses Cyanex 272 as the extractant (Mantuano et al., 2006).

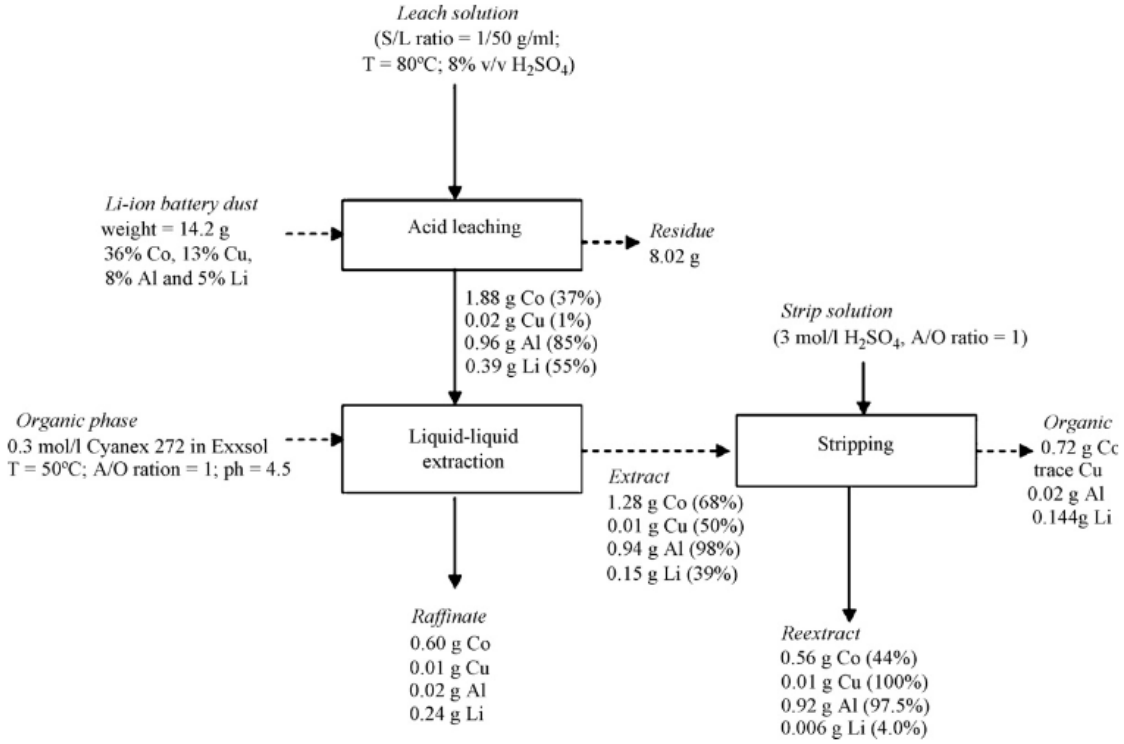

Figure 3: Illustrative of hydrometallurgical route to treat LiB waste (Xu et al., 2008).

1.4.2.3.2 Leaching

The remaining metallic dust and residues from pre-treatment treatment, are then leached by an acidic solution in order to transfer the metals into the bulk aqueous solution (Xu et al., 2008). Zhang et al., found that HCl was the most effective leaching reagent out of the inorganic acids that were tested (Zhang et al., 1998). However, this would require purification steps for the chlorine gas that was evolved, increasing the capital when implemented at industrial scale. The proposed reaction using HCl on LCO residue is described in the chemical reaction below:

$$2LiCoO_2 + 8HCl \Leftrightarrow 2CoCl_2 + Cl_{2\,(g)} + 2LiCl + 4H_2O$$

Hydrometallurgical acid leaching is promising for large scale applications due to its low energy consumption. In addition, it is capable of dealing with varying cathode chemistries, whilst allowing the metals to be recovered in high purity (Or et al., 2020). A range of leaching acids have been tested in literature and are summarised in Table 15 and 16.

Table 15: Leaching systems used for recycling lithium-ion batteries modified from (Chagnes et al., 2013).

Reference	Leaching Reagents	Concentration ($molL^{-1}$)	T (˚C)	Efficiency (%)	
				Li	Co
(Zhang et al., 1998)	HCl	4	80	≈100	≈100
(Lee et al., 2002)	HNO_3	1	75	85	85
(Lee et al., 2002)	H_2O_2	1.7 vol%			
(L. Li et al., 2011)	HNO_3	1	80	≈100	≈100
(L. Li et al., 2011)	H_2O_2	1 vol%			
(Castillo et al., 2002)	HNO_3	2	80		≈100
(Sun et al., 2011)	H_2SO_4	2	80	>99	>99
(Zhu et al., 2012)	H_2SO_4	2	60	≈88	≈96
(Zhu et al., 2012)	H_2O_2	2 vol%			
(Swain et al., 2007)	H_2SO_4	2	75	94	93
(Swain et al., 2007)	H_2O_2	5 vol%			
(Kang et al., 2010)	H_2SO_4	2	60	≈99	≈99
(Kang et al., 2010)	H_2O_2	6 vol%			
(Shin et al., 2005)	H_2SO_4	2	75	≈100	≈100
(Shin et al., 2005)	H_2O_2	15 vol%			
(Nan et al., 2005)	H_2SO_4	3	70	98	98
(Nan et al., 2006)	H_2SO_4	3	70	≈100	≈100
(Nan et al., 2006)	H_2O_2	3 vol%			
(Mantuano et al., 2006)	H_2SO_4	8 vol%	80	95	80
(Dorella et al., 2007)	H_2SO_4	6 vol%	65	37	55
(Dorella et al., 2007)	H_2O_2	4 vol%			
(L. Li et al., 2011)	$C_4H_5O_6$	1.5	90	93	94
(L. Li et al., 2011)	H_2O_2	2 vol%			
(L. Li et al., 2011)	$C_6H_8O_7H_2O$	1.25	90	≈100	>90
(L. Li et al., 2011)	H_2O_2	1			

Table 16: Leaching systems used for recycling lithium-ion batteries modified from (Or et al., 2020)

Reference	Cathode Type	Optimised Conditions				Leaching Efficiency (%)			
		Reagent	L:S (mL/g)	T (˚C)	Time (h)	Li	Ni	Mn	Co
(Wang et al., 2009)	LCO, LMO, NMC	HCl	50	80	1	99.0	99.8	99.8	99.5
(J. Li et al., 2009)	NMC, LFP	HCl, H_2O_2	8	60	2		>95	>95	>95
(Barik et al., 2017)	Mixed	HCl	5	50	2	99.2		99.0	98.0
(Joulié et al., 2014)	NCA	HCl	20	90	18	≈100	≈100		≈100
(Dhiman et al., 2019)	Mixed	HCl	50	80	1	99.0	94.5	93.4	98.7
(Meshram et al., 2015)	Mixed	H_2SO_4	20	95	4	94.3	96.3	50.2	66.2
(L.-P. He et al., 2017)	NMC, LCO	H_2SO_4, H_2O_2	25	40	1	≈99	≈99	≈99	≈99
(Lv et al., 2018)	NMC	H_2SO_4, NH_4Cl	10	60	1	99.1	97.5	97.3	97.6
(Meshram et al., 2015)	Mixed	H_2SO_4, $NaHSO_3$	50	95	4	96.7	96.4	87.9	91.6
(X. Zhang et al., 2018)	NMC	H_2SO_4	3.5	55	2.5		98.0	98.0	96.0
(Liu et al., 2019)	NMC	H_2SO_4	10	90	0.5		99.6	99.9	99.9
(Sattar et al., 2019)	Mixed	H_2SO_4, H_2O_2	20	50	2	>98	>98	>98	>98
(Zhuang et al., 2019)	NMC	H_3PO_4, Citric Acid	50	90	0.5	≈100	93.4	92.0	91.6
(Guan et al., 2017)	Mixed	HNO_3	-	25	2	77.2	99.9	≈100	91.3
(Peng et al., 2019)	Mixed	HNO_3	-	70	5	85.0			80.0
(L. Li et al., 2018)	LCO, LMO, NMC	Citric Acid, H_2O_2	50	90	1	96.0	97.8	99.8	99.2
(X. Chen et al., 2015)	NMC	Citric Acid, H_2O_2	30	80	1.5	99.0	97.0	94.0	95.0
(Musariri et al., 2019)	Mixed	Citric Acid, H_2O_2	50	95	0.5	97.0	99.0		95.0
(L. Li et al., 2018)	NMC	Maleic Acid, H_2O_2	50	50	0.5	99.5	95.1	96.4	94.3
(Y. He et al., 2017)	NMC, LCO	Tartaric Acid, H_2O_2	59	70	0.5	99.1	99.3	99.3	98.6
(L. Li et al., 2017)	NMC	Lactic Acid, H_2O_2	20	70	0.33	97.7	98.2	98.9	98.4
(Gao et al., 2018)	NMC	Acetic Acid, H_2O_2	25	60	1	100	92.7	96.3	93.6
(L. Li et al., 2018)	NMC	Acetic Acid, H_2O_2	50	70	1	98.8	97.9	97.7	97.9

1.4.2.3.3 Solvent extraction

Solvent extraction relates to the selective movement of metallic ions from the aqueous to organic phase (Schulz et al., 1987). The selected metal is stripped from the aqueous phase, whereby the extractant is recycled and the metal can then be physically recovered by precipitation or reduction. Most studies reviewed have used sulphuric acid or hydrogen peroxide as the lixiviant. Whereas Cyanex 272 is often used as the extractant that separates Ni and Co (Yang et al., 2017).

1.4.2.3.4 Electrochemical

Electrochemical recycling methods involve metal oxide deposition from aqueous electrolytes such that these form on in situ electrodes. Myoung et al., applied electrochemical deposition to prepare cobalt oxide from waste LCO cathodes. Under specific pH levels, cobalt hydroxide was precipitated on the titanium electrode and heat treatment of the cobalt hydroxide resulted in the formation of cobalt oxide (Myoung et al., 2002).

1.4.2.4 Biological Processes

1.4.2.4.1 Biometallurgy

Biometallurgy is an effective method for extracting metals from waste LiBs. The metabolites excreted help make soluble metals from insoluble waste (Mishra et al., 2008). Both bacteria and fungi are used in bio-metallurgy, with funguses able to grow over a wider range of pH values and leach at a faster rate (Bahaloo-Horeh et al., 2017). The work of Bahaloo-Horeh et al., used biometallurgy techniques on mixed LiB scrap. This was achieved using Aspergillus Niger, a fungi known to secrete citric, gluconic, malic, and oxalic acids (Bahaloo-Horeh et al., 2017; Or et al., 2020). A numerical model was used to establish initial conditions. Wherein, sucrose was found to be the most important input parameter and was positively correlated with the production of the secreted acids except oxalic acid, which is associated with cobalt precipitation. The process required a long incubation period in the order of two weeks, with high liquid-solid ratios (Or et al., 2020).

1.4.3 Current Practice

lithium-ion batteries are being recycled on an international scale. This is largely due to environmental pressures, but also attributed to the economic benefit of recovering metallic lithium-ion battery constituents. Several companies have developed methods to handle the influx of end-of-life lithium-ion batteries entering the waste stream. The methods used to recycle lithium-ion batteries, from a range of companies, are categorised by country in Figure 4 below and includes overall capacity. Although, comprehensive the list below is not exhaustive, and many recycling companies were not included. Many of the companies excluded utilise novel, environmentally friendly, recycling methods, but were omitted due to insufficient data or limited capacity. Most recycling companies surveyed use a form of pyrometallurgy treatment. However, recent awareness as to the adverse environmental effects of such recycling techniques have prompted a move to reduce this reliance (Or et al., 2020). It should be noted, that for the data collected, it is unclear whether the processing capacities indicated are inclusive of other types of batteries, ores, or manufacturing scraps.

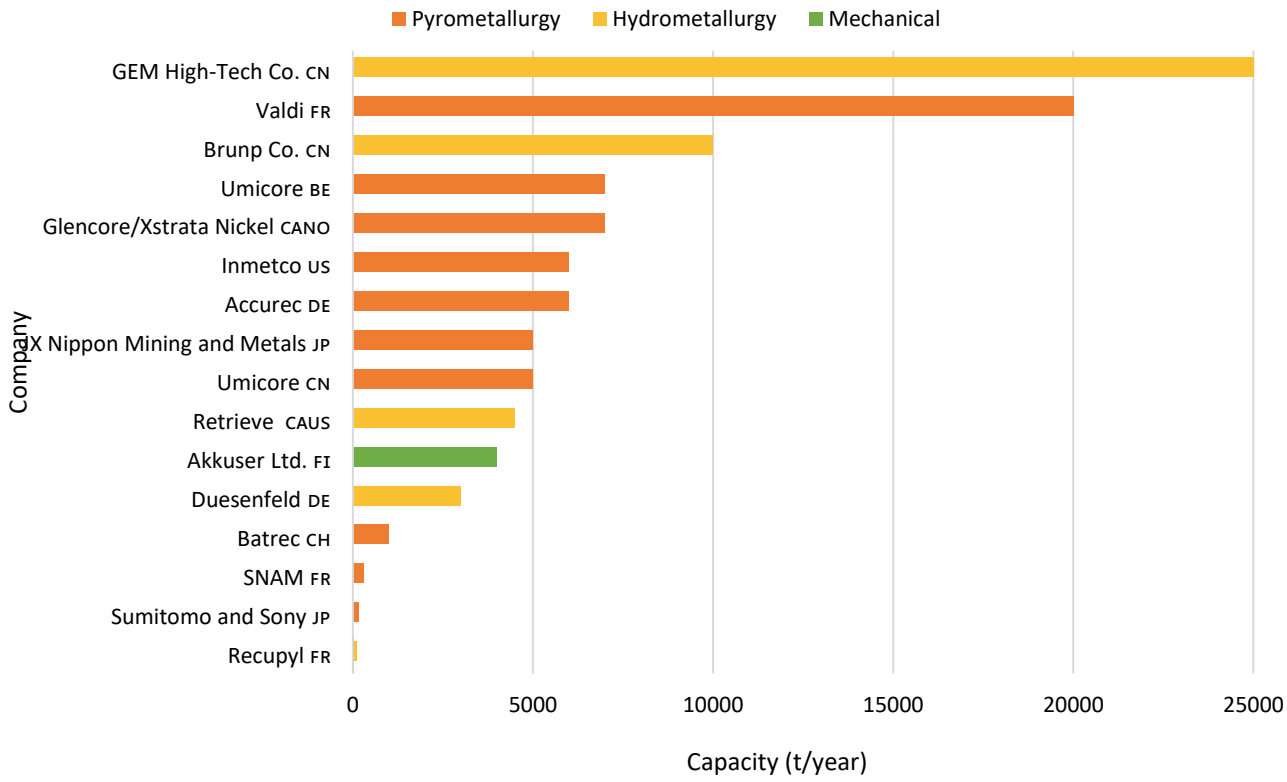

Figure 4: Capacity and methods used by lithium-ion battery recycling companies categorised by origin country (Dahllöf et al., 2019; Lv et al., 2018; Pinegar et al., 2019; Winslow et al., 2018).

Many recycling companies, such as the ones above are continuously expanding to make recycling more economic, efficient and less environmentally impacting. Development and integration of the 3-R model offers a step towards a circular lithium-ion battery economy. However, a shift in perspective is needed to move away from currently dominant, environmentally detrimental, pyrometallurgy methods.

LiBs are being recycled on an international scale. This is largely due to environmental pressures, but also attributed to the economic benefit of recovering LiB constituents such as precious metals. Several companies outlined in Table 17 have developed methods to handle the influx of EoL LiBs entering the waste stream. A generalised process for industrial practice is given in Figure 5.

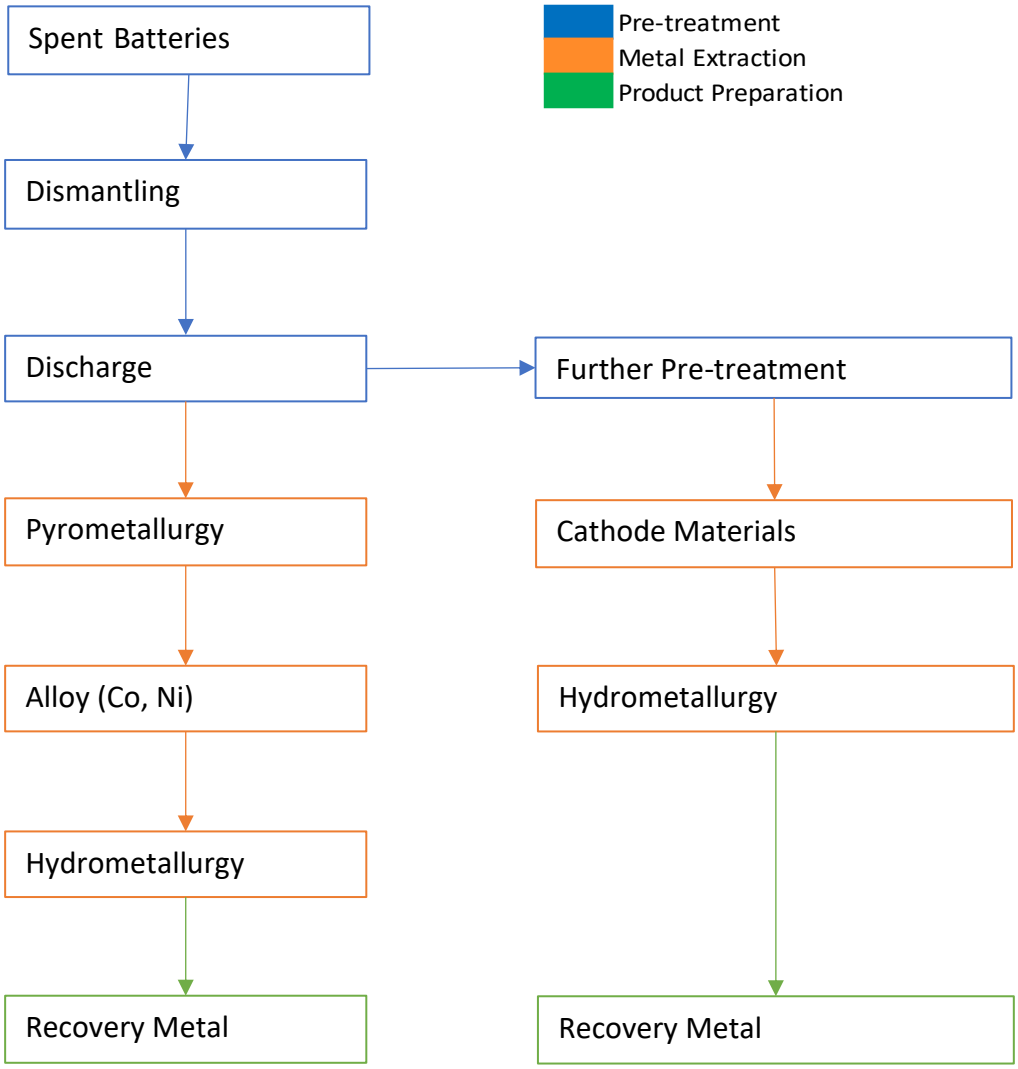

Figure 5: Generalised process to recover LiB constituents used in industry.

Table 17: LiB recycling companies, collated from a range of sources (Dahllöf et al., 2019; Fan et al., 2020; Vector, 2019; Zheng et al., 2018).

Company	Country	Pre-treatment/Extraction Technologies	Capacity (t/year)	Main Products
Accurec	Germany	Collection of the organic solvents in electrolyte by vacuum pyrolysis; recovery of Li by vacuum evaporation	1000	Co alloy, Li_2CO_3
AEA	UK	Hydrometallurgy. Uses organic solvent to remove electrolysis and binder (PVDF); recovery of Co in LiOH solution by electrodeposition	-	Co_2O_3, LiOH
AkkuSer (Boliden)	Finland	Mechanical. The coarse fraction is delivered to Boliden for copper refining	-	Cu and black mass
ARetriev	USA	Hydrometallurgy	3500	Co cake, Li_2CO_3, Cu and Al foil
BatRec (Sarpi/Veoila)	Switzerland	Mechanical, pyrometallurgical. The spent LiBs are stored and shredded under CO_2 atmosphere	1000	Co, MnO_2, Ni-based alloys
Brunp	China	Hydrometallurgical methods including leaching, purification, solvent extraction and resynthesise of materials	-	Cathode materials
Duesenfeld	Germany	Combination of mechanical and hydrometallurgical. Based on processes developed in the project LithoRec	3000	Co, Ni, Mn as active materials, electrolyte
GEM	China	hydrometallurgical methods including pre-treatment, leaching, purification, solvent extraction, and the resynthesise of materials	-	Cathode materials
Glencore	Switzerland	Combines pyro- and hydrometallurgy methods	-	Co, Ni, Cu-alloys
IME	Germany	pyrometallurgy and hydrometallurgy. Collecting electrolyte through evaporation and condensation; separating particles with magnetic separation; Co-base alloys produced by melting small particles in an electric arc furnace; Li_2CO_3 is obtained by dissolving the slag	-	Li_2Co_3, Co-base alloys
Inmetco	USA	Pyrometallurgy. Scrap processed in a rotary hearth furnace and further refined in an electric arc furnace	-	Ni-base alloys

JX Nippon Mining and Metals	Japan	Hydrometallurgy. Solvent extraction	-	Ni, Co, Mn and Li
Kobar	South Korea	Pyrometallurgy and hydrometallurgy	>1000	Li, Na, Co, Al, Cu and Fe
Mitsubishi	Japan	Pyrometallurgy Freezing and disassembling under cryogenic liquid nitrogen environment; $LiCoO_2$ is obtained by burning; the exhaust gas is absorbed by $Ca(OH)_2$	-	$LiCoO_2$
Neometals	Austria	Mechanical and hydrometallurgy	Lab scale	Possible to recover Co, Ni, Cu, Li, Gr
Onto Technology	USA	Direct recycling. CO_2 supercritical fluid	-	Cathode materials
Recupyl/TES-AMM	France	Mechanical and hydrometallurgy	110	Possible to recover Mn, Co, Li, Ni
Redux	Germany/Austria	Mechanical and hydrometallurgy	-	Plastics, Fe, Cu, Al and others
Rockwood Lithium GmbH	Germany	Hydrometallurgy. Solvent extraction		
SNAM	France	Pyrometallurgic	-	Co, Ni, Cu
Sumitomo and Sony	Japan	Pyrometallurgy and Hydrometallurgy The electrolyte and plastics are removed through calcination; pyrometallurgical processes are used to recover alloy containing Co−Ni−Fe; hydrometallurgical process is conducted to recover Co	-	Co, Ni, Fe alloys and CoO
Umicore	Belgium	Pyrometallurgy with subsequent hydrometallurgy	7000	Co, Ni, Cu
uRecycle	Sweden	Mechanical: makes black mass, which is sold	-	Black mass
Xstrata Nickel	Canada	Pyrometallurgy	3000	Ni, Co, Cu alloys

1.5 Conclusions

lithium-ion battery recycling is rapidly developing. However, the manufacturing of new lithium-ion batteries surpasses current recycling efforts. Promising advances at lab scale offer a path towards future industrial scale recycling processes that can compete with lithium-ion battery production. These processes must be able to adapt to new mixed cathode chemistries – that diverge from the use of cobalt – and a comingled scrap of spent lithium-ion batteries from a variety of chemistries. As reviewed in this work, a combination of pre-treatment and hydrometallurgical processes were identified as a potential mechanism that could meet this criterion, which not only focuses on the recovered metal commodity value, but rather the cumulative environmental benefits, reduced energy consumption and lowered reliance on raw material extraction. The recycling of lithium-ion batteries will require political pressure from economic incentives, legislative requirements and public education.

One way to mitigate the incoming stream of LiB waste, is to extend the lifetime of the battery. This requires overcoming the degradation methods outlined in section 5. This is an ongoing area of research. Currently, the lifetime of a LiB battery pack in the EV market is estimated at 10 years (Amarakoon et al., 2013). If the lifetime of LiBs can be extended further, this will alleviate some of strain on future LiB recycling infrastructure.

A reduction in cobalt and nickel use is already being established in new-generation LiBs. Overall, these metals posed a higher carcinogenic risk than other metals and in addition to having a higher toxicity (Amarakoon et al., 2013). Therefore, reducing the use of these metals in the manufacturing, and EoL stages would be expected to reduce the overall potential environmental impacts associated with spent LiBs although would make future metal recovery processes less profitable.

Metal recovery and use in new LiBs poses an environmentally beneficial and economically viable route for a cyclic LiB economy. Recovery around precious metals, such as Ni and Co, are abundant. However, there are few studies on the recovery of graphite and the electrolyte in spent LiBs.

Biological based extraction mechanisms such as bioleaching, are gaining prominence and offer a viable recycling route. However, more research is needed in this field before it progresses from lab scale testing.

The changing nature of LiB manufacturing requires not just finding ways to recover precious metals, but also to recover other materials which may harm the environment (Ordoñez et al., 2016).

2 Lithium-ion Battery Characteristics: A Survey of Used Cells

2.1 Introduction

End-of-life lithium-ion batteries are often disposed with residual capacity (Or et al., 2020). EV battery packs that are unable to meet automotive standards are disposed with up to 80% capacity still remaining (Pistoia et al., 2018). Therefore, there is a niche within the lithium-ion battery market for second-use alternatives, whereby cells with sufficient residual capacity can be integrated within stationary storage systems, increasing the lifespan of individual cells and reducing the waste stream of spent LiBs, whilst supplementing renewable energy infrastructure. A design-and-build solar solution was examined in Chapter 5. However, to better understand the characteristics of spent LiBs, a survey of spent 18650 cells was undertaken. Although EV cells are predicted to become the largest market share in the future (Richa et al., 2016), LiB cells from consumer devices are currently dominant in the NZ LiB market (Vector, 2019). Therefore, 18650 cells were chosen for the survey as they reflect the NZ market, and are the most common type of LiB; used in both consumer devices and EVs.

2.2 Testing Methodology

Discarded battery packs were obtained from a variety of consumer devices and suppliers. The battery packs were then dismantled to remove the cells housed within Figure 6.

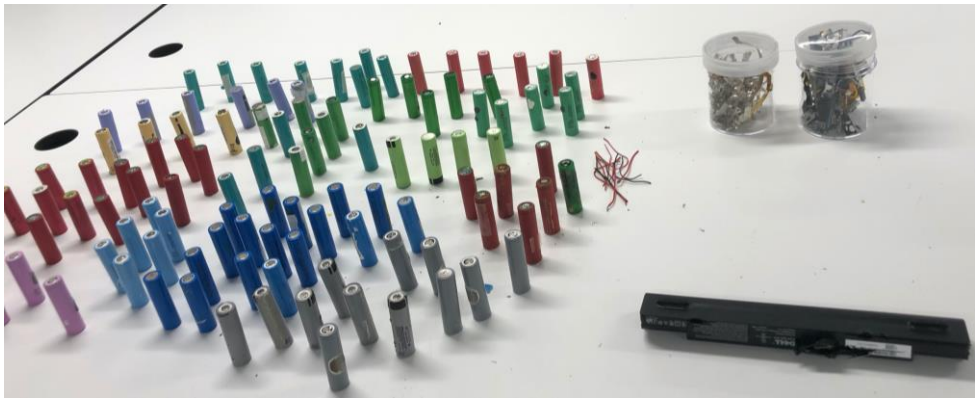

Figure 6: Lithium-ion 18650 cells from disassembled consumer devices.

Following disassembly, the plastic housing was recycled, and the 18650 cells were removed. For each of the cells gathered, the voltage, serial number and manufacturer were recorded

as shown in Appendix F1. A random sample of these cells were then chosen to characterise by potentiostat through subsequent charge-discharge cycles. Measurements for this application were performed on the 18650 cells from consumer devices. The batteries were placed into a custom battery holder for 18650 cells, as in Figure 7 below.

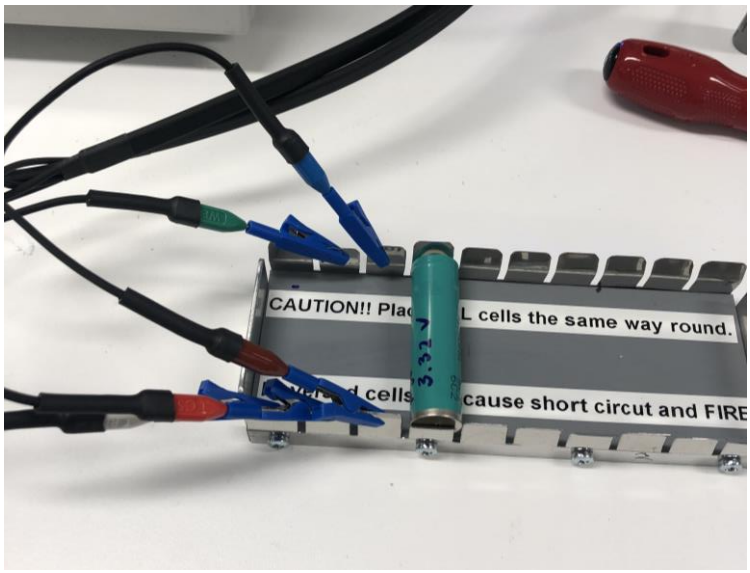

Figure 7: Custom housing unit used to perform cell characterisation on Gamry potentiostat.

2.3 Results and Discussion

The voltage distribution of the surveyed cells is shown in Figure 8, with 40% of the cells functional and above the minimum capacity threshold of 3 V as outlined by the manufacturer, and 60% of the cells above 2 V – the minimum safe discharge voltage.

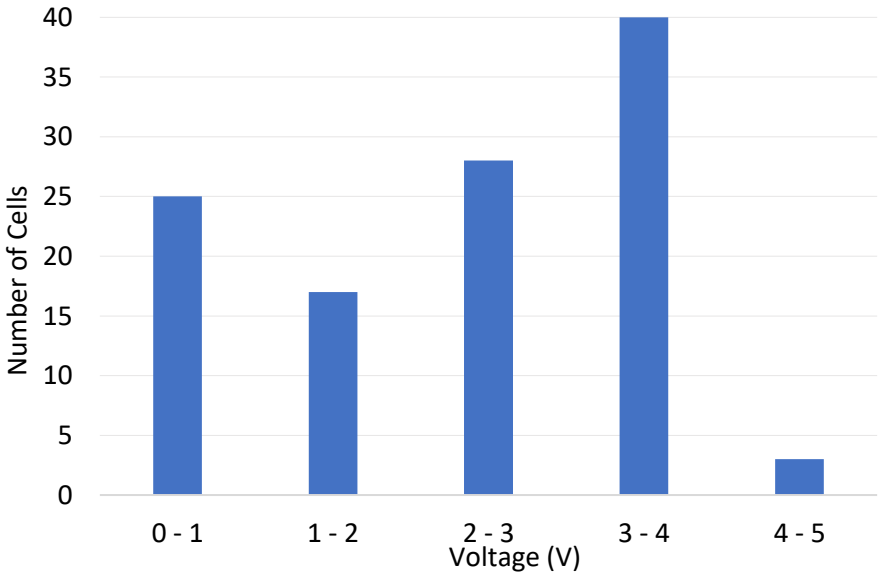

Figure 8: End-of-life 18650 cell voltage ranges from battery survey of consumer devices.

The results show that a large proportion of discarded cells – from a variety of consumer devices, manufacturers and a range of cell chemistries, are still functional. Infrastructure to directly reuse these cells for their intended purpose could then reduce the waste stream of LiBs from consumer devices by up to 40%.

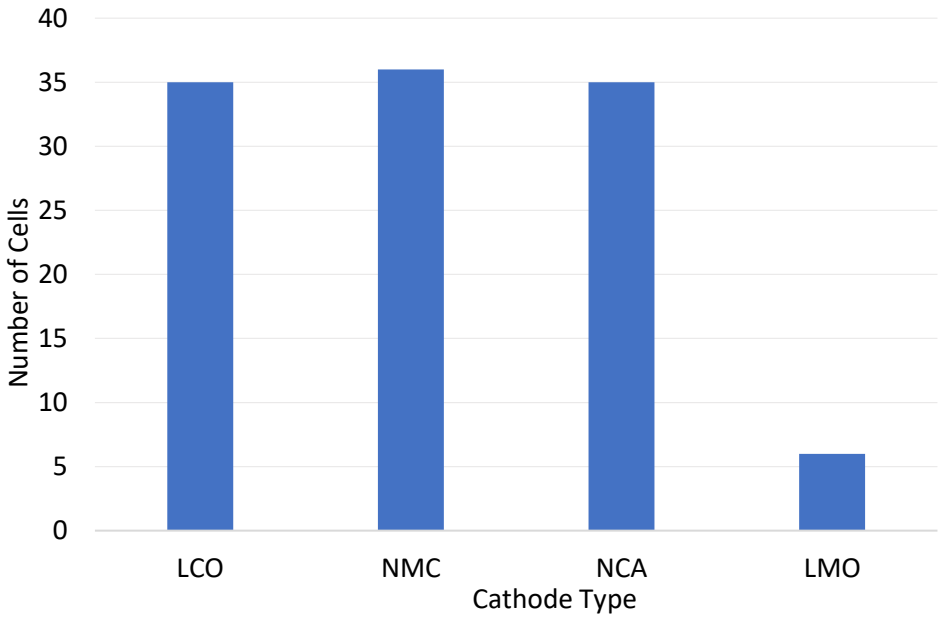

Figure 9: Distribution of cell chemistries among surveyed cells form consumer devices.

Figure 10 shows a typical charge curve and Figure 11 a discharge curve of several of the 18650 cells tested. Voltage is plotted against time. The cell was charged and discharged with a current of approximately 40 mA between 3 V and 4.2 V. Voltage increases steadily while charging the battery. During this step, lithium ions are extracted from the cathode and are intercalated into the graphitic anode layers.

The cell is held at 4.2 V after reaching the upper voltage limit. This step lasts until the current reaches approximately 0.5 mA which corresponds to a C rate of 0.01 C. This ensures that the battery is fully charged. The battery's state of charge SoC (State of Charge) is 100%.

The voltage initially drops at the beginning of the discharge step. According to Ohm's law, this voltage decrease is proportional to the ESR (Equivalent Series Resistance) as in (4).

$$\Delta V = (I)(ESR) \quad (4)$$

Where I is the applied current, ESR is the sum up resistances from electrodes, electrolyte, and electrical contacts. Whereby, the lower the voltage drop the higher the maximum output energy that can be drawn from a cell.

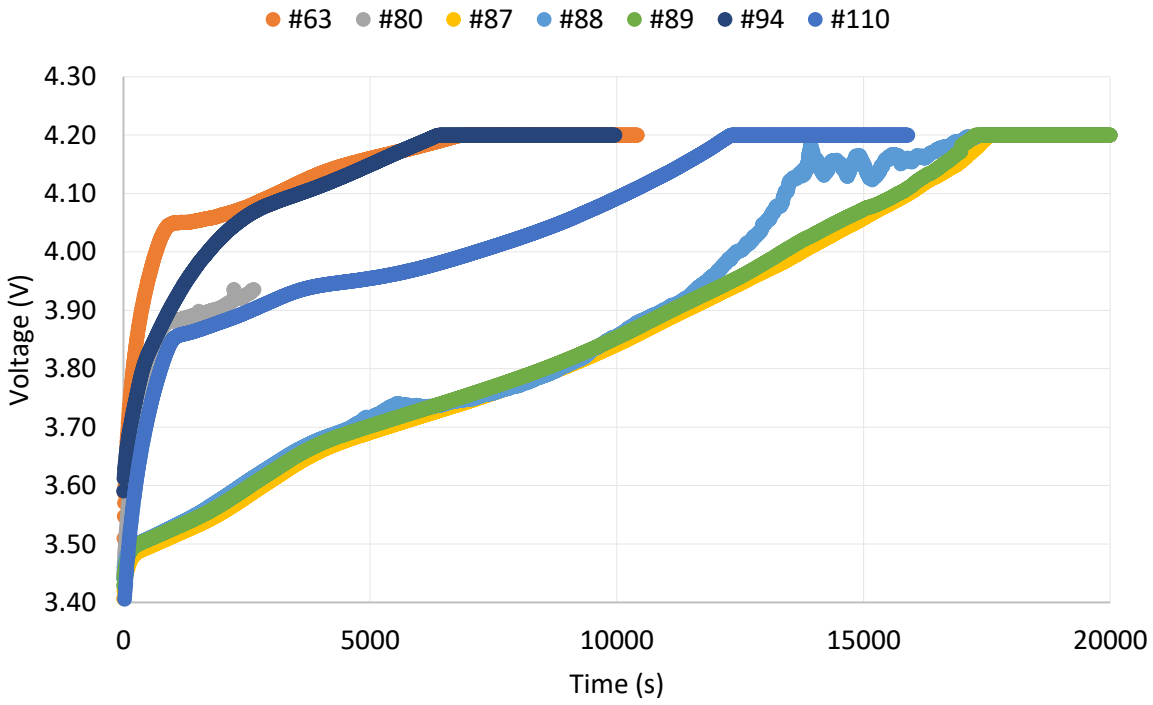

Figure 10: Charge profile of selected cells on Gamry potentiostat.

$$E = (V_0 - \Delta V)(I)(t) \quad (5)$$

In (5) V_0 is the actual voltage of the battery and t the charge or discharge time respectively. The limit of a battery's usable capacity is reached when the voltage declines sharply. The discharge step is stopped at 3 V. At this potential, the SOC is defined to be 0% and the depth of discharge (DoD) is 100%.

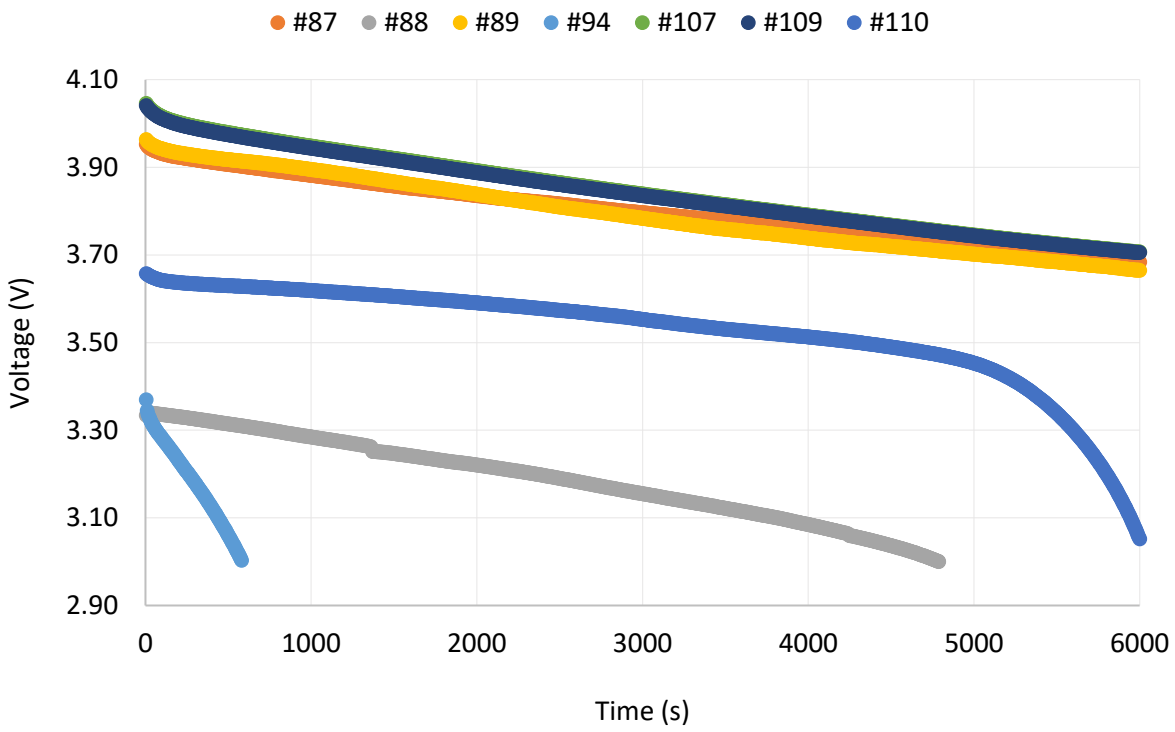

Figure 11: Discharge profile of selected cells from Gamry potentiostat.

Figure 12 shows a Nyquist diagram for various cells characterised under Potentiostatic EIS (Electrochemical Impedance Spectroscopy). Generally, the impedance of the cell increases at higher potentials. For a better understanding, an EIS circuit model is provided in Figure 13.

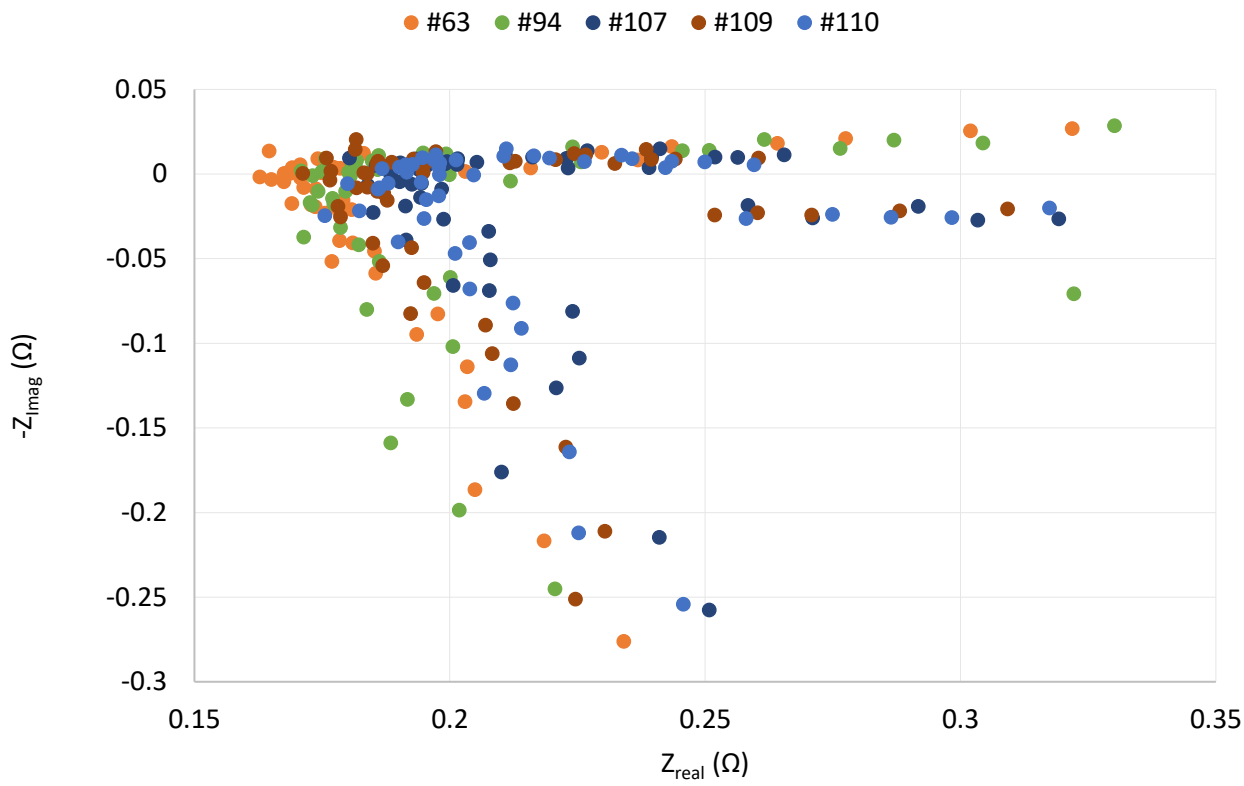

Figure 12: Nyquist plot from characterisation of 18650 cells by EIS.

The change in internal resistance with potential is studied by EIS measurements during charging. This resistance was determined by using the Gamry Model Editor to fit the EIS graphs to the equivalent model below.

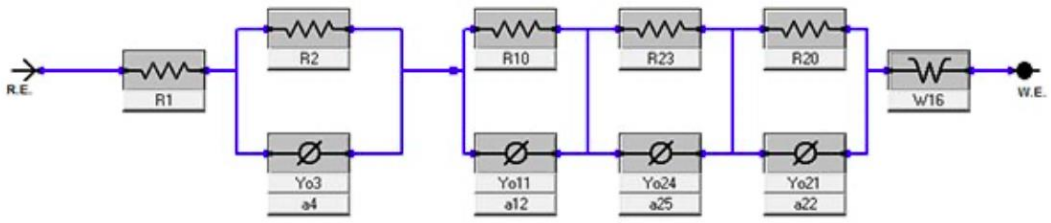

Figure 13: Equivalent circuit generated by Gamry best fit model.

2.4 Conclusions

Characterisation of spent 18650 cells from consumer devices showed that 60% of the sampled cells remained operational and held a SoC above 80%. The results from this

investigation confirm the plausibility for use in secondary storage applications, such as the solar application outlined in Chapter 3.

3 Lithium-ion Battery Second Use: A Solar Solution

A 7 series 15 parallel (7s15p) battery pack was designed using 105 Panasonic second-use 18650 cells, capable of 25 V and 150 A output generating 1.2 kWh of storage. The pack utilises a 150 A separate port battery management system (BMS) with heat sink to control the system. The pack is constrained by the power input of a 170 W monocrystalline photovoltaic (PV) unit and the output of a 400 W modified sinewave inverter. The system is capable of being upgraded to a 320 W PV unit and a larger inverter for higher output loads in the future.

3.1 Introduction

Lithium-ion batteries have second-use applications within the stationary storage sector. Electrical vehicle performance standards, typically include 80% of total usable capacity and a self-discharge rate of only about 5% over a 24-hour period (Heymans et al., 2014). Therefore, lithium-ion batteries from electrical vehicles still remain usable for stationary storage applications where power density is not a significant constraint. Therefore, the following design utilises second-use 18650 cells, which are typically found in electric vehicles and consumer devices.

The battery pack was sized according to solar and inverter availability and economic constraints as described in sections 2.3 and 2.5 respectively. It was found that 105 Panasonic NCR18650bd cells in a 7s15p configuration as shown in Figure 14 could meet these constraints, providing 25.2 V at a capacity of 47.7 Ah with a total current of 150 A; with subsequent components sized accordingly. The design calculations are given in Appendix E1 and E2. Cell cases were used opposed to cell holders to ease the replacement of spent cells. The potential for a cell monitoring system is included in Future Directions.

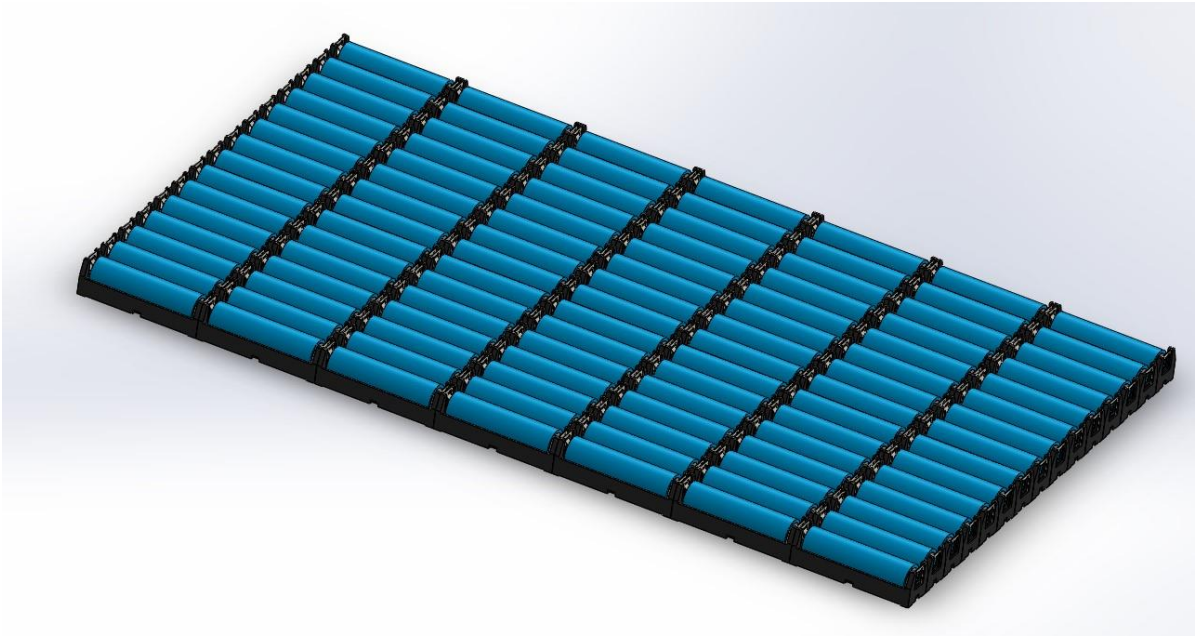

Figure 14: Battery pack design in 7s15p configuration as per constraints, designed on SolidWorks.

3.2 Background

3.2.1 Voltage in Series

In a series connection, the positive terminal of one cell is connected to the negative terminal of the next battery. Where the total voltage of the system is multiplied by the number of cells in series. In a parallel connection it is imperative the individual cell voltages are almost identical to prevent self-equalisation.

3.2.2 Capacity in Parallel

Parallel connections are made by connecting the same terminals together. For example, the positive terminal of one cell to the positive terminal of a second cell, and likewise for the negative terminal of each cell. Whereby the total capacity of the system is multiplied by the number of cells in parallel.

3.3 Experimental Method

3.3.1 Components

3.3.1.1 Lithium-ion Cells

Panasonic NCR18650bd cells were used for the build. Chemically, these cells are NCA, which use a lithium-nickel-cobalt-aluminium oxide for the cathode and graphite for the anode. These cells were sourced from a local supplier and extracted from faulty consumer goods, with the performance characteristics given in Table 18. The voltages of each cell were measured before use and were required to be within 0.1 V to prevent equalisation of the cells in parallel. These cells were purchased for $3.16 per cell and equate to $331.58 for the 105 cells used in the build. In praxis, these cells could be salvaged from spent battery packs from EVs.

Table 18: NCR18650bd cell capacity, voltage and charging characteristics

	
Capacity	3000 mAh
Nominal Voltage	3.6 V (2.5 V – 4.2 V)
Standard Charging	900 mA
Discharging	610 mA (10000 mA max)

3.3.1.2 Battery Management System

A separate port BMS was chosen for simultaneous charge and discharge capability. The BMS chosen is rated for 150 A and 24 V, which aligns with the battery pack design. A lower rated BMS, down to 60 A was considered as the current rating for the inverter load was only 25 A and significantly reduced the cost of the build. However, for future consideration of inverter upgrade and to optimise the capacity of the battery pack a 150 A unit was chosen. The wiring diagram from the manufacturer is given in Figure 15 below. The unit was $135.73.

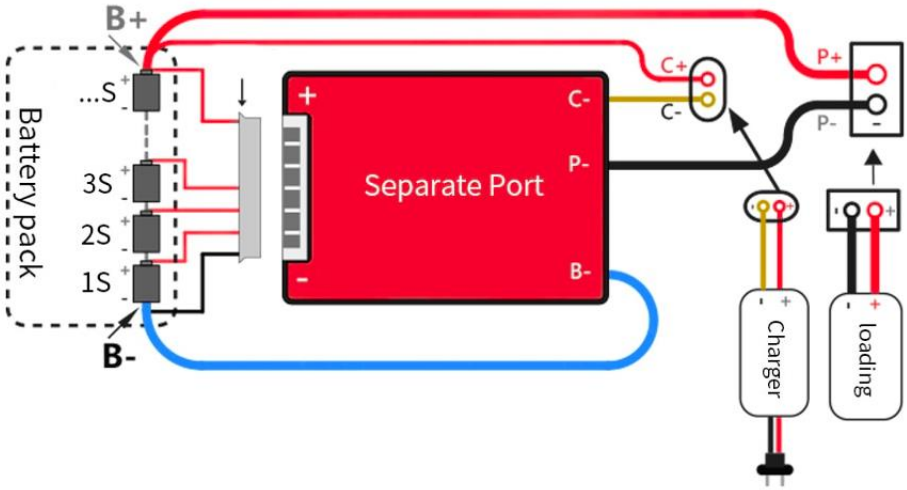

Figure 15: Wiring diagram for separate port 150 A, 24 V BMS as provided by supplier.

3.3.1.3 Solar Panel

The power of the solar panel is proportional to the time taken to charge the battery pack. A higher rated PV system could charge the pack in less time but would be more expensive. For this reason, a monocrystalline, 170 W, 12 V unit was chosen and is shown in Figure 16 below. Under optimal conditions the panel could charge the battery pack over the course of the day (7.5 hours) and would require a controller capable of 6.3 A. This panel is comprised of 36 pieces of 156x156mm A-grade solar cells with 900 mm leads. The panel can be combined with subsequent panels in the future to increase its power output and decrease the charge time of the battery pack. The unit will cost $239.99.

Figure 16: Photovoltaic unit rated at 170 W and 12 V.

3.3.1.4 Solar Controller

The solar controller was sized at 6.3 A given by the PV power over battery pack voltage ($160\ W/25.2\ V$). The controller chosen is capable of 10 A and so another panel can be added to the system in the future. The MPPT controller is shown in Figure 17, which is capable of boost power supply and able to perform under variable input-output conditions such as 12 V on the solar side to the 24 V to the battery pack. The unit will cost $50.26.

Figure 17: Variable input-output MPPT solar controller rated to 10 A with boost.

3.3.1.5 Inverter

A 500 W modified sinewave inverter was chosen, capable of 24 V DC from the battery pack to 240 V AC to the load with 1500 W surge capability. The inverter is shown in Figure 18. The unit will cost $99.90.

Figure 18: Modified sinewave inverter, 500 W, 24 V DC to 240 V AC.

3.3.1.6 Cell Case

Cell cases were chosen over holders to ease the replacement of spent cells. Single cell cases were chosen over grouped cell cases due to their manipulability. Furthermore, grouped cell

cases offered an insignificant saving when compared to single cases. The cases were $0.13 per cell case for a total cost of $13.65 for 105 cell cases. The individual cases are pictured below in Figure 19.

Figure 19: Single cell cases, which will be joined in a 7s 15p configuration to house the cells.

3.4 Results and Discussion

Initially the BMS, inverter, controller and XT90 connector were connected and mounted on a rigid alloy frame, as in Figure 20 below.

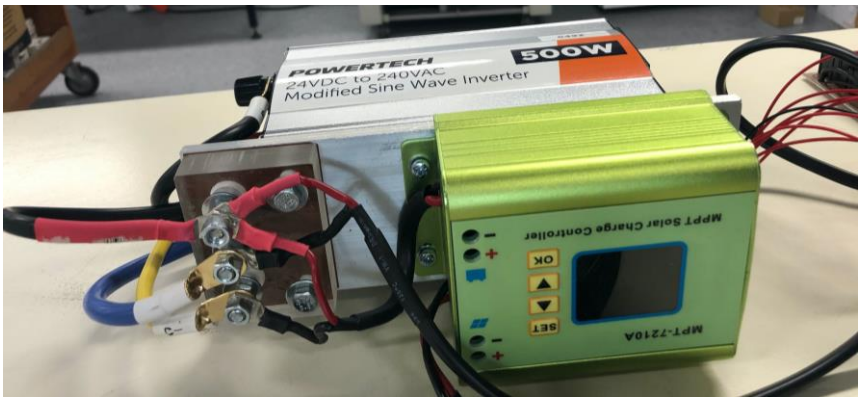

Figure 20: BMS (underneath), solar controller (front), inverter (back) and connector mounted on a rigid alloy frame.

The BMS was mounted opposite the inverter, with a profile view shown in Figure 21 and a view of the underneath in Figure 22.

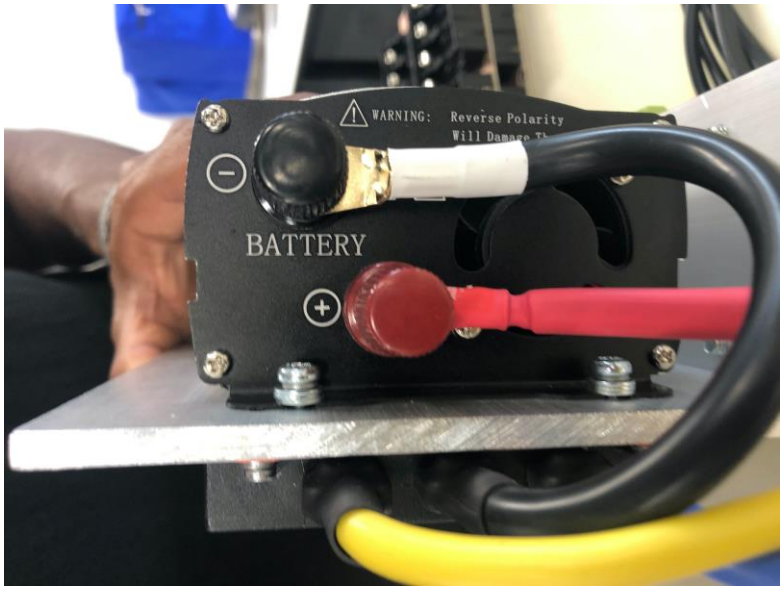

Figure 21: Profile view of BMS (bottom) and inverter (top).

Figure 22: Underneath of housing unit, highlighting BMS.

The mounting for the parallel cells were achieved through an acrylic PCB backing with a copper current collector coating. A single 7s1p test pack was initially used to test the system which proved the system was operating, as shown in Figure 23 below.

Figure 23: Battery pack connected to 7s1p test unit.

Following the successful testing of the single parallel unit, 15 individual cell holders were attached in series as in Figure 24 below.

Figure 24: Individual 1s15p cell holder unit.

The intial 1s15p board was replicated several times and stacked ontop of each other as in Figure 25. Each board is held together with a threaded rod and spacers. Testing showed correct voltages when populated with cells and proves the operability of the pack. The holders are arranged such that each board is positive on the top plane and negative on the

bottom plane, with cells inserted with their positive ends to the outside and negative ends to the middle of each board to avoid blowing the 10 A fuses.

Figure 25: Final battery pack housing in 7s15p arrangement.

The final product is shown in Figure 26, which shows the connector to the BMS, inverter, controller and the 7s15p battery pack housing.

Figure 26: Completed 7s15p battery pack with BMS, inverter and solar controller.

3.5 Future Directions

There is further development opportunities for the as-built battery pack, which was limited by the time constraints of the project. These include a monitoring system of the 7s15p build, such that individual cell characteristics can be mapped over time to validate the performance of second-use LiB cells in stationary storage applications. Additional monitoring systems could be used to identify cells that require replacement and allow the battery pack to function continuously by replacing individual cells throughout the lifetime of the battery pack.

3.6 Conclusions

The 7s15p battery pack is capable of 25 V and 150 A output with 1.2 kWh of storage. The proof-of-concept build shows the plausibility of second-life options for LiBs, particularly from EVs into stationary storage applications. The battery pack is currently being commissioned at GNS in Wellington.

4 Lithium-ion Battery Metal Recovery: A Sustainable Approach

4.1 Introduction

The hydrometallurgy process can recover metals from spent LiBs. It provides high metal recovery efficiencies, with less energy consumption when compared to pyrometallurgy (Aaltonen et al., 2017). Prior to hydrometallurgical treatment spent LiBs undergo discharge, mechanical, and separation pre-treatment steps. Subsequently, there are two types of leaching processes, acid leaching and alkaline leaching which use a range of reagents as discussed in section 1.4. Metals are then reclaimed by several chemical approaches, including solvent extraction, solvent precipitation, and electrolytic deposition. The leaching results can then be processed using kinetic models to predict the leaching rate of the metals extracted.

4.1.1 Health and Safety

The processing of spent LiBs have potential health and safety implications, which were considered prior to conducting this investigation. The safety hazards of LiB constituents were considered, taking the recommended precautions as outlined in the MSDS sheets.

The dissection step of recovering metals from LiB cells posed the greatest risk, as there was a risk of thermal runaway through residual metallic lithium reacting exothermically with the moisture in the atmosphere. Similarly, gas released by LiBs include vaporised electrolyte consisting of hydrogen fluoride from 20 – 200 mg/Wh, and phosphoryl fluoride from 15 – 22 mg/W, which is toxic (Marshall et al., 2020). Therefore, all experiments were conducted in a fume-hood and with appropriate PPE.

4.2 Background

4.2.1 Leaching Kinetics

The shrinking core model, describes systems in which solid particles are being consumed through dissolution or reaction (Sethurajan et al., 2019). The shrinking core model is well

established and was used to describe the leaching kinetics during the metal recovery of LiBs. The kinetic model for the shrinking core model shown in Figure 27 consists of the following steps: mass transfer of the liquid layer, chemical reactions at the surface, and diffusion processes of the residue layer.

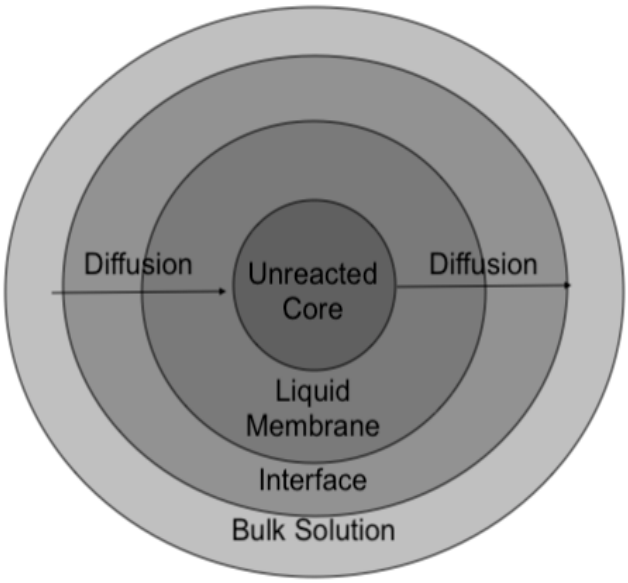

Figure 27: Shrinking–core model for the leaching of metal ions.

To determine the leaching parameters in the kinetic models used, kinetic analyses were carried out during the metal recovery of LiBs. Wherein, the leaching process is divided into several steps (Gao et al., 2018). The leaching process of metal material from the cathode of spent LiBs, was considered a solid-liquid-gas heterogeneous process, which can be modelled kinetically by (6).

$$\frac{x}{3k_m} + \frac{R_0}{6D_e}\left[1 - 3(1-x)^{\frac{2}{3}} + 2(1-x)\right] + \frac{1}{k_r}\left[1 - (1-x)^{\frac{1}{3}}\right] = \frac{MC_0}{y\rho R_0}t \qquad (6)$$

Where k_m is the liquid boundary layer mass transfer coefficient, x is the leaching rate, R_0 is the radius of the particle, D_e is the residue layer mass transfer coefficient, k_r is the reaction rate constant, M is the molar weight of the cathode metal-oxide, t is the reaction time, C_0 is the acid concentration at $t = 0$, ρ is the density of the cathode material and y is the electron transfer number in the leaching reaction.

Under constant conditions the rate constant can be determined by the Arrhenius equation (7).

$$k = Ae^{\frac{-E_a}{RT}} \tag{7}$$

Where R is the universal gas constant in $J/molK$, A is the pre-exponential factor in $1/\text{min}$, E_a is the activation energy in J/mol and T is absolute temperature in K. However, as A is variable under different leaching conditions, the kinetic equation for the leaching of metal-oxides from the cathode of spent LiBs can be modelled by (8).

$$k = k_0 C_{acid}^{M} \left(\frac{S}{L}\right)^{N} e^{\frac{-E_a}{RT}} \tag{8}$$

where k_0 is the pre-exponential factor, C_{acid} is the acid concentration in mol/L, M is the acid concentration index constant, S/L is the S/L ratio g/L, and N is the S/L ratio index constant. This can be simplified to (9), such that M, N, E_a and k_0 can be calculated under the specific experimental conditions.

$$lnk = lnk_0 + MlnC_{acid} + N\left(\frac{S}{L}\right) - \frac{E_a}{RT} \tag{9}$$

The leaching rate can be assumed to be controlled by the following kinetic models: mass transfer of the liquid layer (10), chemical reaction at the surface (11), or diffusion of the residue layer (12). Where k_1, k_2 and k_3 are the slopes of the fitted lines, t is the reaction time in minutes.

$$x = k_1 t \tag{10}$$

$$1 - (1 - x)^{\frac{1}{3}} = k_2 t \tag{11}$$

$$1 - 3(1 - x)^{\frac{2}{3}} + 2(1 - x) = k_3 t \tag{12}$$

4.2.2 Analytical Techniques

4.2.2.1 MP-AES

The concentration of metal constituents in solution were measured by MP-AES (Microwave Plasma Atomic Emission Spectroscopy). MP-AES is an atomic emission technique that uses the characteristic wavelengths of excited atoms. The cobalt, nickel and manganese calibration lines were selected at 340.512 nm, 361.939 nm, and 403.076 nm respectively with 5% calibration error and 3 subsequent replicates. The calibration data for the leaching results can be found in Appendix B1- B18. Figure 28 shows the MP-AES used throughout this investigation.

Figure 28: Agilent Technologies 4120 MP-AES used to characterise leached cathode samples.

4.3 Experimental Methods

4.3.1 Materials and Reagents

LiBs were sourced from a range of suppliers and different devices, which were then dismantled with the cells removed. All chemical reagents were of analytical grade and prepared with Milli-Q water when applicable.

4.3.2 Pre-treatment

4.3.2.1 Discharge

LiBs discharged in brine solution under ventilation, leave organic constituents in solution, as outlined by Xiao et al. (Xiao et al., 2020). Brine discharge has the potential to corrode the electrodes before full discharge is achieved. The reaction follows the water splitting half reactions at the anode and cathode respectively:

$$2H_2O \rightarrow O_2 + 4e^- + 4H^+ \;\; E_0 = 1.23\,V$$

$$2H^+ + 2e^- \rightarrow H_2 \;\; E_0 = 0.00\,V.$$

Additionally, a reaction leading to the formation of chlorine gas at the anode can also occur (Ojanen et al., 2018).

$$2Cl^- \rightarrow Cl_2 + 2e^- \;\; E_0 = 1.36\,V$$

This step can be omitted if cells are sufficiently discharged at less than 2 V, which reduces the loss of metal particulates in solution and prevents the corrosion of terminals. Therefore, the 18650 cells were discharged to avoid short-circuiting and self-ignition, using a Gamry 3000 potentiostat in a custom housing.

4.3.2.2 Dissection

The cells were then dissected manually by peeling away the aluminium casing using plyers after a shallow incision with a craft knife. Thereby, the cell components could be unravelled while remaining intact.

4.3.2.3 Electrode Separation

Usually, the anode is copper lined with graphite, and the cathode aluminium plated with the metal-oxide. The anode was separated through simple washing, which removed graphite from copper.

Figure 29: Dissection of 18650 cells, with graphite lined, copper current collector visible.

The active cathode material was separated from the aluminium foil after immersion in 2 M alkaline sodium hydroxide solution and sonicated at 35 kHz for approximately 1 hour following the reaction below (L.-P. He et al., 2017; L. Li et al., 2017).

$$2Al + 2NaOH + 2H_2O \rightarrow 2NaAlO_2 + 3H_2$$

As leaching is an interfacial reaction, the boundaries of the two phases can influence the reaction rate significantly. Therefore, the materials were milled to a small particle size and subsequently filtered, and dried.

Figure 30: Cathode powder sieved from aluminium current collector post milling.

4.3.3 Leaching Studies

The extraction and pre-treatment of cathode powder was done for a range of cell chemistries. The Leaching experiments were conducted using a 500 ml glass reactor fitted with a punctured condenser (to avoid the evaporation of leachate) and placed over a hot plate with magnetic stirring system under a fume hood as shown in Figure 31.

Figure 31: Reactor, hot plate and agitator used in the leaching experiments for LiB cathode powder.

For each leaching experiment, 50 g/L of cathode powder was added to the reactor with a predetermined concentration of acidic solution for different temperatures, time periods and acid concentrations. The system was maintained under normal operating conditions at 50 ˚C and 400 rpm (to minimise the effects of external diffusion). At specific time intervals, 1 ml of sample solution was withdrawn, diluted, filtered and analysed through MP-AES to determine the metal ion concentration in the solution after appropriate dilutions. The leaching experiments conducted are summarised in Table 19 below.

Table 19: Summary of leaching experiments conducted.

Cathode Type	Reagent	Concentration (mol/L)
LCO	HCl	1.3
NMC	HCl	1.3

NMC	H2SO4	1, 2, 3, 4, 5
NMC	H2SO4 + H2O2	2+1.3

4.4 Results and Discussion

4.4.1 Leaching Results

The practical implications of the leaching results are profound. Insomuch as the majority of LiBs reaching end-of-life are currently LCO based cell chemistries. However there has been an influx in NMC LiBs attributed to the increase in EVs, motivated by an avoidance for reliance on cobalt. Therefore, an experimental method was devised to recover polluting and valuable metals from both LCO and NMC cell chemistry. The major findings from the leaching of cathode scrap are summarised in Figures 32 – 34. The leaching method outlined above was successful in leaching up to 95% of metal constituents from LiB cathode powder. Notably lithium was excluded from the investigation due to a relatively low metallic content in the cathode powder as well as a low economic benefit.

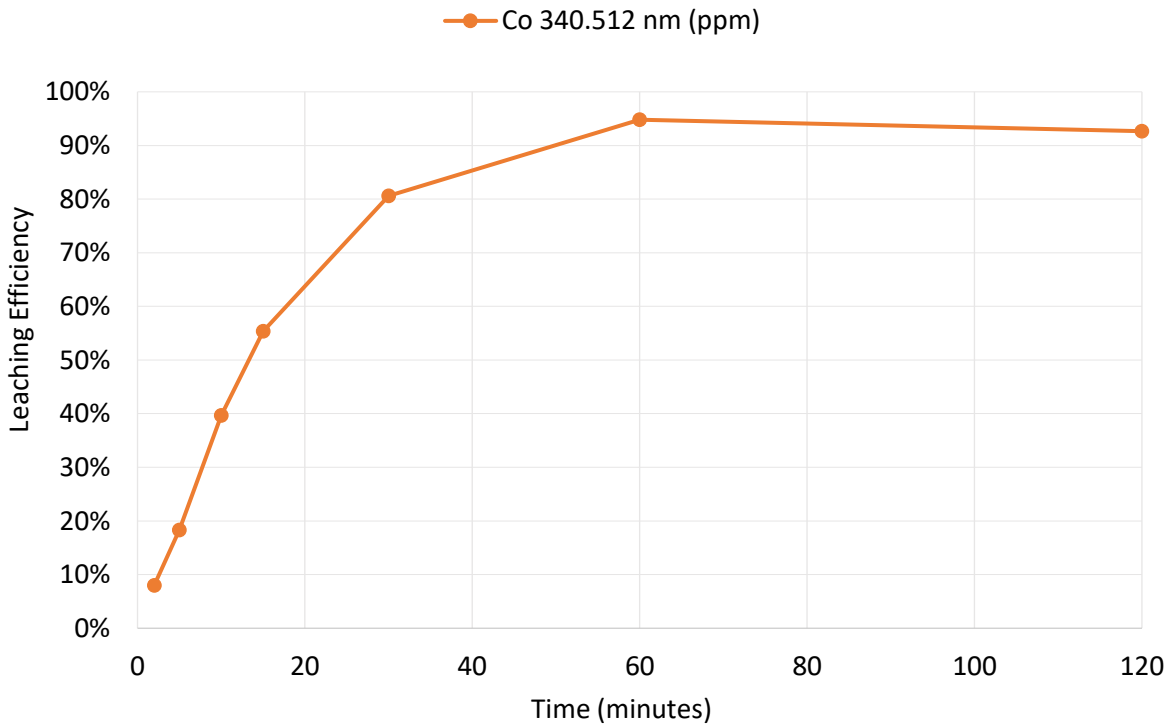

Figure 32: Leaching efficiency determined from MP-AES characterisation for LCO cathode powder in 1.3 M HCl.

Initially, a low HCl concentration was trialled to test the leaching procedure. However, once it was shown that under the experimental conditions the leaching of cathode scrap was plausible, H_2SO_4 was trialled with H_2O_2 dosing to increase the leaching efficiency, as shown by Sattar et al. (Sattar et al., 2019).

LCO cathode scrap was pre-treated and characterised according to the method outlined above. The leaching conditions were determined from literature review and the leaching results are shown in Figure 32. Cobalt leaching efficiencies of 95% (9.4 g/L) were achieved after 60 minutes of leaching. The calibration data can be found in Appendix B4.

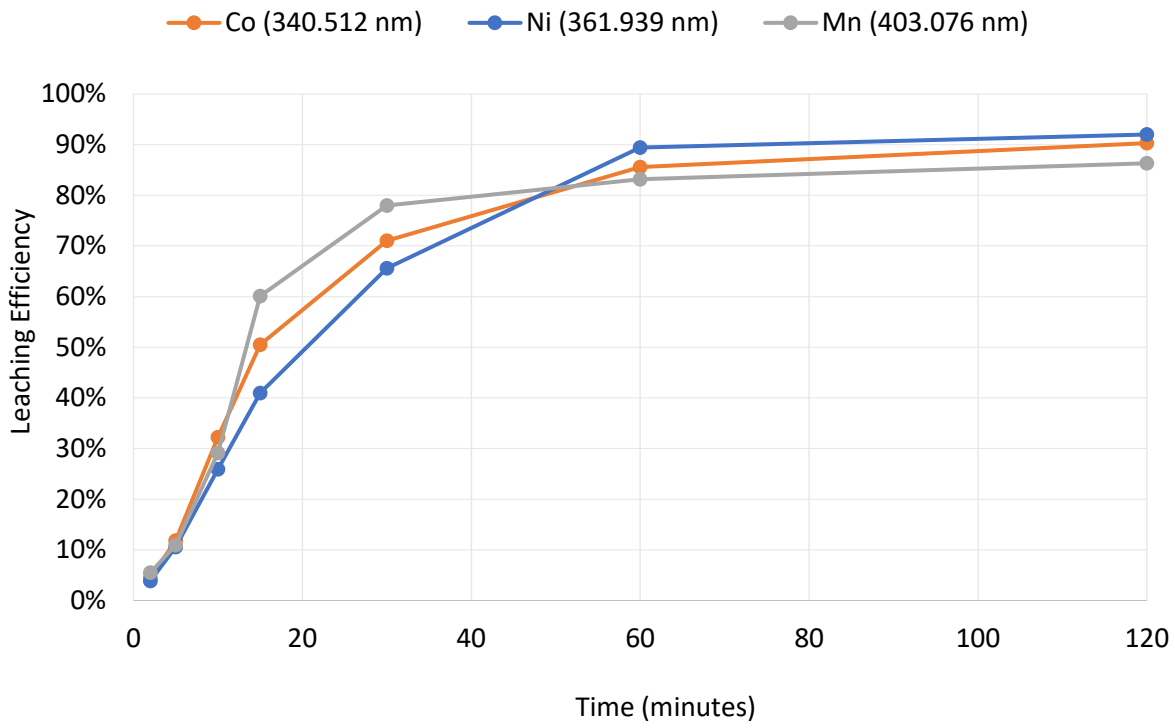

Figure 33: Leaching efficiency determined from MP-AES characterisation for NMC cathode powder in 1.3 M HCl

Following the leaching of cobalt from LCO cathode powder with 1.3 M HCl, alternate cell chemistries were trialled to validate the process under different initial concentrations and metallic species. The leaching results suggest that, the recovery of nickel and manganese measured under these experimental conditions follow a similar trend to that seen for LCO cell chemistries. The leaching of NMC cathode powder under 1.3 M HCl achieved leaching efficiencies for cobalt, nickel and manganese of 90% (9.3 g/L), 92% (8.9 g/L) and 86% (8.4

g/L) respectively. The results were below estimates found by Gao et al. (Gao et al., 2018). Therefore, further investigation utilising a combination of sulphuric acid and hydrogen peroxide were used to increase these leaching efficiencies.

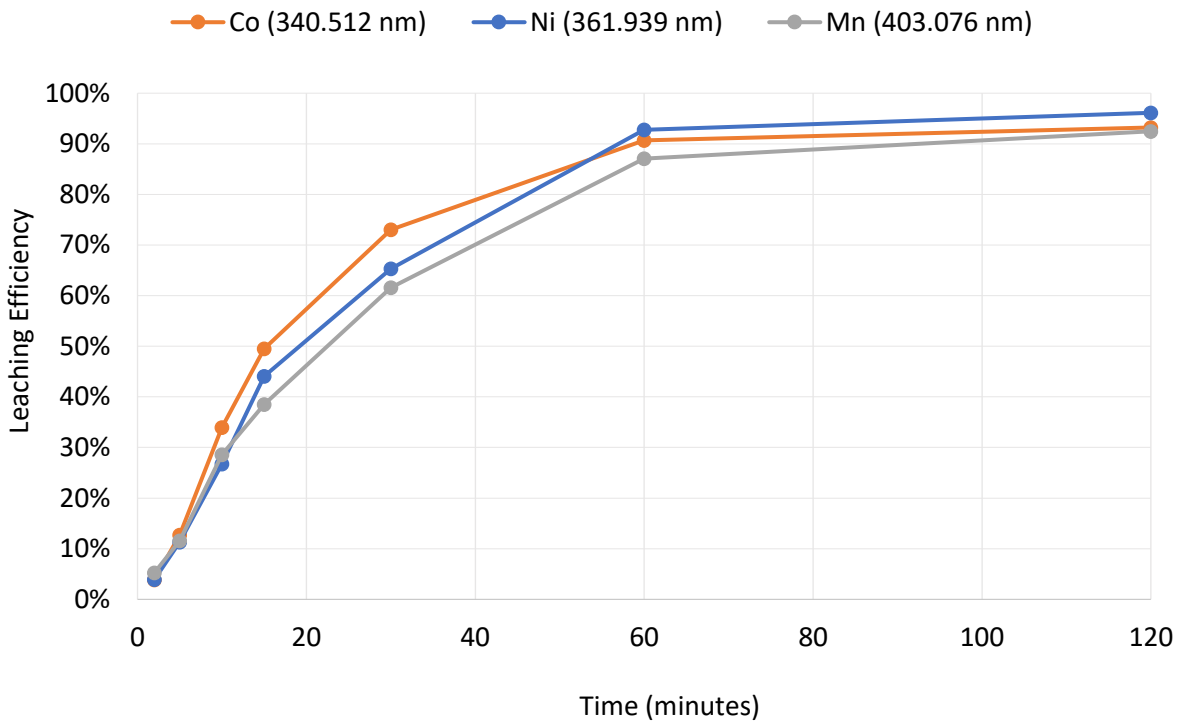

Figure 34: Leaching efficiency determined from MP-AES characterisation for NMC cathode powder in 2 M H_2SO_4, 1.3 M H_2O_2.

The method used to extract cobalt, nickel and manganese from cathode scrap utilising sulphuric acid with hydrogen peroxide dosing was modified from the methods outlined by Sattar et al., Gao et al., Li et al. and Contestabile et al. (Contestabile et al., 2001; Gao et al., 2018; L. Li et al., 2018; Sattar et al., 2019). Specifically, the experiments were performed under the following conditions: S/L ratio of 50 g/L at 50 ˚C and agitation of 400 RPM. A series of samples were taken, ranging from 0 to 120 minutes. As shown in Figure 34, the leaching rates of cobalt, nickel and manganese increased with time. Within the initial 45 minutes there was a rapid increase in leaching rate, which trended to stabilise after 60 minutes. The leaching rates for cobalt, nickel and manganese reached 93% (9.5 g/L), 96% (9.3 g/L), 92% (9 g/L) respectively. Nickel was more readily leached from solution than the other metals characterised. After 60 minutes there was no obvious increase in the leaching

rates across both LCO and NMC chemistries. Therefore, for kinetic investigation the leaching period was limited to 60 minutes.

4.4.2 Kinetic Results

An investigation of the leaching mechanisms for sulphuric acid (without hydrogen peroxide reductant) was done to establish kinetic parameters, which could be used to predict the leaching rates for cobalt, nickel and manganese. The conditions, which were optimised in the leaching investigation were maintained. The following kinetic model ignored the effects of mass transfer attributed to the relatively high reagent concentrations, temperature and agitation rate. Therefore, the solubility of the metal ions within the cathode powder lead to a rapid release into the bulk solution and can be assumed to be negligible. Instead, the kinetic model below considers the chemical reaction and diffusion contributions associated with the leaching process. The leaching efficiencies of NMC cathode scrap are summarised in Figures 35 – 37. In general, the leaching efficiencies increased with increasing sulphuric acid concentration.

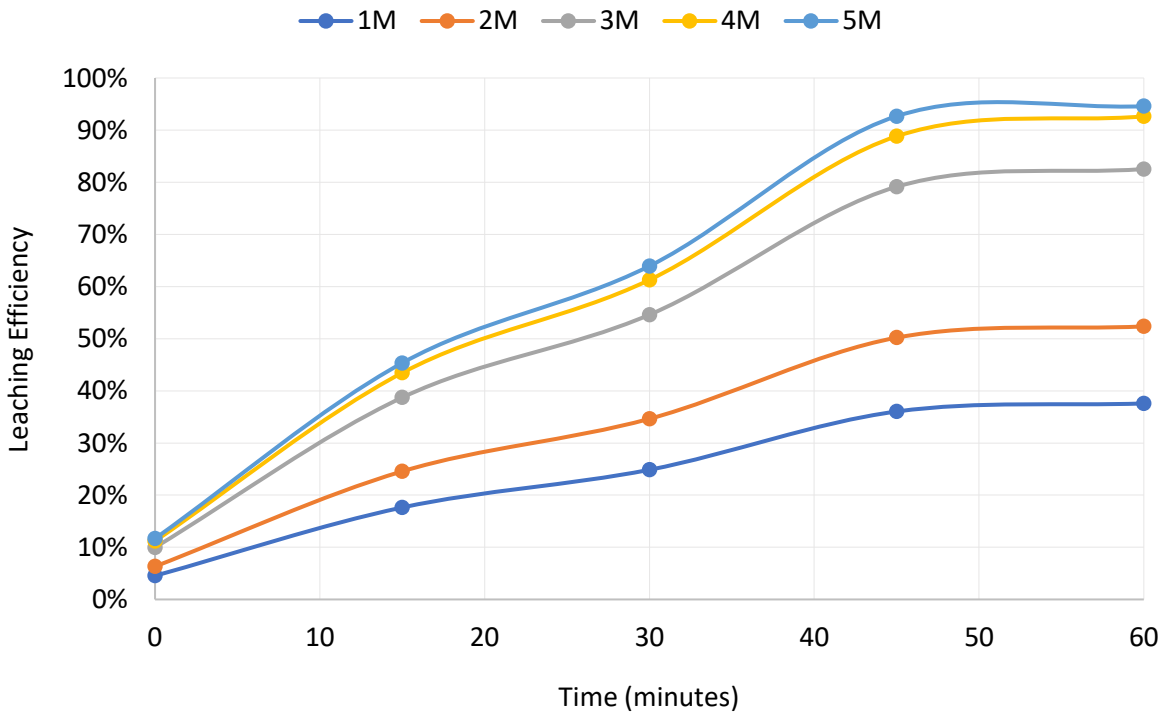

Figure 35: Cobalt leaching efficiencies for NMC LiBs at varying H_2SO_4 concentrations.

The leaching efficiencies for cobalt in varying sulphuric acid concentrations (1 M – 5 M) are shown in Figure 35. The highest leaching rates were achieved at 5 M, with little difference in leaching efficiencies down to 3 M. Significantly, the leaching efficiency at 2 M and below are poor and highlight the significance of utilising hydrogen peroxide as a reductant as per previous leaching investigations.

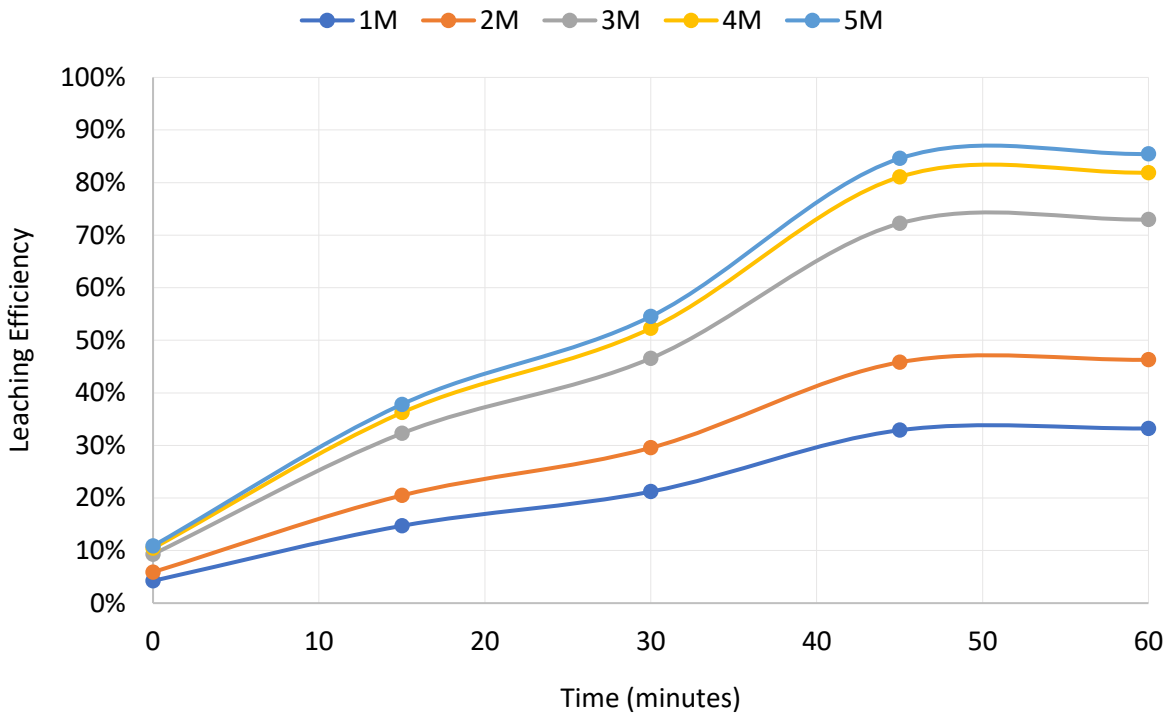

Figure 36: Nickel leaching efficiencies for NMC LiBs at varying H2SO4 concentrations.

The leaching efficiencies of nickel for varying sulphuric acid concentrations (1 M – 5 M) are show above in Figure 36, with similar trends to that of the cobalt leaching efficiencies. Both metals have characteristic periods of stasis punctuated with rapid leaching steps, which are justified in the kinetic models outlined below.

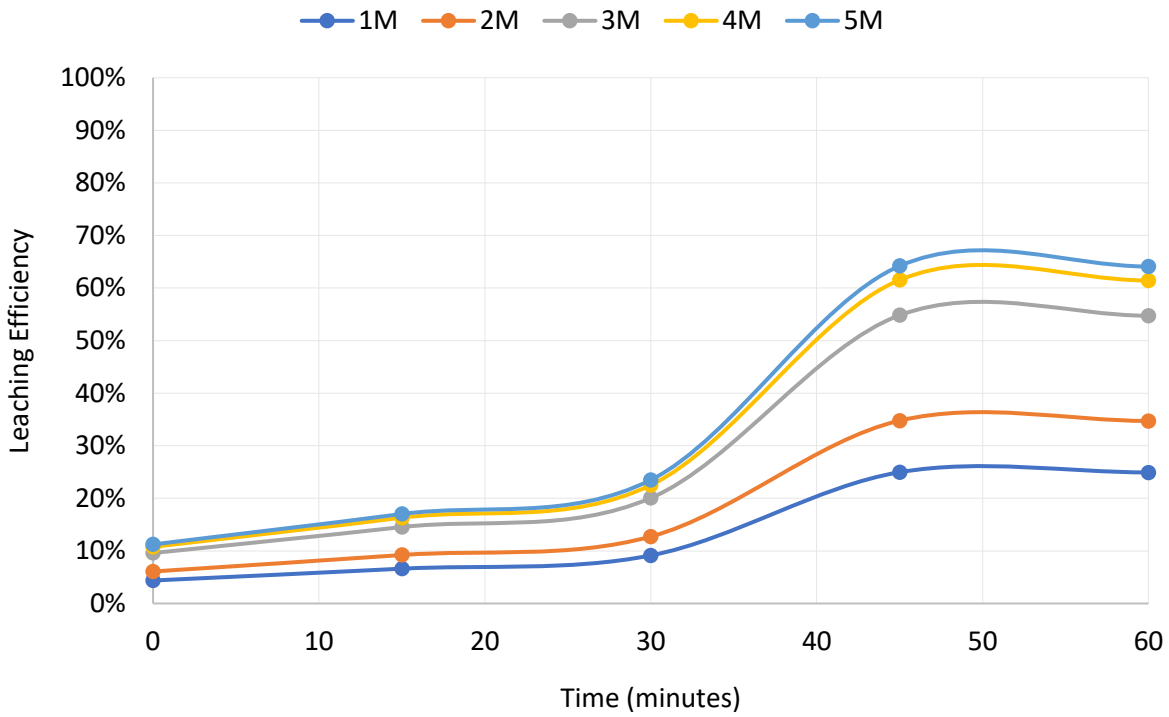

Figure 37: Manganese leaching efficiencies for NMC LiBs at varying H2SO4 concentrations.

The leaching of manganese at varying sulphuric acid concentrations (1 M – 5 M) is shown above in Figure 37. Manganese showed poor leaching characteristics attributed to a lower initial chemical reactivity and higher diffusive contributions as highlighted in the empirical rate equations derived in section 4.4.2 Kinetic Results.

4.4.2.1 Reaction Model Results

The kinetic results for the reaction model of cobalt, nickel and manganese are presented in Figures 38 – 30. The correlation coefficients for the kinetic curves are relatively high, greater than 0.95. This could be a result of the relatively low reactivity of sulphuric acid towards the metal oxide during leaching, resulting in moderate reaction kinetics, with the contribution of the surface reaction being significant over time.

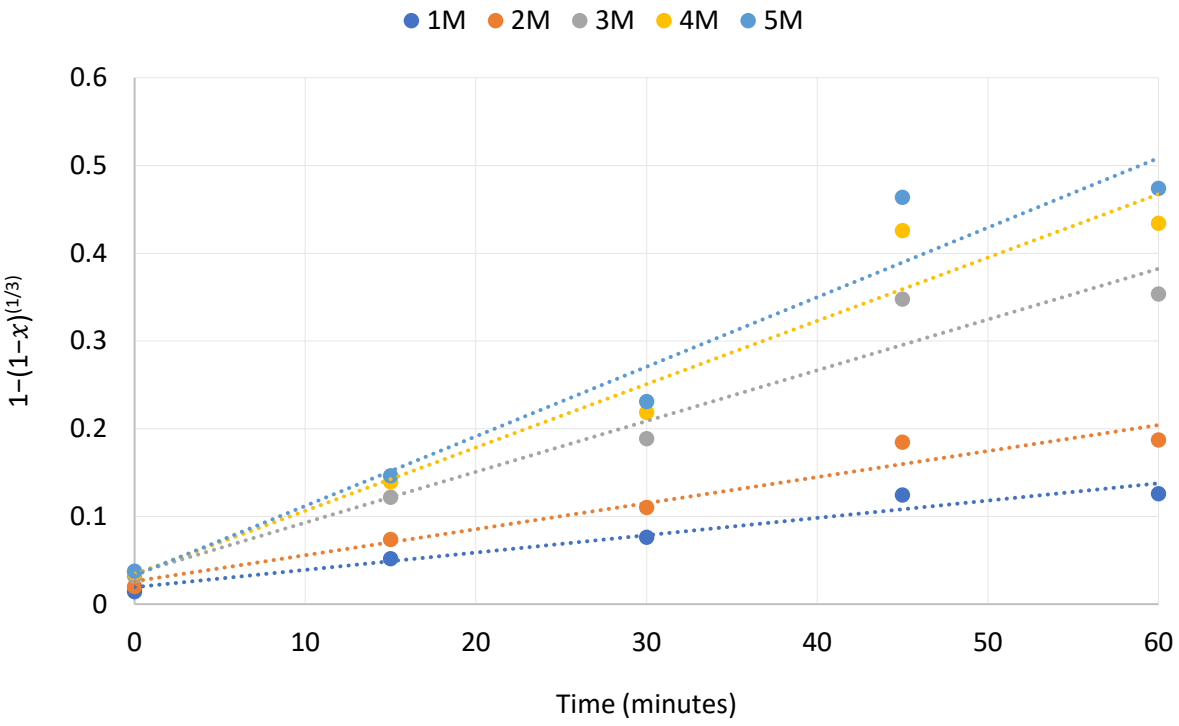

Figure 38: Reaction model plot for leaching fraction of cobalt for k_2 against time as per (7).

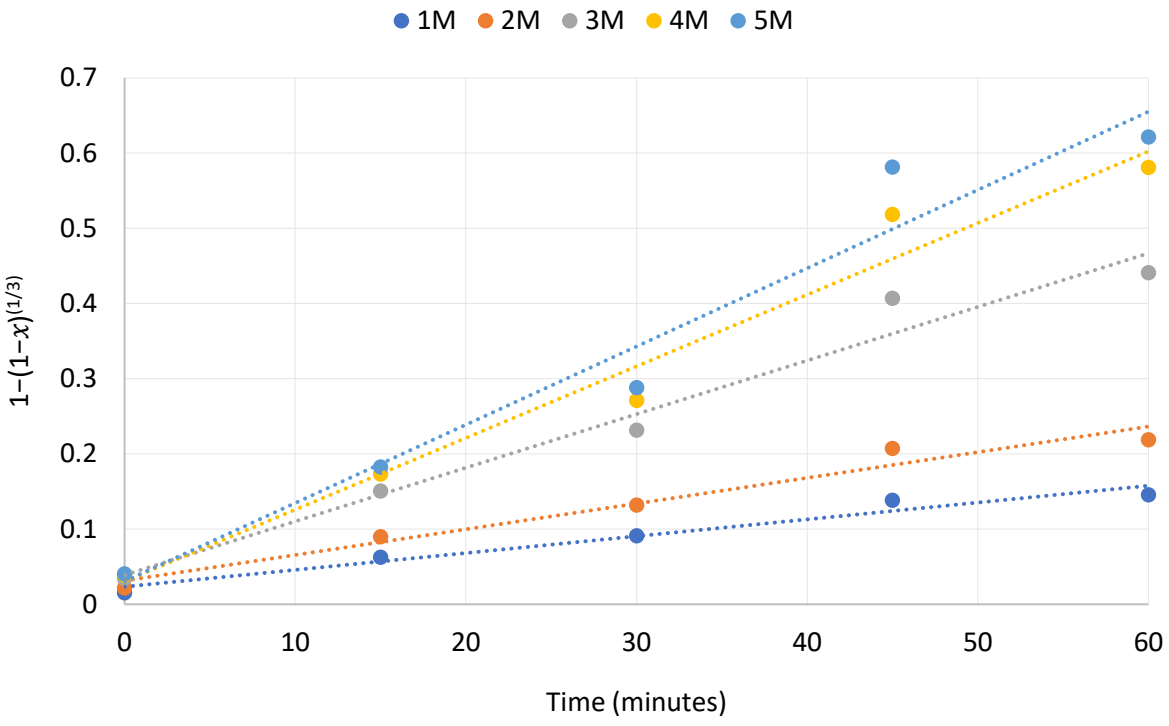

Figure 39: Reaction model plot for leaching fraction of nickel for k_2 against time (7).

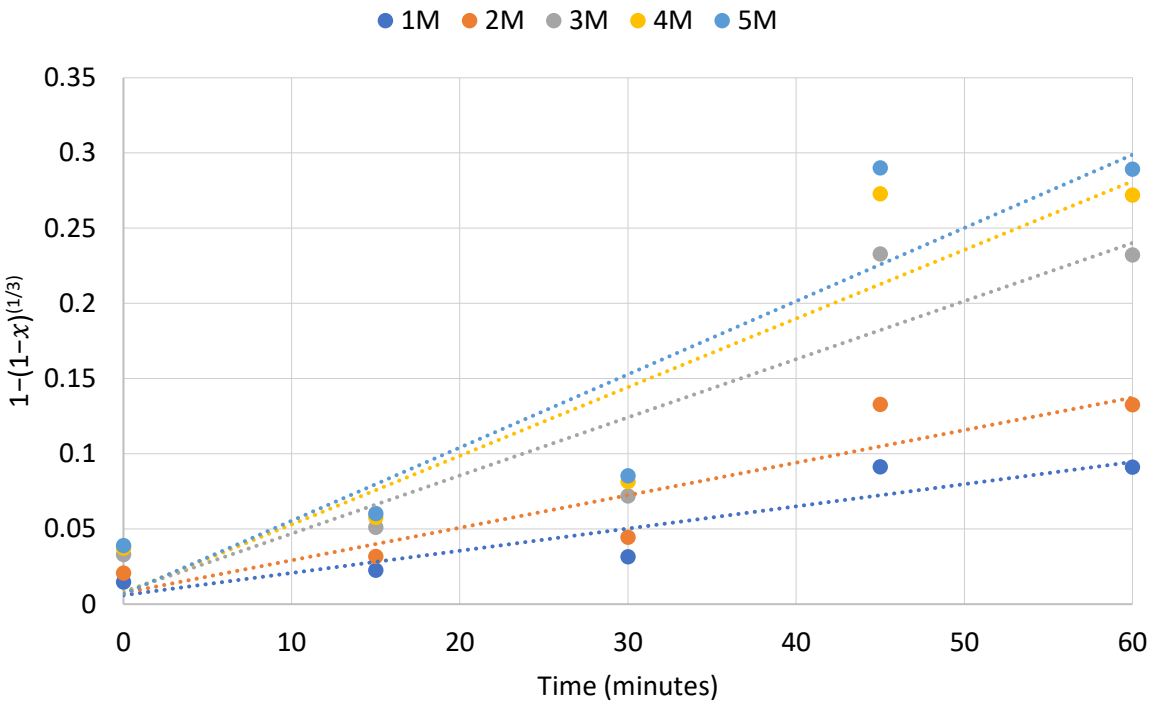

Figure 40: Reaction model plot for leaching fraction of manganese for k_2 against time (7).

The findings from the reaction model plots are summarised below in Table 20. Whereby the rate constant is given at different concentrations for the metal species. The rate constant is determined by the gradient of the figures above and the natural log of these values are presented adjacent. Therefore, a plot of $ln(k_x)$ against of $ln(C_{acid})$ as in Figure 41, gives the associated acid concentration index constant and the ratio index constant.

Table 20: Summary of kinetic model reaction variables for cobalt, nickel and manganese.

Conc. (M)	k_{Co}	$ln(k_{Co})$	k_{Ni}	$ln(k_{Ni})$	k_{Mn}	$ln(k_{Mn})$
1	0.002	-6.2	0.002	-6.1	0.002	-6.5
2	0.003	-5.8	0.003	-5.7	0.002	-6.1
3	0.006	-5.2	0.007	-5.0	0.004	-5.6
4	0.007	-4.9	0.01	-4.7	0.005	-5.4
5	0.008	-4.8	0.01	-4.6	0.005	-5.3

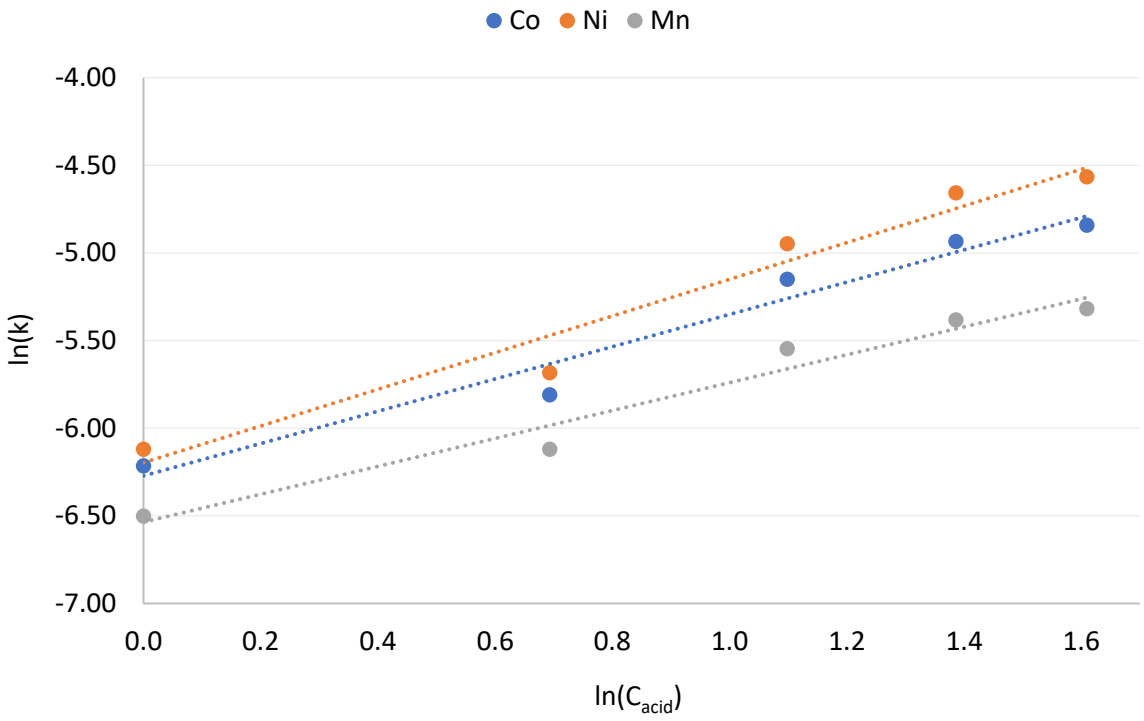

Figure 41: Natural log of rate constant and concentration for varying metallic species to determine index constants.

The associated acid concentration index constants (M) and the ratio index constant (N) for cobalt, nickel and manganese are shown in Table 21 below.

Table 21: Index constants for cobalt, nickel and manganese.

	Cobalt	Nickel	Manganese
M	0.9	1.1	0.8
N	-6.3	-6.2	-6.5

To determine the activation energy as per (10), the natural log of the rate constants for cobalt, nickel and manganese was plotted against the inverse of temperature steps. Thereby the gradient gives the activation energy for the metal species as per the Arrhenius equation (7). This is shown in Figure 42 and summarised in Table 22 below.

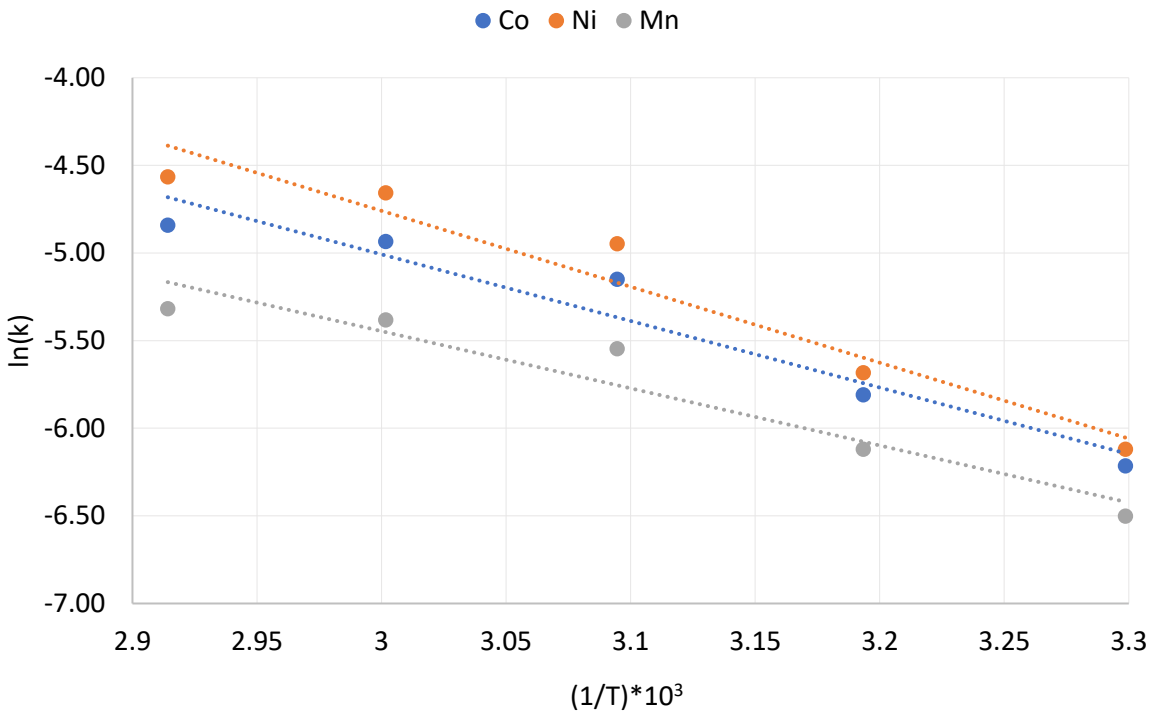

Figure 42: Natural log of rate constant against inverse temperatures to determine activation energy for metal species.

Table 22: Activation energy determined from gradient of $ln(k)$ against $1/T$.

	Cobalt	Nickel	Manganese
E_a (kJ/mol)	-32	-36	-27

4.4.2.1.1 Determination of Kinetic Equations

The following kinetic equations are based on the leaching rates under different sulphuric acid concentrations in the absence of the hydrogen peroxide reductant. The equations are derived from the plot of $1-(1-x)^{\frac{1}{3}} = k_2$ vs. t, which show high correlation coefficients of approximately 0.99. Therefore, according to (11), the plot of $\ln(k)$ vs $\ln(C_{acid})$, is a linear correlation with gradient M, if the S/L ratio, and reaction temperature are kept constant at 50 g/L and 50 ˚C respectively. The M values of the metal constituents are given in Table 21.

As shown in Table 23, the pre-exponential factor k_0 can be determined from the calculated values of that M, N, E_a at specific conditions.

Table 23: Summary of variables used to establish empirical model based on reaction kinetics.

Variable	Cobalt	Nickel	Manganese
C_{acid} (M)	3	3	3
M	0.9	1.0	0.8
S/L (g/L)	50	50	50
N	-6.3	-6.2	-6.5
E_a (kJ/mol)	-31	-36	-27
R (J/molK)	8.3	8.3	8.3
T (K)	323	323	323
k	0.006	0.007	0.004
k_0	$9.4 * 10^7$	$7.5 * 10^7$	$2.1 * 10^8$

This is based on the kinetic parameters under a range of sulphuric acid concentrations at a S/L ratio of 50 g/L, 323.15 K and for a leaching time of 60 minutes. Under the average k_0 values given in Table 23, the kinetic equations during leaching of cobalt, nickel, and manganese are determined under the empirical reaction model:

$$Co: 1 - 3(1-x)^{\frac{2}{3}} + 2(1-x) = 9.42 \times 10^7 C_{acid}^{0.921} \left(\frac{S}{L}\right)^{-6.272} e^{\frac{-3152}{RT}} t \quad (13)$$

$$Ni: 1 - 3(1-x)^{\frac{2}{3}} + 2(1-x) = 7.48 \times 10^7 C_{acid}^{1.046} \left(\frac{S}{L}\right)^{-6.197} e^{\frac{-3602}{RT}} t \quad (14)$$

$$Mn: 1 - 3(1-x)^{\frac{2}{3}} + 2(1-x) = 2.05 \times 10^8 C_{acid}^{0.796} \left(\frac{S}{L}\right)^{-6.536} e^{\frac{-2711}{RT}} t \quad (15)$$

4.4.2.2 Diffusion Model Results

The kinetic results for the diffusion model for cobalt, nickel and manganese are presented in Figure 43 – 45. The correlation coefficients for the kinetic curves are relatively high, greater than 0.95, suggesting a high fitting degree of this kinetic model.

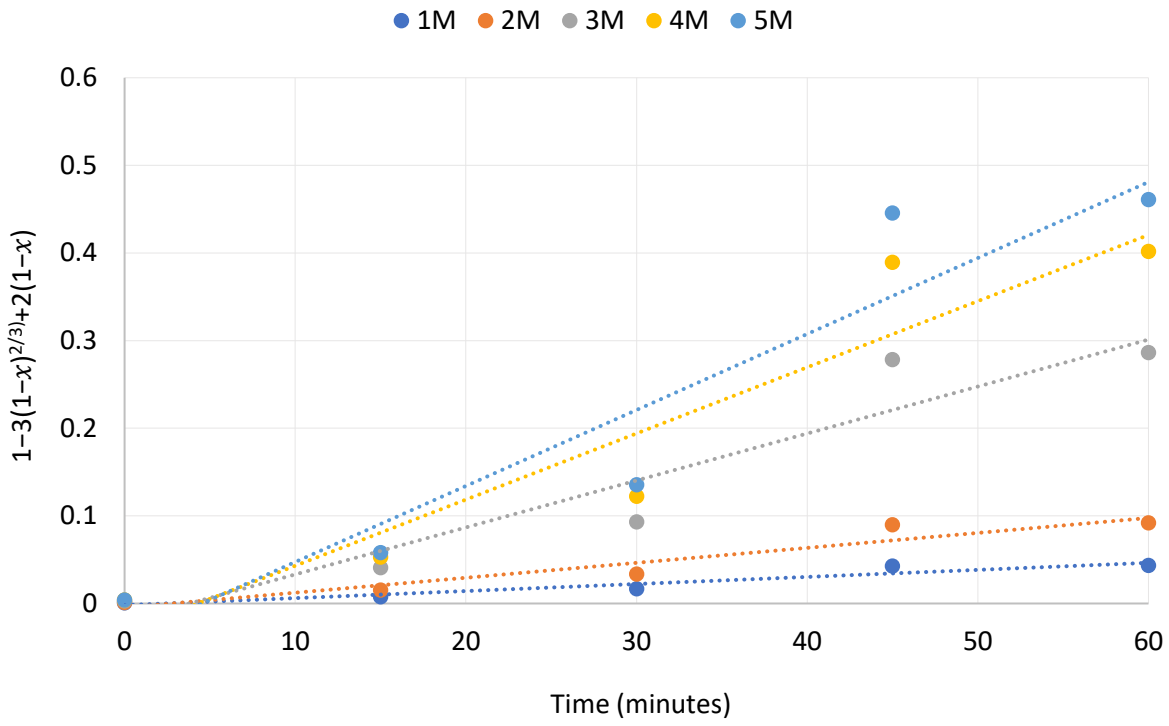

Figure 43: Diffusion model plot for leaching fraction of cobalt for k_3 against time as per (8).

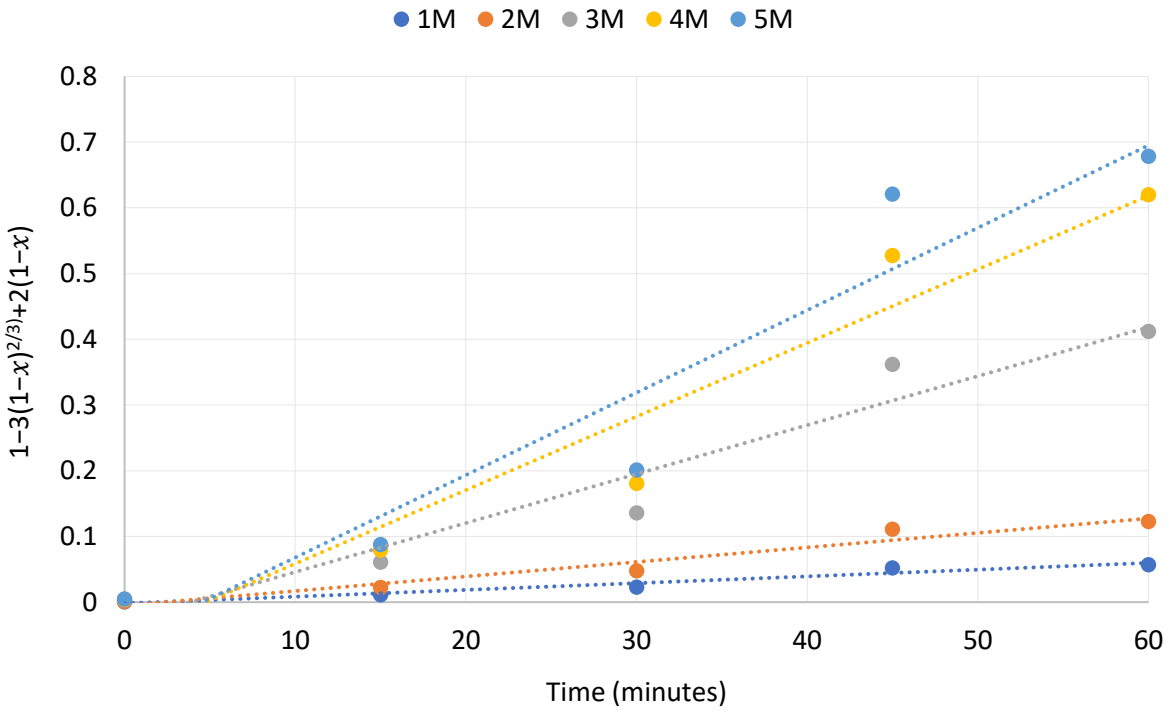

Figure 44: Diffusion model plot for leaching fraction of nickel for k_3 against time as per (8).

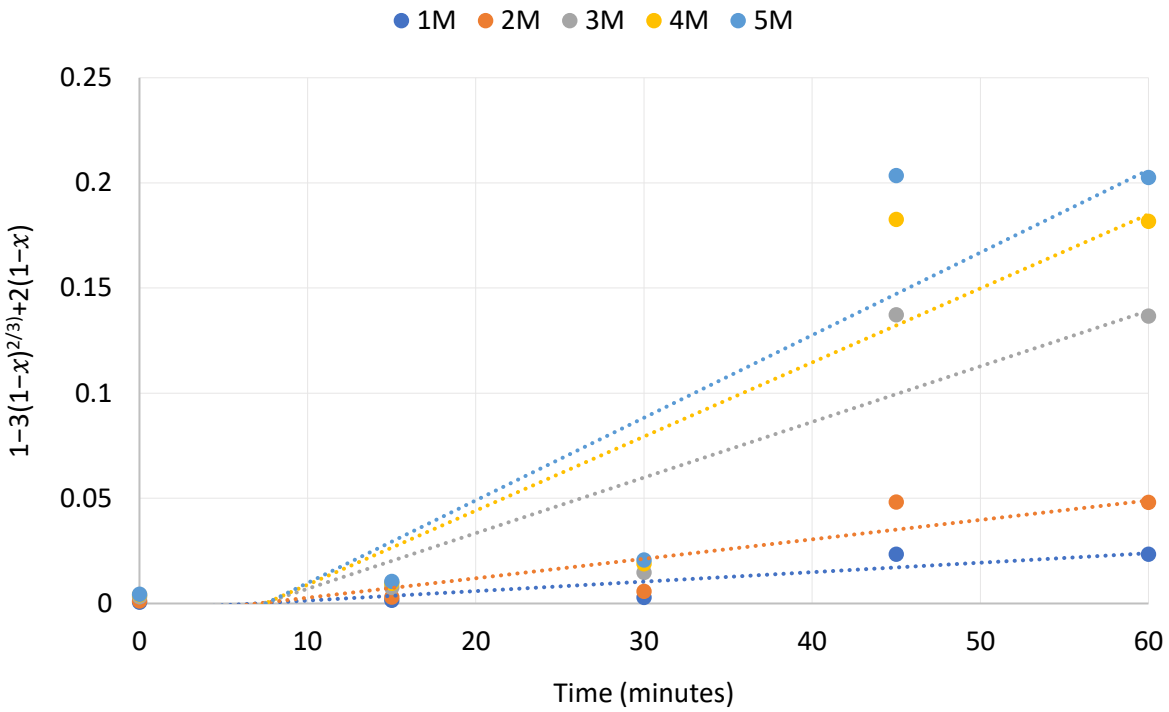

Figure 45: Diffusion model plot for leaching fraction of manganese for k_3 against time as per (8).

The findings from the diffusion model plots are summarised below in Table 24. Whereby the rate constant is given for the metallic species at the given concentrations. The rate constant is determined by the gradient of the figures above and the natural log of these values are presented adjacent. Therefore, a plot of $ln(k_x)$ against of $ln(C_{acid})$ as in Figure 46, gives the associated acid concentration index constant and the ratio index constant.

Table 24: Summary of kinetic model diffusion variables for cobalt, nickel and manganese.

Conc. (M)	k_{Co}	$ln(k_{Co})$	k_{Ni}	$ln(k_{Ni})$	k_{Mn}	$ln(k_{Mn})$
1	0.0008	-7.1	0.001	-6.9	0.0004	-7.8
2	0.002	-6.4	0.002	-6.1	0.0009	-7.0
3	0.005	-5.2	0.008	-4.9	0.003	-6.0
4	0.008	-4.9	0.01	-4.5	0.004	-5.7
5	0.009	-4.7	0.01	-4.4	0.004	-5.6

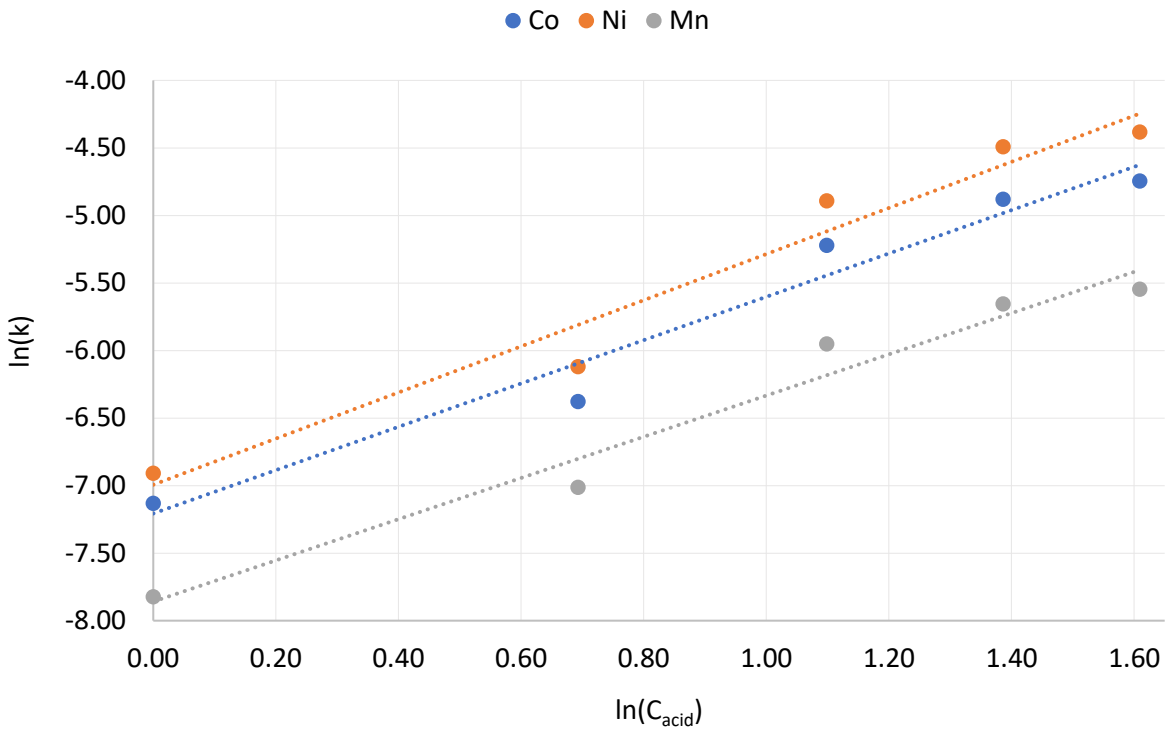

Figure 46: Natural log of rate constant and concentration for varying metallic species to determine index constants.

The associated acid concentration index constants (M) and the ratio index constant (N) for cobalt, nickel and manganese are shown in Table 25 below.

Table 25: Index constants for cobalt, nickel and manganese

	Cobalt	Nickel	Manganese
M	1.6	1.7	1.5
N	-7.2	-7.0	-7.9

To determine the activation energy as per (10), the natural log of the rate constants for cobalt, nickel and manganese was plotted against the inverse of temperature steps. Thereby the gradient gives the activation energy for the metal species as per the Arrhenius equation (7). This is shown in Figure 47 and summarised in Table 26 below.

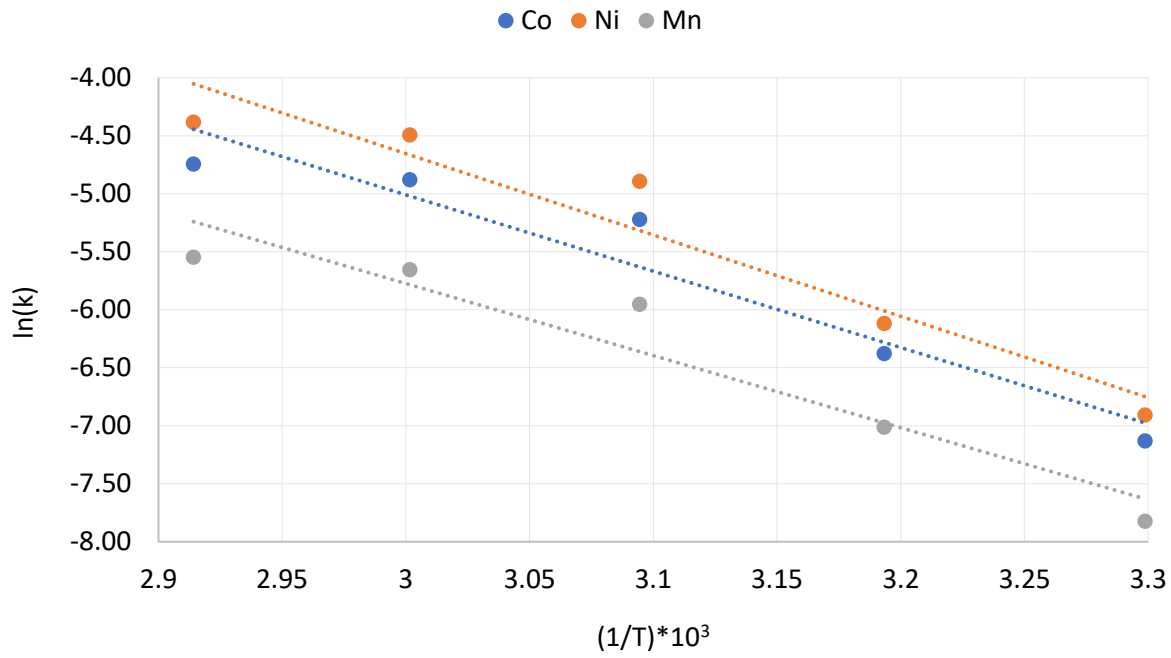

Figure 47: Natural log of rate constant against inverse temperatures to determine activation energy for metal species

Table 26: Activation energy determined from gradient of $ln(k)$ against $1/T$.

	Cobalt	Nickel	Manganese
E_a (kJ/mol)	-54	-58	-52

4.4.2.2.1 Determination of Kinetic Equations

The following kinetic equations are based on the leaching rates under different sulphuric acid concentrations in the absence of the hydrogen peroxide reductant. The equations are derived from the plot of $1-3(1-x)^{\frac{2}{3}}+2(1-x)$ vs. t, which show high correlation coefficients of approximately 0.99. Therefore, according to (12), the plot of $\ln(k)$ vs $\ln(C_{acid})$, is a linear correlation with gradient M, if the S/L ratio, and reaction temperature are kept constant at 50 g/L and 50 ˚C respectively. The M values of the metal constituents are given in Table 25.

As shown in Table 27, the pre-exponential factor k_0 can be determined from the calculated values of that M, N, E_a at constant conditions.

Table 27: Summary of variables used to establish empirical model based on diffusion kinetics

Variable	Cobalt	Nickel	Manganese
C_{acid} (M)	3	3	3
M	1.6	1.7	1.5
S/L (g/L)	50	50	50
N	-7.2	-7.0	-7.9
E_a (kJ/mol)	-55	-58	-52
R (J/molK)	8.3	8.3	8.3
T (K)	323	323	323
k	0.005	0.008	0.003
k_0	$1.6 * 10^9$	$8.6 * 10^8$	$1.1 * 10^{10}$

This is based on the kinetic parameters under a range of sulphuric acid concentrations at a S/L ratio of 50 g/L, 323.15 K and for a leaching time of 60 minutes. Under the average k_0 values given in Table X, the kinetic equations during leaching of Co, Ni, and Mn are determined under the diffusion model:

$$Co: 1 - 3(1-x)^{\frac{2}{3}} + 2(1-x) = 1.59 \times 10^9 C_{acid}^{1.604} \left(\frac{S}{L}\right)^{-7.207} e^{\frac{-5473}{RT}} t \quad (16)$$

$$Ni: 1 - 3(1-x)^{\frac{2}{3}} + 2(1-x) = 8.57 \times 10^8 C_{acid}^{1.708} \left(\frac{S}{L}\right)^{-6.994} e^{\frac{-5830}{RT}} t \quad (17)$$

$$Mn: 1 - 3(1-x)^{\frac{2}{3}} + 2(1-x) = 1.07 \times 10^{10} C_{acid}^{1.526} \left(\frac{S}{L}\right)^{-7.859} e^{\frac{-5167}{RT}} t \quad (18)$$

4.5 Conclusions

A lab-scale, hydrometallurgical process utilising selective leaching was developed to aid in the recovery of potentially polluting metals from LiB scrap. The process centred around the recovery of cobalt, nickel and manganese. There is potential to extract lithium, but under current market rates this is not economically viable – see Literature Review. An analysis of the kinetics of the leaching process was performed quantitatively to determine an empirical model to predict the leaching rate of the metals investigated. Several factors were modified

throughout the leaching experiments: acid type, concentration, temperature, reductant dosing and cathode type; these conditions were modified at a constant S/L ratio of 50 g/L, 50 ˚C and at 400 rpm. A maximum leaching rate of cobalt, nickel and manganese was achieved with 2 M sulphuric acid and dosed with 12 vol% (1.3 M) hydrogen peroxide reductant. This achieved leaching efficiencies for cobalt, nickel and manganese of 93 wt%, 96 wt% and 92 wt% respectively. It is understood that by the addition of hydrogen peroxide reductant, the rate-determining step is altered from residue layer diffusion to the surface chemical reaction during leaching, with the associated activation energy of the reaction reduced. Through the calculation of the kinetic parameters: k_0, M, N, E_a the kinetic equations of each metal in the leaching process can be determined. Thus, a lab-scale process for the metal recovery of metals from spent Libs was demonstrated.

5 Lithium-ion Battery Recycling Design: A New Zealand Context

5.1 Feasibility

5.1.1 Project Description

This report discusses the feasibility of LiB (lithium-ion battery) recycling in NZ (New Zealand). The key challenges for the project include: lack of local regulatory requirements, changing chemical composition of LiBs, and emerging technologies within the recycling market. A combination of internationally feasible chemical processes will be adapted to suit NZ's demands. The need for sustainable metal extraction is a constraint on the project; therefore, novel processes utilising hydrometallurgical methods must take precedence over energy intensive and environmentally detrimental processes such as pyrometallurgy.

5.1.2 Market Analysis

5.1.2.1 Demographic

To better understand the current stock of LiBs in traction vehicles, the total number of registered electric vehicles are summarised by model in Figure 48. Thereby, the total mass in tons of LiBs for New Zealand is shown in Figure 49.

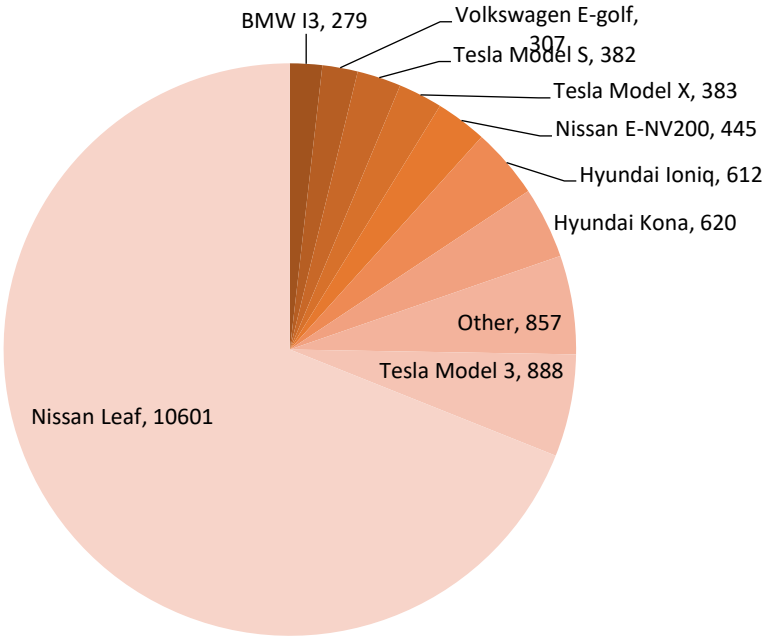

Figure 48: New Zealand registrations by Model.

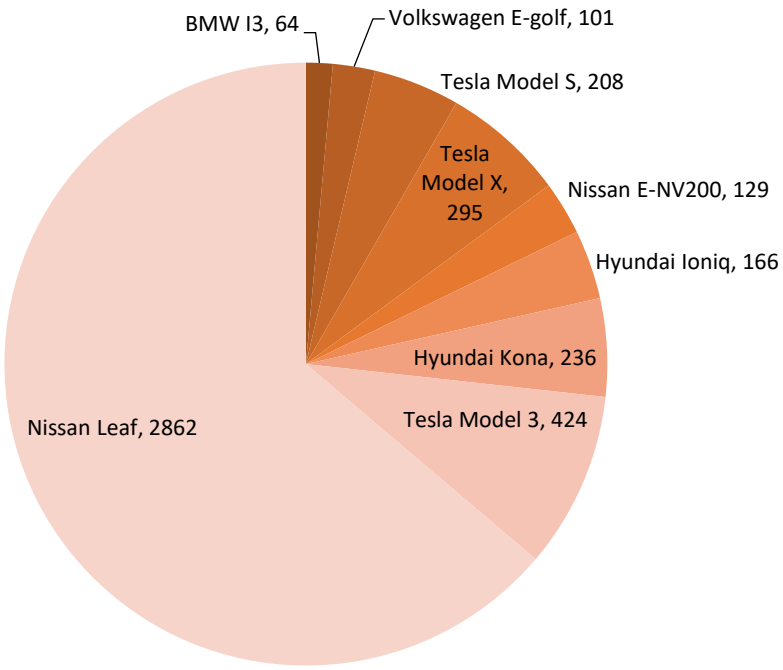

Figure 49: Total mass of LiBs per model in tons.

Battery recycling and operation is determined by local councils. Current data of NZ's LiB consumption is unknown and must be estimated. These estimations were done through data from Transport NZ and WMINZ (Waste Management Institute of New Zealand) and are summarised in Section 2.2. Statistics NZ and MFE (Ministry for the Environment) were contacted but were unable to give relevant estimates.

5.1.2.2 Growth

The market prediction is that lithium-ion batteries will continue to grow in NZ. This is attributed to the rapid influx in EVs (electric vehicles) and the propagation of LiBs in consumer devices (Vector, 2018, 2019).

Email correspondence with WMINZ found that there was between 600 – 800 tonnes of small consumer batteries disposed of annually in New Zealand; of which 80% are LiBs according to the IFRI (French Institute of International Relations) (Danino-Perraud, 2020; WasteMINZ, 2020). This suggests an annual waste stream, of LiBs from small consumer devices, between 480 – 640 tonnes in NZ – this estimation does not account for the exponential trend of LiB usage in consumer devices.

Similarly, the rapid growth of EVs in NZ and subsequent increase in spent LiBs are environmentally concerning. Data from Transport NZ on EV registrations were analysed; it was found that between Q1 2015 – Q4 2019 there were 18,000 (2SF) EVs registered, which equates to approximately 3,600 (2SF) tonnes of LiBs from EVs over the 5-year period. The trend in EV registrations in NZ was then extrapolated until 2030 as shown in Figure 50.

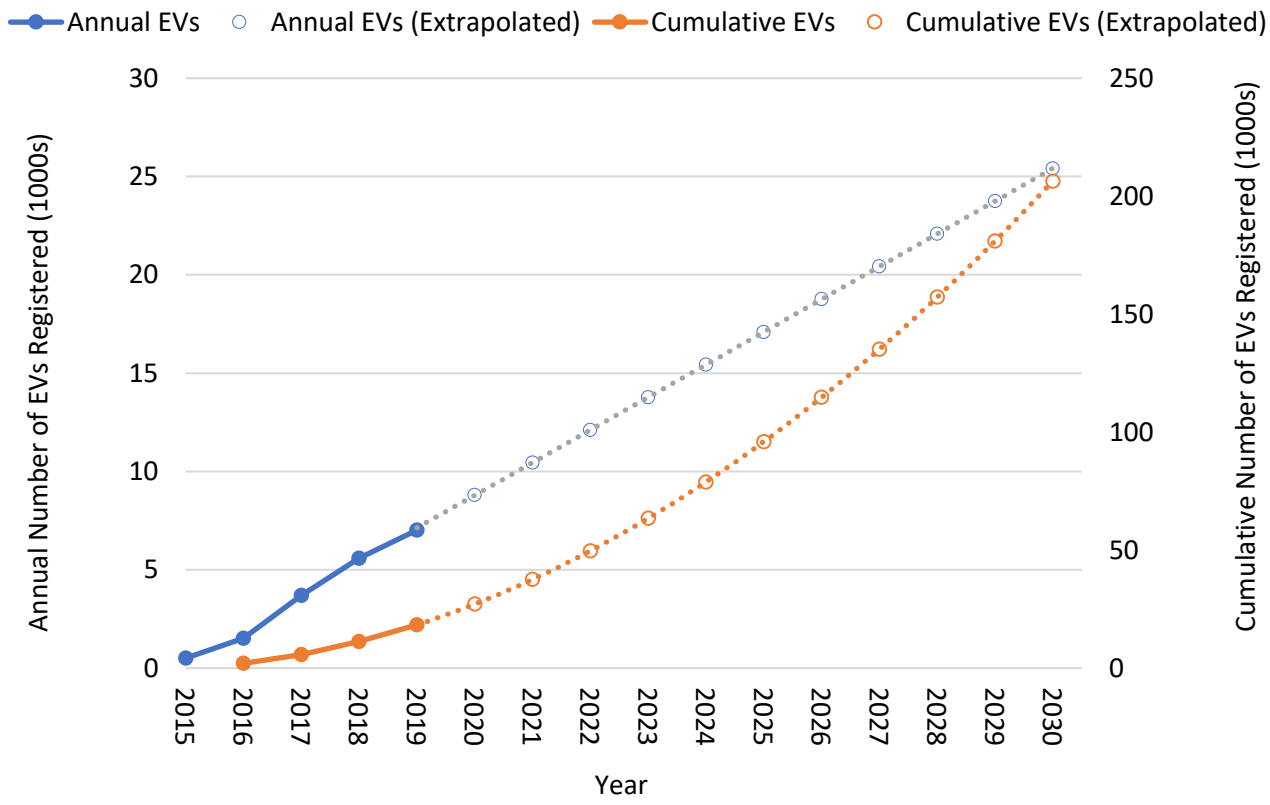

Figure 50: Annual and cumulative EV registrations for New Zealand between 2015 - 2019 as given by Transport NZ, extrapolated until 2030 (Transport NZ, 2020).

The forecast predicts that between Q1 2020 – Q4 2030 there will be approximately 210,000 (2SF) EVs registered. Therefore, assuming a 10-year lifespan of EV battery packs – as given in Vector's Technical Addendum (Vector, 2019), an estimated 40,000 (2SF) tonnes of waste LiBs from EVs is predicted to be generated between 2015 – 2040, refer to Appendix X for detailed calculations and assumptions.

In summary, the waste stream of LiBs in NZ is expected to grow exponentially, with an estimated 50,000 (2SF) tonnes of collective LiB waste generated between 2015 - 2040 from small consumer devices and EVs. The waste stream for this period is summarised in Figure 2.

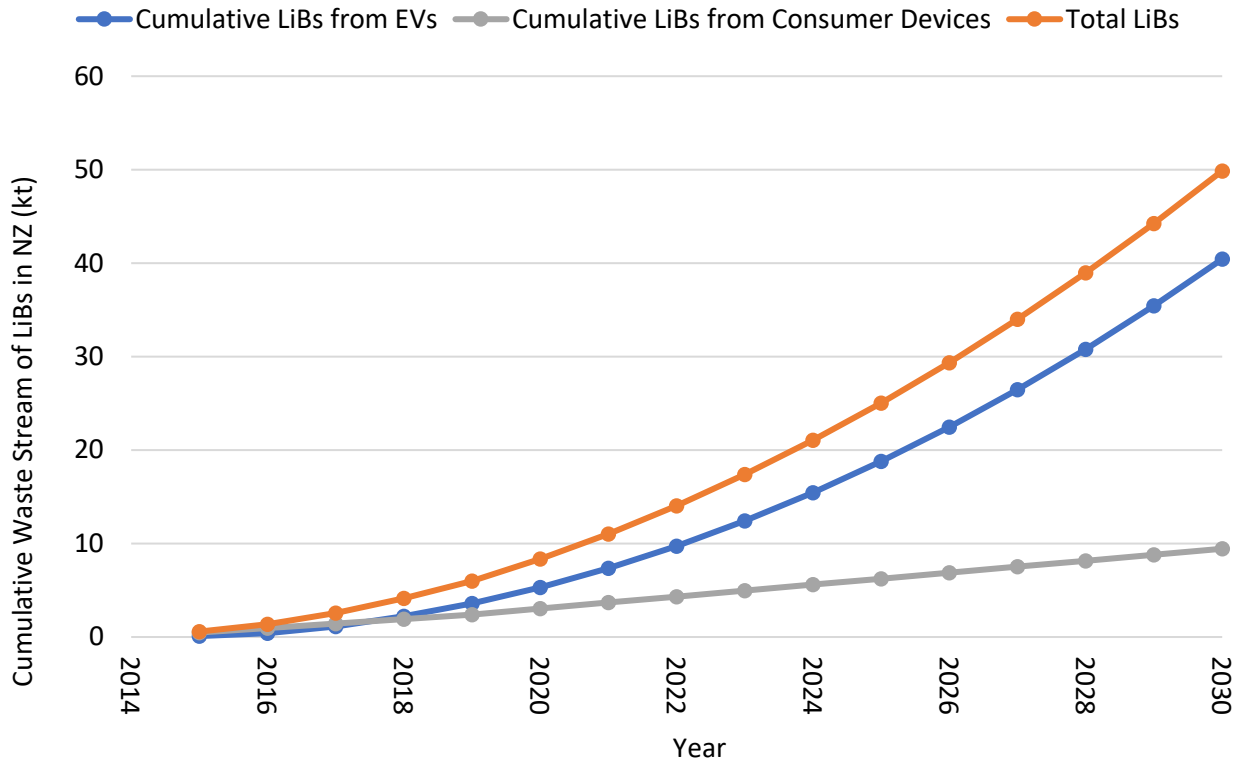

Figure 51: Timeseries estimate of LiB waste in New Zealand, based off EV registrations from Transport NZ and information provided from WasteMINZ (Transport NZ, 2020; WasteMINZ, 2020).

These trends align with an investigation done by Vector, which estimated 84,000 end of life EV battery packs by 2030 requiring management each year in NZ (Vector, 2019).

5.1.2.3 Regulation

5.1.2.3.1 Resource Management Act

The RMA (Resource Management Act) is NZ's main environmental legislation and provides a framework for managing the effects on the environment. The RMA provides definitions for sustainable management, catering for social, economic and cultural well-being, whilst maintaining environmental regulations of recycling facilities, such as in the treatment and disposal of LiBs (MFE, 2020).

5.1.2.3.2 Local Government Act

The LCA (Local Government Act) enables local decision-making and action, and holds responsible the local authority for solid waste collection and disposal, which will be crucial in the preliminary stages of building LiB recycling policy and infrastructure (MFE, 2020).

5.1.2.3.3 Waste Minimisation Act

The WMA (Waste Minimisation Act) encourages a reduction in the amount of waste generated and disposed of. The Act allows for regulations to be made to control the disposal of products, materials or waste. It also allows for mandatory regulations on waste reporting to improve information on waste minimisation. Currently, there is deficient data on the waste stream of LiBs. However, the WMA could facilitate active monitoring of this waste stream in NZ (MFE, 2020).

5.1.2.3.4 Climate Change Response Act

The CCRA (Climate Change Response Act) places a legal framework to allow NZ to ratify the Kyoto Protocol and to meet its obligations under the UN (United Nations) Framework Convention on Climate Change. This Act enables the NZ ETS (New Zealand Emissions Trading Scheme), wherein, operators of disposal facilities have specific obligations under the NZ ETS (MFE, 2020).

5.1.2.3.5 Hazardous Substances and New Organisms Act

The HSNOA (Hazardous Substances and New Organisms Act) controls the import, manufacture, use and disposal of manufactured substances that have hazardous properties, such as LiBs. The approval covers the lifecycle of these substances until they are disposed of; treating it so that it is no longer a hazardous substance or exporting it from NZ as a waste (MFE, 2020).

5.1.2.4 Barriers to Entry

For lithium-ion batteries, there are numerous design barriers to establishing a recycling market. These include:

- Lack of standardisation among LiB chemistries;
- Changing chemical composition of LiB cathodes;

- An underdeveloped market for recycling processes; and
- Non-automated systems for processing and pre-treatment.

There is rapid development in alternate cathode chemistry such as carbon-based or compostable batteries, which could make this method of recycling redundant. Similarly, as LiB cathode chemistries evolve to remove high-value metals such as cobalt, LiB recycling becomes economically unfeasible. This poses the greatest risk to the project as these unknowns cannot be incorporated into the design process. Therefore, the LiB market must be constantly reassessed and recycling processes adapted accordingly.

5.1.3 Process Selection

At full scale, the recycling plant would have to cope with 50,000 (2SF) tonnes of LiB waste between 2015 – 2040, which equates to a yearly average of 2,500 (2SF) tonnes per year or 7 tonnes per day. Albeit, this estimate does not include a collection rate, which would likely reduce the mass flow significantly. Similarly, this estimation does not account for the exponential increase of spent LiBs over time, insomuch as the daily inflow is expected to increase towards maximum capacity throughout the lifetime of the plant. Similarly, this estimation assumes that all spent LiBs from EVs and consumer devices are directed towards the recycling plant, which in praxis is unlikely.

Although specific process options will be comprehensively discussed in Chapter 2 – Process Alternatives, a generalised process description is outlined as follows. In general, there are two routes followed in the metal extraction of spent LiBs: pyrometallurgy and hydrometallurgy, the former being energy intensive and the latter chemically intensive.

Pyrometallurgy is cheaper on the industrial scale, and involves less disassembly, whilst being able to process a variety of LiB cathodes. However, this process is highly energy intensive and requires a significant embodied carbon cost through harmful gas emissions all for a low metal recovery rate. Comparatively, hydrometallurgy offers a high metal recovery rate and is not energy intensive. However, this process is expensive and requires a large volume of reagents. Although hydrometallurgy has an opportunity cost, it offers a more sustainable approach to LiB metal recovery when coupled with forward thinking design options such as:

decentralised mechanical pre-treatment, reagent recycle lines, heat exchange and electrolyte capture. This method of metal recovery will create mineral wealth in key metals, which NZ currently depends on external suppliers for.

5.1.4 Site Selection

Pre-treatment decentralised across NZ, with main processing plants for north and South Island.

5.1.4.1 Personnel Requirement

The processing plant will operate 5 days per week, 8 hours per day. It will be staffed by permanent employees, based on standard 40 hour working weeks.

5.1.5 Community and Iwi Engagement

Throughout the project, it is essential to integrate the local community and iwi. Engagement will begin in the initial stages of the project to establish a positive relationship with key stakeholders. These stakeholders include local government, local iwi and rūnanga, and other affected parties. Stakeholders will be invited to meetings and be given opportunities to voice their ideas or concerns. Information on progress of the project will also be provided.

Under the Ngāi Tahu Claims Settlement Act 1998, nohoanga sites are specific areas of Crown owned land adjacent to lakeshores or riverbanks. This entitles Ngāi Tahu to occupy temporarily and exclusively approximately one hectare of land bordering lakes or rivers for lawful fishing and interactions with natural resources.

Although the proposed LiB recycling plant will not be on a direct nohoanga site, it is important to consider its proximity and potential implications in the consent application process. Iwi are responsible for ensuring their requirements for kaitiakitanga are satisfied, while the local governments must ensure the key requirements under the RMA are met.

Bicultural confidence and competence are essential aspects of this project. Without it, the project faces significant risk of social and governmental persecution. New Zealand's culture is built on Māori tradition and acknowledgment. Approval from iwi poses a large risk, as often, aspects of projects do not align with cultural beliefs. However, this project is

concerned with Kaitiakitanga for New Zealand and so Iwi opinion and the project objectives should remain aligned.

5.1.6 Future Directions

An understanding of project barriers is vital for future design steps. By acknowledging these barriers, assumptions can be made, and measures can be taken to reduce the impact of these barriers in later design stages. Further study of process options should be undertaken to design an effective and economical plant. Design for exponential increase in the number of spent LiBs over the next 20 years must be considered. When proceeding with the project, the input of the community and iwi is vital to ensure success. Following the initial economic analysis, a full analysis will be conducted to provide more definitive evaluations. Similarly, a preliminary P&ID will be developed to highlight the most feasible process options moving forward.

5.2 Process Alternatives

To treat lithium-ion battery influent, a 3-step process was identified from literature, pre-treatment, mechanical and hydrometallurgy extraction. The process involves leaching, precipitation and liquid-liquid extraction in recovering lithium-ion battery constituents. Phase ratio, temperature, pH and concentration were important parameters, determined through review with opportunities for optimisation through modelling and experimental analysis. The combination of 5% pulp density, 2 M sulphuric acid mixed with 4 vol% hydrogen peroxide resulted in leaching efficiencies exceeding 98% at below 50 ˚C. The lithium-ion battery influent was assumed to be composed of mainly NMC type cathode materials and from the initial feasibility report, the waste stream of lithium-ion batteries was estimated at 2,500 tonnes per year or 7 tonnes per day – across New Zealand. However, these estimates are averages based on 40-year estimates, with high uncertainty associated with the domestic electric vehicle market. Similarly, initial recycling rates will be low, with only a portion of the estimated lithium-ion battery waste stream being captured. Each process in the preliminary process flow diagram was described, explaining the purpose, significant reaction chemistry and intended equipment used. The process was shown to have overall extraction efficiencies equivalent to $630/kg of influent lithium-ion batteries, based on consumer costs.

5.2.1 Process Description

The following process is a hydrometallurgy solution for the metal recovery of primary and secondary LiBs. Preliminary review found a net increase in GHG (Greenhouse Gas) emissions when pyrometallurgy was involved in metal recovery (Ciez et al., 2019). Therefore, the following PFD (Process Flow Diagram), outlined in Figure 52, addresses these gas emissions directly. The process utilises a combination of industrially recognised processes, supplemented with additional unit operations as per project constraints.

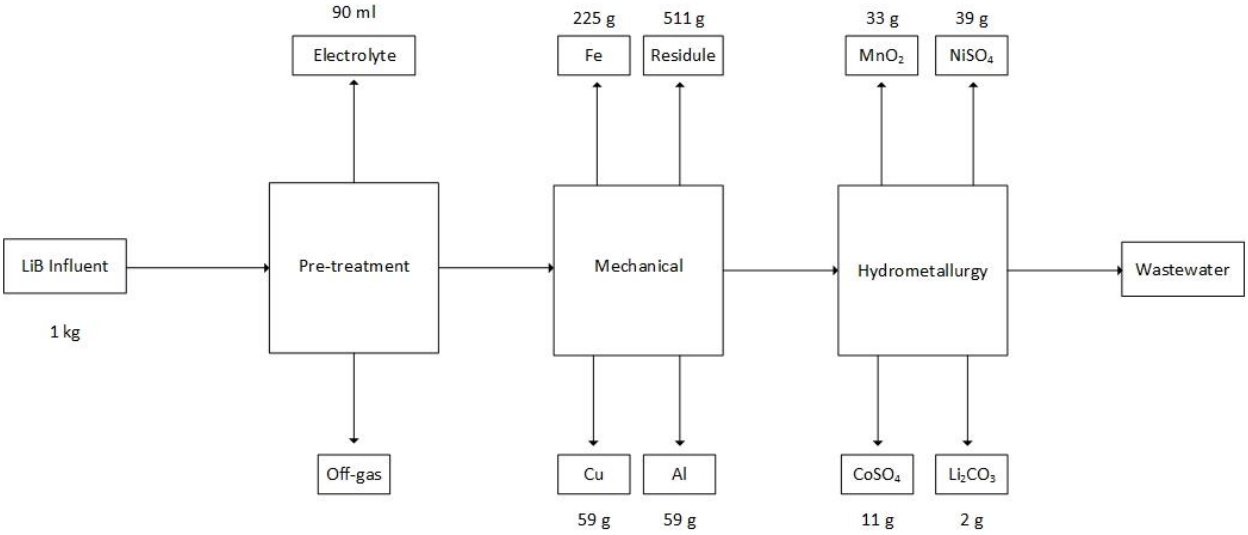

Figure 52: PFD of proposed hydrometallurgy process for metal recovery form LiBs.

The PFD above provided a basis for preliminary economic estimates of product revenue. The relative economic benefit from the constituents extracted are summarised in Figure 53.

5.2.1.1 Feeds

The LiB (Lithium-ion Battery) influent was assumed to be composed of $LiNi_xCo_yMn_zO_2$ type cathode materials with an elemental balance of 7.6% lithium, 20.5% cobalt, 19.5% manganese, and 19.4% nickel. The cell itself was assumed to comprise of 27% cathode, 25% casing, 17% anode, 13% foils, 10% electrolyte and 8% separator.

5.2.1.2 Products

The LiB recycling process in Figure 54 shows the metal extraction of: cobalt, nickel, iron, manganese, aluminium, copper and lithium. The process has options to recycle the chemical solvents used thereby reducing the overall environmental impact associated with solvent disposal.

In Figure 53, the LiB electrolyte was shown to be a valuable co-product. Therefore, the recycling process was adapted to facilitate electrolyte extraction through liquid CO_2 (Carbon dioxide) extraction. Similarly, graphite extraction was integrated into the preliminary recycling process, although is not economically feasible.

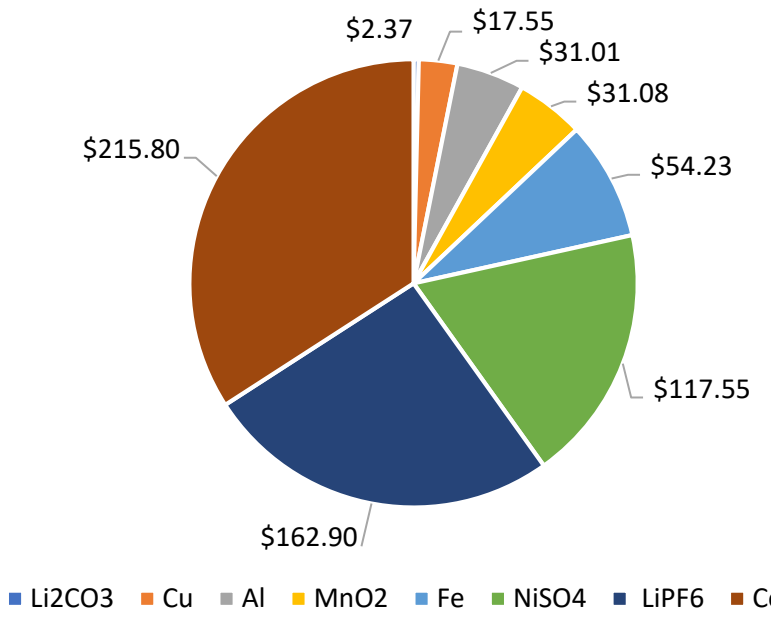

Figure 53: Associated value of 1 kg of LiB cells, based on approximate value from Sigma Aldrich.

The as extracted cobalt, electrolyte and nickel are the most valuable of the constituents extracted. Overall, the constituents extracted equate to approximately $630/kg at consumer prices estimated from Sigma Aldrich. However, these estimates are expected to reduce significantly for commercial pricing.

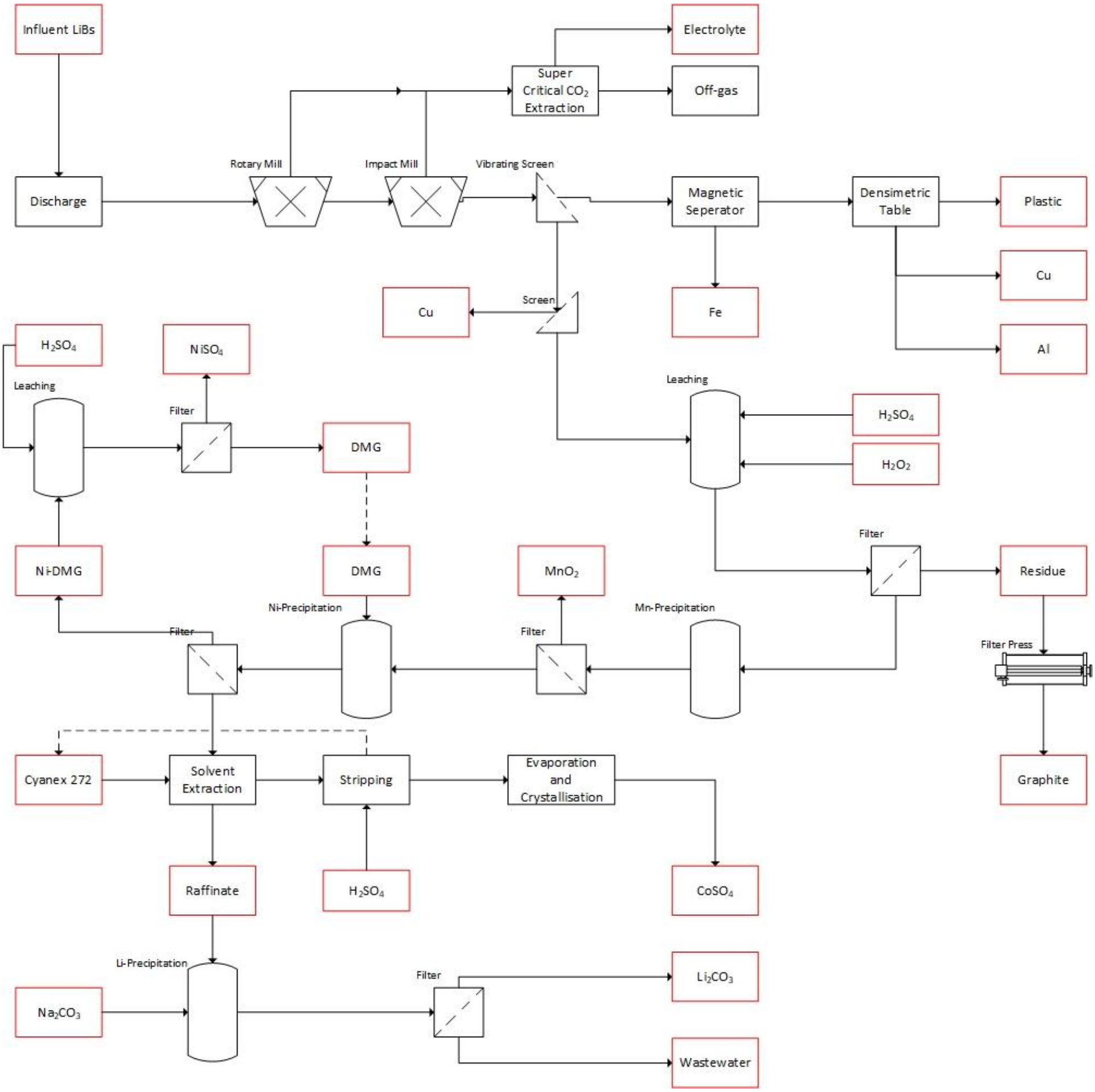

Figure 54: Process flow diagram of proposed recycling process to extract LiB constituents.

5.2.1.3 Preliminary Treatment

5.2.1.3.1 Sorting

The mechanical treatment of influent LiBs removes non-metallic fractions in addition to copper and aluminium constituents. However, influent batteries, which could pollute downstream processes, such as nickel-cadmium cells should be removed prior to mechanical treatment.

5.2.1.3.2 Discharge

Second-life options to utilise the residual energy of inbound LiB packs should be integrated to sustain process requirements or can be adopted in grid power applications to complement renewable infrastructure and absorb peak loading. However, this exceeds the constraints of this design project, which will focus on the metal extraction aspect of recycling.

5.2.1.4 Mechanical

5.2.1.4.1 Rotary Milling

Influent LiBs enter the rotary mill operating at approximately 10 RPM under inert conditions. An atmosphere of carbon dioxide (or argon) is used to achieve an inert environment and passivate potential metallic lithium. An insulating lithium carbonate layer is formed thereby reducing the risk associated with an exothermic reaction. Alternative methods include cryogenic cooling of influent LiBs using liquid nitrogen, however this is dependent on availability and environmental suitability.

5.2.1.4.2 Impact Milling

Subsequent grinding, at approximately 100 RPM, reduces the particles to less than 3 mm, which is then passed through a vibrating screen. This secondary mechanical step ensures the separation of the metal oxide cathode from the aluminium foil. Additional dosing of sodium hydroxide could increase recovery of cathodic material and could be implemented as a future process option.

5.2.1.4.3 Electrolyte Recovery

The electrolyte of LiBs typically consist of lithium salts, such as $LiPF_6$ (Lithium hexafluorophosphate) with a concentration of 1 $molL^{-1}$, dissolved in an equal mixture of EC (Ethylene Carbonate) and DMC (Dimethyl Carbonate), which is a highly combustible solvent (Heelan et al., 2016). Liquid CO_2 extraction was shown to effectively recover electrolyte from LiBs in literature. Whereby, Grützke et al., found that extraction for 30 minutes with

liquid CO_2 at 25 ˚C, 60 bar and 0.5 mL/min ACN (Acetonitrile) in a ratio of 3:1 with PC (Propylene carbonate) followed by an additional 20 minutes liquid CO_2 extraction yielded 90% of the original electrolyte (Grützke et al., 2015). This process must be further developed in the future to cater for increased scale.

5.2.1.5 Screening

5.2.1.5.1 Vibrating Screen

The vibrating screen separates the mechanically pre-treated LiB influent into over and under sized fractions. Whereby, the oversized fractions are passed to the magnetic separator with undersized fractions passed to hydrometallurgy-based metal recovery.

5.2.1.5.2 Magnetic Separation

High-induction magnetic separation removes any ferrous metals assuming a recovery rate of 90%, before the remaining oversized fraction is passed to denismetric separation.

5.2.1.5.3 Densimetric Separation

The relative difference in density between the plastic and metal fractions creates a high-density fraction containing copper and aluminium and a low-density fraction containing plastic and paper. The high-density fraction of electrode foils was assumed to have an overall recovery rate of 90%.

5.2.1.6 Hydrometallurgy

5.2.1.6.1 Screening

Secondary screening, post mechanical treatment, ensures a filtrate that is largely free of copper, which could negatively impact downstream leaching and precipitation reactions. This is achieved through a 500 µm sieving step.

5.2.1.6.2 Leaching

The electrode-rich fine fractions are then leached (according to the chemical reaction below), for 120 minutes at 50 ˚C using a mixed lixiviant of 2 M sulphuric acid with a dosage of 4 vol% hydrogen peroxide, and 5% pulp density. This method achieves leaching efficiencies of approximately 98% (Ciez et al., 2019; Gaines, 2018; L.-P. He et al., 2017; Sattar et al., 2019).

$$6LiNi_{\frac{1}{3}}Co_{\frac{1}{3}}Mn_{\frac{1}{3}}O_{2\,(s)} + 9H_2SO_{4(aq)} + 3H_2O_{2(aq)} \rightarrow$$
$$3Li_2SO_{4(aq)} + 2NiSO_{4(aq)} + 2CoSO_{4(aq)} + 2MnSO_{4(aq)} + 12H_2O_{(aq)} + 2O_{2(g)}$$

The leach liquour is then passed through a solid-liquid separator, which removes the final residue, mainly comprising of graphite, which is then passed through a filter press for graphite extraction.

5.2.1.6.3 Manganese Precipitation

The oxidative precipitation of manganese (according to the chemical reaction below) was achieved through the addition of potassium permanganate at a relatively low pH of 2.5, in a ratio of 1.2:1 manganese. At this ratio and maintained for 1 hour at 80 ˚C, 98% of manganese is precipitated (Granata et al., 2012; Pinegar et al., 2020; Sattar et al., 2019).

$$3{Mn^{2+}}_{(aq)} + 2{MnO_4^-}_{(aq)} + 2{H_2O}_{(aq)} \rightarrow 5{MnO_2}_{(s)} + 4{H^+}_{(aq)}$$

The manganese precipitate is then recovered by passing it through a solid-liquid separator. The final manganese precipitate is then washed and dried resulting in an overall recovery rate of 62.4%.

5.2.1.6.4 Nickel Precipitation

The manganese recovered solution is adjusted to a pH of 5 before DMG (Dimethylglyoxime) is added in a ratio of 2:1 to nickel, thus achieving nickel precipitation efficiencies greater than 99%. The DMG can then be reclaimed and recycled through sulphuric acid leaching of the Ni-DMG complex (Rath et al., 2018). The precipitation reaction of nickel (according to the chemical reaction below).

$$Ni^{2+}_{(aq)} + 2{C_4H_8N_2O_2}_{(aq)} + 2{OH^-}_{(aq)} \rightarrow Ni - {(2C_4H_7N_2O_2)_2}_{(s)} + 2{H_2O}_{(aq)}$$

After DMG dosing, the Nickel-DMG precipitate is recovered through a solid-liquid separator, is washed then dried with an overall recovery rate of 20.3%.

5.2.1.6.5 Cobalt Extraction

Geopolitical and ethical issues limit the extraction of cobalt from the abundant DRC reserves. Insomuch as, high purity cobalt recovery is necessary to prevent further resource depletion. To achieve this purity, a 2-stage, counter-current, solvent extraction process,

using Cyanex 272 was optimised at a pH of 5, equal phase ratio, and 0.64 M Cyanex 272 in kerosene diluent at room temperature (according to the chemical reaction below).

$$Co^{2+} + 2(RH)_2 \leftrightarrow Co(R.RH)_2 + 2H^+_{(aq)}$$

The extraction conditions were optimised with 50% of the Cyanex 272 saponified with 4 M sodium hydroxide solution prior to addition (according to the chemical reaction below). The raffinate is then passed to the lithium precipitation step.

$$Na^+_{(aq)} + \frac{1}{2}(RH)_2 \leftrightarrow NaR + H^+_{(aq)}$$

The stripping reaction to recover cobalt sulphate from the organic solution is understood by (according to the chemical reaction below). This is achieved through a 10-minute contact with 2 M sulphuric acid under a phase ratio of 10:1. Whereby, Cyanex 272 can be recycled back to the solvent extraction step.

$$Co(R.RH)_2 + 2H_2SO_{4(aq)} \leftrightarrow CoSO_{4(aq)} + 2(RH)$$

High quality cobalt crystals are then obtained through evaporation under slow agitation resulting in an overall recovery rate of 20.5%.

5.2.1.6.6 Lithium Precipitation

The raffinate, from the solvent extraction step is further processed to extract lithium carbonate. Therefore, the lithium solution is evaporated until it has doubled its initial concentration, to approximately 7.5 g/L, before the pH was neutralised with the subsequent addition of sodium carbonate in a ratio of 1.2:1 lithium. The reaction (according to the chemical reaction below), is maintained at 90 ˚C for 1 hour.

$$2Li^{2+}_{(aq)} + {CO_3^{2-}}_{(aq)} \rightarrow Li_2CO_{3(s)}$$

Subsequently, the lithium carbonate precipitate is passed through a solid-liquid separator before being washed, dried and collected at an overall recovery rate of 10.3%. Wastewater from the final separator can then be sent for further treatment.

5.2.2 Future Directions

The process outlined above is a sustainable recycling solution to New Zealand's rapidly increasing waste stream of LiBs. The mass and energy balances will be refined and specific conditions for unit operations determined. Equipment sizing will also be completed. Modelling could allow for process optimisation. However more accurate data on the waste stream of LiBs in New Zealand is required, which can be achieved in the future through policy and regulation around monitoring.

6 Conclusions

A circular approach to the sustainable recycling of lithium-ion batteries was taken. An initial battery survey of spent lithium-ion batteries in New Zealand revealed that upwards of 60% of cells surveyed held a state-of-charge above 80% confirming that cells remained usable once disposed. Subsequently, a design and build battery pack utilised second-life cells in a 7s15p battery pack, capable of 1.2 kWh of solar power storage. To continue the 3-R concept in the context of recycling lithium-ion batteries; a lab-scale, hydrometallurgical process utilising selective leaching steps was developed to aid in the recovery of potentially polluting metals from LiB scrap. An analysis of the kinetics of the leaching process was performed quantitatively to determine an empirical model to predict the leaching rate of the metals investigated, which achieved leaching efficiencies for cobalt, nickel and manganese of 93 wt%, 96 wt% and 92 wt%. A design process, drawing on lab-scale results guided the design of potential process for lithium-ion battery recycling in a New Zealand context

6.1 Future Directions

6.1.1 Lithium-ion Battery Characteristics: A Survey of Used Cells

The sample size of cells could be increased to better validate the second-use supply chain model proposed for lithium-ion batteries in New Zealand. Whereby, cells from electric vehicles could be included in the survey.

6.1.2 Lithium-ion Battery Second Use: A Solar Solution

The design and build of second-use battery packs could be scaled up, optimised and regulated such that their use could be used to supplement renewable energy solutions, such as wind and solar. The use of end of life electric vehicle battery packs for stationary storage could be investigated.

6.1.3 Lithium-ion Battery Metal Recovery: A Sustainable Approach

It has been proven in literature and confirmed at lab-scale that lithium-ion batteries can be recycled and the metals within recovered. This research should be progressed to a pilot scale project and prove that it could offer a solution to New Zealand's growing waste-stream of lithium-ion batteries.

6.1.4 Lithium-ion Battery Recycling Design: A New Zealand

Further to the design piece, the process flow diagram can be developed, including associated P&IDs. Following a preliminary hazard assessment, a HAZOP can be conducted along with the progression of subsequent design reports: Process Description, Process Design, Safety Community and Environment, Equipment Design, Process Operations and Economics. The concepts outlined in the recycling design of lithium-ion battery recycling should be rolled out in a commercial application as a solution to end of life lithium-ion batteries.

Appendix

Appendix A1: Potentiostat Sample Data (Cell #63)

	A	B	C	D	E	F	G	H	I	J	K	L
59		Pt	T	Vf	Im	Vu	Pwr	Sig	Ach	Temp	IERange	Over
60		#	s	V	A	V	W	V	V	deg C	#	bits
61		0	5	3.38	0.50	0.00	1.69	2.50	0.00	-327.64	11	.....a
62		1	10	3.51	0.50	0.00	1.75	2.50	0.00	-327.64	11	.....a
63		2	15	3.55	0.50	0.00	1.77	2.50	0.00	-327.64	11	.....a
64		3	20	3.57	0.50	0.00	1.79	2.50	0.00	-327.64	11	.....a
65		4	25	3.59	0.50	0.00	1.79	2.50	0.00	-327.64	11	.....a
2116		2055	10275	4.20	0.31	0.00	1.32	1.57	0.00	-327.64	11	.....a
2117		2056	10280	4.20	0.31	0.00	1.32	1.57	0.00	-327.64	11	.....a
2118		2057	10285	4.20	0.31	0.00	1.32	1.57	0.00	-327.64	11	.....a
2119		2058	10290	4.20	0.31	0.00	1.32	1.57	0.00	-327.64	11	.....a
2120		2059	10295	4.20	0.31	0.00	1.31	1.57	0.00	-327.64	11	.....a
2121		2060	10300	4.20	0.31	0.00	1.31	1.56	0.00	-327.64	11	.....a
2122		2061	10305	4.20	0.31	0.00	1.31	1.56	0.00	-327.64	11	.....a
2123		2062	10310	4.20	0.31	0.00	1.31	1.56	0.00	-327.64	11	.....a
2124		2063	10315	4.20	0.31	0.00	1.31	1.56	0.00	-327.64	11	.....a
2125		2064	10320	4.20	0.31	0.00	1.31	1.56	0.00	-327.64	11	.....a
2126		2065	10325	4.20	0.31	0.00	1.31	1.56	0.00	-327.64	11	.....a
2127		2066	10330	4.20	0.31	0.00	1.31	1.56	0.00	-327.64	11	.....a
2128		2067	10335	4.20	0.31	0.00	1.31	1.56	0.00	-327.64	11	.....a
2129		2068	10340	4.20	0.31	0.00	1.31	1.56	0.00	-327.64	11	.....a
2130		2069	10345	4.20	0.31	0.00	1.31	1.55	0.00	-327.64	11	.....a
2131		2070	10350	4.20	0.31	0.00	1.30	1.55	0.00	-327.64	11	.....a
2132		2071	10355	4.20	0.31	0.00	1.30	1.55	0.00	-327.64	11	.....a
2133		2072	10360	4.20	0.31	0.00	1.30	1.55	0.00	-327.64	11	.....a
2134		2073	10365	4.20	0.31	0.00	1.30	1.55	0.00	-327.64	11	.....a
2135		2074	10370	4.20	0.31	0.00	1.30	1.55	0.00	-327.64	11	.....a
2136		2075	10375	4.20	0.31	0.00	1.30	1.55	0.00	-327.64	11	.....a
2137		2076	10380	4.20	0.31	0.00	1.30	1.55	0.00	-327.64	11	.....a
2138		2077	10385	4.20	0.31	0.00	1.30	1.54	0.00	-327.64	11	.....a
2139		2078	10390	4.20	0.31	0.00	1.30	1.54	0.00	-327.64	11	.....a
2140		2079	10395	4.20	0.31	0.00	1.30	1.54	0.00	-327.64	11	.....a
2141		2080	10400	4.20	0.31	0.00	1.29	1.54	0.00	-327.64	11	.....a
2142		2081	10405	4.20	0.31	0.00	1.29	1.54	0.00	-327.64	11	.....a
2143		2082	10410	4.20	0.31	0.00	1.29	1.54	0.00	-327.64	11	.....a
2144		2083	10414.5	4.20	0.31	0.00	1.29	1.54	0.00	-327.64	11	.....a

Appendix A2: Potentiostat Sample Data (Cell #80)

	B	C	D	E	F	G	H	I	J	K	L
59	Pt	T	Vf	Im	Vu	Pwr	Sig	Ach	Temp	IERange	Over
60	#	s	V	A	V	W	V	V	deg C	#	bits
61	0	5	3.45E+00	5.00E-01	0.00E+00	1.72E+00	2.50E+00	-1.99E-05	-3.28E+02	11	.....a
62	1	10	3.46E+00	5.00E-01	0.00E+00	1.73E+00	2.50E+00	-1.59E-05	-3.28E+02	11	.....a
63	2	15	3.47E+00	5.00E-01	0.00E+00	1.73E+00	2.50E+00	-1.87E-05	-3.28E+02	11	.....a
64	3	20	3.48E+00	5.00E-01	0.00E+00	1.74E+00	2.50E+00	-1.87E-05	-3.28E+02	11	.....a
65	4	25	3.48E+00	5.00E-01	0.00E+00	1.74E+00	2.50E+00	-1.92E-05	-3.28E+02	11	.....a
66	5	30	3.49E+00	5.00E-01	0.00E+00	1.75E+00	2.50E+00	-1.69E-05	-3.28E+02	11	.....a
67	6	35	3.50E+00	5.00E-01	0.00E+00	1.75E+00	2.50E+00	-2.12E-05	-3.28E+02	11	.....a
68	7	40	3.50E+00	5.00E-01	0.00E+00	1.75E+00	2.50E+00	-2.46E-05	-3.28E+02	11	.....a
69	8	45	3.51E+00	5.00E-01	0.00E+00	1.75E+00	2.50E+00	-2.66E-05	-3.28E+02	11	.....a
70	9	50	3.52E+00	5.00E-01	0.00E+00	1.76E+00	2.50E+00	-2.63E-05	-3.28E+02	11	.....a
71	10	55	3.52E+00	5.00E-01	0.00E+00	1.76E+00	2.50E+00	-3.08E-05	-3.28E+02	11	.....a
72	11	60	3.53E+00	5.00E-01	0.00E+00	1.76E+00	2.50E+00	-3.81E-05	-3.28E+02	11	.....a
73	12	65	3.53E+00	5.00E-01	0.00E+00	1.77E+00	2.50E+00	-4.39E-05	-3.28E+02	11	.....a
74	13	70	3.54E+00	5.00E-01	0.00E+00	1.77E+00	2.50E+00	-5.50E-05	-3.28E+02	11	.....a
75	14	75	3.54E+00	5.00E-01	0.00E+00	1.77E+00	2.50E+00	-4.15E-05	-3.28E+02	11	.....a
76	15	80	3.55E+00	5.00E-01	0.00E+00	1.77E+00	2.50E+00	-4.36E-05	-3.28E+02	11	.....a
77	16	85	3.55E+00	5.00E-01	0.00E+00	1.78E+00	2.50E+00	-4.36E-05	-3.28E+02	11	.....a
78	17	90	3.56E+00	5.00E-01	0.00E+00	1.78E+00	2.50E+00	-4.20E-05	-3.28E+02	11	.....a
79	18	95	3.56E+00	5.00E-01	0.00E+00	1.78E+00	2.50E+00	-3.91E-05	-3.28E+02	11	.....a
80	19	100	3.57E+00	5.00E-01	0.00E+00	1.78E+00	2.50E+00	-4.46E-05	-3.28E+02	11	.....a
81	20	105	3.57E+00	5.00E-01	0.00E+00	1.79E+00	2.50E+00	-4.64E-05	-3.28E+02	11	.....a
82	21	110	3.58E+00	5.00E-01	0.00E+00	1.79E+00	2.50E+00	-3.89E-05	-3.28E+02	11	.....a
83	22	115	3.58E+00	5.00E-01	0.00E+00	1.79E+00	2.50E+00	-5.09E-05	-3.28E+02	11	.....a
84	23	120	3.59E+00	5.00E-01	0.00E+00	1.79E+00	2.50E+00	-5.19E-05	-3.28E+02	11	.....a
85	24	125	3.59E+00	5.00E-01	0.00E+00	1.79E+00	2.50E+00	-5.39E-05	-3.28E+02	11	.....a
580	519	2600	3.93E+00	5.00E-01	0.00E+00	1.97E+00	2.50E+00	-8.43E-05	-3.28E+02	11	.....a
581	520	2605	3.93E+00	5.00E-01	0.00E+00	1.97E+00	2.50E+00	-8.18E-05	-3.28E+02	11	.....a
582	521	2610	3.93E+00	5.00E-01	0.00E+00	1.97E+00	2.50E+00	-7.97E-05	-3.28E+02	11	.....a
583	522	2615	3.93E+00	5.00E-01	0.00E+00	1.97E+00	2.50E+00	-7.77E-05	-3.28E+02	11	.....a
584	523	2620	3.93E+00	5.00E-01	0.00E+00	1.97E+00	2.50E+00	-7.73E-05	-3.28E+02	11	.....a
585	524	2625	3.93E+00	5.00E-01	0.00E+00	1.97E+00	2.50E+00	-7.89E-05	-3.28E+02	11	.....a
586	525	2630	3.94E+00	5.00E-01	0.00E+00	1.97E+00	2.50E+00	-7.93E-05	-3.28E+02	11	.....a
587	526	2635	3.94E+00	5.00E-01	0.00E+00	1.97E+00	2.50E+00	-8.29E-05	-3.28E+02	11	.....a
588	527	2640	3.94E+00	5.00E-01	0.00E+00	1.97E+00	2.50E+00	-7.83E-05	-3.28E+02	11	.....a
589	528	2645	3.94E+00	5.00E-01	0.00E+00	1.97E+00	2.50E+00	-7.92E-05	-3.28E+02	11	.....a

Appendix A3: Potentiostat Sample Data (Cell #87)

	A	B	C	D	E	F	G	H	I	J	K	L
59		Pt	T	Vf	Im	Vu	Pwr	Sig	Ach	Temp	IERange	Over
60		#	s	V	A	V	W	V	V	deg C	#	bits
61		0	5	3.41E+00	5.00E-01	0.00E+00	1.70E+00	2.50E+00	-1.08E-04	-3.28E+02	11	.....a
62		1	10	3.42E+00	5.00E-01	0.00E+00	1.71E+00	2.50E+00	-1.14E-04	-3.28E+02	11	.....a
63		2	15	3.42E+00	5.00E-01	0.00E+00	1.71E+00	2.50E+00	-1.13E-04	-3.28E+02	11	.....a
64		3	20	3.43E+00	5.00E-01	0.00E+00	1.71E+00	2.50E+00	-1.13E-04	-3.28E+02	11	.....a
65		4	25	3.43E+00	5.00E-01	0.00E+00	1.72E+00	2.50E+00	-1.14E-04	-3.28E+02	11	.....a
66		5	30	3.44E+00	5.00E-01	0.00E+00	1.72E+00	2.50E+00	-1.15E-04	-3.28E+02	11	.....a
67		6	35	3.44E+00	5.00E-01	0.00E+00	1.72E+00	2.50E+00	-1.16E-04	-3.28E+02	11	.....a
68		7	40	3.44E+00	5.00E-01	0.00E+00	1.72E+00	2.50E+00	-1.15E-04	-3.28E+02	11	.....a
69		8	45	3.44E+00	5.00E-01	0.00E+00	1.72E+00	2.50E+00	-1.11E-04	-3.28E+02	11	.....a
4277		4216	21080	4.20E+00	2.28E-01	0.00E+00	9.59E-01	1.14E+00	-1.65E-04	-3.28E+02	11	.....a
4278		4217	21085	4.20E+00	2.28E-01	0.00E+00	9.58E-01	1.14E+00	-1.61E-04	-3.28E+02	11	.....a
4279		4218	21090	4.20E+00	2.28E-01	0.00E+00	9.57E-01	1.14E+00	-1.65E-04	-3.28E+02	11	.....a
4280		4219	21095	4.20E+00	2.27E-01	0.00E+00	9.55E-01	1.14E+00	-1.64E-04	-3.28E+02	11	.....a
4281		4220	21100	4.20E+00	2.27E-01	0.00E+00	9.54E-01	1.14E+00	-1.65E-04	-3.28E+02	11	.....a
4282		4221	21105	4.20E+00	2.27E-01	0.00E+00	9.53E-01	1.13E+00	-1.67E-04	-3.28E+02	11	.....a
4283		4222	21110	4.20E+00	2.27E-01	0.00E+00	9.52E-01	1.13E+00	-1.65E-04	-3.28E+02	11	.....a
4284		4223	21115	4.20E+00	2.26E-01	0.00E+00	9.50E-01	1.13E+00	-1.67E-04	-3.28E+02	11	.....a
4285		4224	21120	4.20E+00	2.26E-01	0.00E+00	9.49E-01	1.13E+00	-1.63E-04	-3.28E+02	11	.....a
4286		4225	21125	4.20E+00	2.26E-01	0.00E+00	9.48E-01	1.13E+00	-1.64E-04	-3.28E+02	11	.....a
4287		4226	21130	4.20E+00	2.25E-01	0.00E+00	9.47E-01	1.13E+00	-1.65E-04	-3.28E+02	11	.....a
4288		4227	21135	4.20E+00	2.25E-01	0.00E+00	9.46E-01	1.13E+00	-1.65E-04	-3.28E+02	11	.....a
4289		4228	21137.3	4.20E+00	2.25E-01	0.00E+00	9.45E-01	1.12E+00	-1.68E-04	-3.28E+02	11	.....a

Appendix A4: Potentiostat Sample Data (Cell #88)

	B	C	D	E	F	G	H	I	J	K	L	M
54	Pt	Time	Freq	Zreal	Zimag		Zsig	Zmod	Zphz	Idc	Vdc	IERange
55	#	s	Hz	ohm	ohm		V	ohm	∞	A	V	#
56	0	3	100078.1	0.311368	0.0944723	-0.0944723	1	0.3253845	16.87834	-2.93E-08	4.126432	8
57	1	4	79453.13	0.3135381	0.0818782	-0.0818782	1	0.3240528	14.63552	-1.95E-08	4.126006	8
58	2	6	63140.62	0.3047008	0.0693619	-0.0693619	1	0.3124959	12.82424	1.88E-07	4.125648	8
59	3	7	50203.12	0.3074426	0.0481582	-0.0481582	1	0.3111916	8.902534	3.94E-08	4.125303	8
60	4	9	39890.62	0.3127382	0.0365808	-0.0365808	1	0.3148703	6.671541	-2.56E-08	4.125027	8
61	5	11	31640.63	0.303829	0.0323549	-0.0323549	1	0.3055469	6.07855	-6.43E-08	4.124755	8
62	6	12	25171.88	0.3079068	0.0371898	-0.0371898	1	0.3101446	6.886971	-2.42E-08	4.124484	8
63	7	14	20015.62	0.3022426	0.0211438	-0.0211438	1	0.3029813	4.001681	1.88E-07	4.124243	8
64	8	16	15890.62	0.2908657	0.0211444	-0.0211444	1	0.2916332	4.157795	8.08E-08	4.124008	8
65	9	17	12609.37	0.2918435	0.0167349	-0.0167349	1	0.2923229	3.281856	-6.30E-08	4.123769	8
66	10	19	10078.13	0.2870721	0.0227254	-0.0227254	1	0.2879702	4.526253	-2.70E-08	4.123582	8
67	11	20	8015.625	0.288413	0.0136215	-0.0136215	1	0.2887345	2.704024	3.58E-07	4.123388	8
68	12	22	6328.125	0.2746572	0.0147918	-0.0147918	1	0.2750552	3.082721	1.97E-07	4.123197	8
69	13	24	5015.625	0.2900443	0.0103116	-0.0103116	1	0.2902276	2.036117	1.20E-07	4.123008	8
70	14	25	3984.375	0.2942255	0.0061763	-0.0061763	1	0.2942903	1.202559	1.96E-07	4.122842	8
93	37	61	19.86229	0.3062165	-0.0007164	0.0007164	1	0.3062174	-0.1340466	8.53E-08	4.119919	8
94	38	62	15.625	0.3093848	-0.0007009	0.0007009	1	0.3093856	-0.1298063	7.80E-08	4.119829	8
95	39	64	12.40079	0.3186038	-0.0009912	0.0009912	1	0.3186054	-0.1782466	7.77E-08	4.119737	8
96	40	65	9.93114	0.3165152	-0.009431	0.009431	1	0.3166556	-1.706693	7.78E-08	4.119651	8
97	41	67	7.944915	0.3191121	-0.0058505	0.0058505	1	0.3191657	-1.05032	7.64E-08	4.119545	8
98	42	69	6.317385	0.3210998	-0.0092228	0.0092228	1	0.3212323	-1.645235	7.69E-08	4.119417	8
99	43	71	5.008013	0.3278409	-0.00216	0.00216	1	0.327848	-0.3774863	7.59E-08	4.119261	8
100	44	74	3.945707	0.3354447	-0.0025546	0.0025546	1	0.3354544	-0.4363361	7.85E-08	4.119072	8
101	45	77	3.158693	0.336215	-0.0036519	0.0036519	1	0.3362348	-0.6223158	7.78E-08	4.118881	8
102	46	81	2.504006	0.3391236	0.026608	-0.026608	1	0.3401658	4.486292	8.00E-08	4.118692	8
103	47	86	1.998082	0.3440786	0.0231032	-0.0231032	1	0.3448534	3.841374	7.49E-08	4.118445	8
104	48	91	1.584686	0.3646946	0.0207792	-0.0207792	1	0.3652861	3.26102	7.77E-08	4.118161	8
105	49	97	1.266892	0.3762045	0.0274952	-0.0274952	1	0.3772079	4.180073	7.50E-08	4.117815	8
106	50	105	0.999041	0.3964183	0.018072	-0.018072	1	0.39683	2.610203	7.65E-08	4.117508	8

Appendix A5: Potentiostat Sample Data (Cell #89)

	B	C	D	E	F	G	H	I	J	K	L
59	Pt	T	Vf	Im	Vu	Pwr	Sig	Ach	Temp	IERange	Over
60	#	s	V	A	V	W	V	V	deg C	#	bits
61	0	5	3.43E+00	5.00E-01	0.00E+00	1.71E+00	2.50E+00	-1.19E-04	-3.28E+02	11	.....a
62	1	10	3.44E+00	5.00E-01	0.00E+00	1.72E+00	2.50E+00	-1.17E-04	-3.28E+02	11	.....a
63	2	15	3.45E+00	5.00E-01	0.00E+00	1.72E+00	2.50E+00	-1.20E-04	-3.28E+02	11	.....a
64	3	20	3.45E+00	5.00E-01	0.00E+00	1.72E+00	2.50E+00	-1.16E-04	-3.28E+02	11	.....a
65	4	25	3.45E+00	5.00E-01	0.00E+00	1.73E+00	2.50E+00	-1.19E-04	-3.28E+02	11	.....a
66	5	30	3.46E+00	5.00E-01	0.00E+00	1.73E+00	2.50E+00	-1.18E-04	-3.28E+02	11	.....a
67	6	35	3.46E+00	5.00E-01	0.00E+00	1.73E+00	2.50E+00	-1.20E-04	-3.28E+02	11	.....a
68	7	40	3.46E+00	5.00E-01	0.00E+00	1.73E+00	2.50E+00	-1.14E-04	-3.28E+02	11	.....a
69	8	45	3.46E+00	5.00E-01	0.00E+00	1.73E+00	2.50E+00	-1.16E-04	-3.28E+02	11	.....a
70	9	50	3.47E+00	5.00E-01	0.00E+00	1.73E+00	2.50E+00	-1.17E-04	-3.28E+02	11	.....a
71	10	55	3.47E+00	5.00E-01	0.00E+00	1.73E+00	2.50E+00	-1.12E-04	-3.28E+02	11	.....a
72	11	60	3.47E+00	5.00E-01	0.00E+00	1.73E+00	2.50E+00	-1.09E-04	-3.28E+02	11	.....a
73	12	65	3.47E+00	5.00E-01	0.00E+00	1.74E+00	2.50E+00	-1.11E-04	-3.28E+02	11	.....a
74	13	70	3.47E+00	5.00E-01	0.00E+00	1.74E+00	2.50E+00	-1.18E-04	-3.28E+02	11	.....a
75	14	75	3.47E+00	5.00E-01	0.00E+00	1.74E+00	2.50E+00	-1.13E-04	-3.28E+02	11	.....a
76	15	80	3.48E+00	5.00E-01	0.00E+00	1.74E+00	2.50E+00	-1.12E-04	-3.28E+02	11	.....a
4212	4151	20755	4.20E+00	2.37E-01	0.00E+00	9.97E-01	1.19E+00	-5.67E-05	-3.28E+02	11	.....a
4213	4152	20760	4.20E+00	2.37E-01	0.00E+00	9.96E-01	1.19E+00	-5.80E-05	-3.28E+02	11	.....a
4214	4153	20765	4.20E+00	2.37E-01	0.00E+00	9.95E-01	1.18E+00	-5.91E-05	-3.28E+02	11	.....a
4215	4154	20770	4.20E+00	2.37E-01	0.00E+00	9.94E-01	1.18E+00	-5.87E-05	-3.28E+02	11	.....a
4216	4155	20775	4.20E+00	2.36E-01	0.00E+00	9.93E-01	1.18E+00	-5.64E-05	-3.28E+02	11	.....a
4217	4156	20780	4.20E+00	2.36E-01	0.00E+00	9.92E-01	1.18E+00	-5.90E-05	-3.28E+02	11	.....a
4218	4157	20785	4.20E+00	2.36E-01	0.00E+00	9.91E-01	1.18E+00	-5.84E-05	-3.28E+02	11	.....a
4219	4158	20790	4.20E+00	2.36E-01	0.00E+00	9.90E-01	1.18E+00	-5.69E-05	-3.28E+02	11	.....a
4220	4159	20795	4.20E+00	2.35E-01	0.00E+00	9.89E-01	1.18E+00	-5.81E-05	-3.28E+02	11	.....a
4221	4160	20800	4.20E+00	2.35E-01	0.00E+00	9.88E-01	1.18E+00	-5.65E-05	-3.28E+02	11	.....a
4222	4161	20805	4.20E+00	2.35E-01	0.00E+00	9.87E-01	1.17E+00	-5.81E-05	-3.28E+02	11	.....a
4223	4162	20810	4.20E+00	2.35E-01	0.00E+00	9.86E-01	1.17E+00	-6.13E-05	-3.28E+02	11	.....a
4224	4163	20815	4.20E+00	2.35E-01	0.00E+00	9.85E-01	1.17E+00	-6.18E-05	-3.28E+02	11	.....a
4225	4164	20820	4.20E+00	2.34E-01	0.00E+00	9.84E-01	1.17E+00	-6.02E-05	-3.28E+02	11	.....a
4226	4165	20825	4.20E+00	2.34E-01	0.00E+00	9.83E-01	1.17E+00	-6.01E-05	-3.28E+02	11	.....a
4227	4166	20830	4.20E+00	2.34E-01	0.00E+00	9.82E-01	1.17E+00	-5.96E-05	-3.28E+02	11	.....a
4228	4167	20835	4.20E+00	2.34E-01	0.00E+00	9.81E-01	1.17E+00	-6.01E-05	-3.28E+02	11	.....a
4229	4168	20840	4.20E+00	2.33E-01	0.00E+00	9.80E-01	1.17E+00	-5.74E-05	-3.28E+02	11	.....a
4230	4169	20845	4.20E+00	2.33E-01	0.00E+00	9.79E-01	1.17E+00	-6.11E-05	-3.28E+02	11	.....a
4231	4170	20850	4.20E+00	2.33E-01	0.00E+00	9.78E-01	1.16E+00	-5.75E-05	-3.28E+02	11	.....a
4232	4171	20855	4.20E+00	2.33E-01	0.00E+00	9.77E-01	1.16E+00	-5.51E-05	-3.28E+02	11	.....a
4233	4172	20858.3	4.20E+00	2.32E-01	0.00E+00	9.76E-01	1.16E+00	-5.92E-05	-3.28E+02	11	.....a

Appendix A6: Potentiostat Sample Data (Cell #94)

	B	C	D	E	F	G	H	I	J	K	L
59	Pt	T	Vf	Im	Vu	Pwr	Sig	Ach	Temp	IERange	Over
60	#	s	V	A	V	W	V	V	deg C	#	bits
61	0	5	3.59E+00	5.00E-01	0.00E+00	1.80E+00	2.50E+00	-1.26E-04	-3.28E+02	11	.....a
62	1	10	3.61E+00	5.00E-01	0.00E+00	1.81E+00	2.50E+00	-1.26E-04	-3.28E+02	11	.....a
63	2	15	3.62E+00	5.00E-01	0.00E+00	1.81E+00	2.50E+00	-1.23E-04	-3.28E+02	11	.....a
64	3	20	3.62E+00	5.00E-01	0.00E+00	1.81E+00	2.50E+00	-1.26E-04	-3.28E+02	11	.....a
65	4	25	3.63E+00	5.00E-01	0.00E+00	1.81E+00	2.50E+00	-1.27E-04	-3.28E+02	11	.....a
66	5	30	3.63E+00	5.00E-01	0.00E+00	1.82E+00	2.50E+00	-1.30E-04	-3.28E+02	11	.....a
67	6	35	3.64E+00	5.00E-01	0.00E+00	1.82E+00	2.50E+00	-1.35E-04	-3.28E+02	11	.....a
68	7	40	3.64E+00	5.00E-01	0.00E+00	1.82E+00	2.50E+00	-1.37E-04	-3.28E+02	11	.....a
69	8	45	3.65E+00	5.00E-01	0.00E+00	1.82E+00	2.50E+00	-1.36E-04	-3.28E+02	11	.....a
70	9	50	3.65E+00	5.00E-01	0.00E+00	1.83E+00	2.50E+00	-1.37E-04	-3.28E+02	11	.....a
71	10	55	3.66E+00	5.00E-01	0.00E+00	1.83E+00	2.50E+00	-1.32E-04	-3.28E+02	11	.....a
72	11	60	3.66E+00	5.00E-01	0.00E+00	1.83E+00	2.50E+00	-1.34E-04	-3.28E+02	11	.....a
73	12	65	3.66E+00	5.00E-01	0.00E+00	1.83E+00	2.50E+00	-1.36E-04	-3.28E+02	11	.....a
2041	1980	9900	4.20E+00	2.43E-01	0.00E+00	1.02E+00	1.21E+00	-1.01E-04	-3.28E+02	11	.....a
2042	1981	9905	4.20E+00	2.43E-01	0.00E+00	1.02E+00	1.21E+00	-1.05E-04	-3.28E+02	11	.....a
2043	1982	9910	4.20E+00	2.42E-01	0.00E+00	1.02E+00	1.21E+00	-1.03E-04	-3.28E+02	11	.....a
2044	1983	9915	4.20E+00	2.42E-01	0.00E+00	1.02E+00	1.21E+00	-9.99E-05	-3.28E+02	11	.....a
2045	1984	9920	4.20E+00	2.42E-01	0.00E+00	1.02E+00	1.21E+00	-1.01E-04	-3.28E+02	11	.....a
2046	1985	9925	4.20E+00	2.42E-01	0.00E+00	1.02E+00	1.21E+00	-1.00E-04	-3.28E+02	11	.....a
2047	1986	9930	4.20E+00	2.42E-01	0.00E+00	1.01E+00	1.21E+00	-1.03E-04	-3.28E+02	11	.....a
2048	1987	9935	4.20E+00	2.41E-01	0.00E+00	1.01E+00	1.21E+00	-1.03E-04	-3.28E+02	11	.....a
2049	1988	9940	4.20E+00	2.41E-01	0.00E+00	1.01E+00	1.21E+00	-9.93E-05	-3.28E+02	11	.....a
2050	1989	9945	4.20E+00	2.41E-01	0.00E+00	1.01E+00	1.20E+00	-1.02E-04	-3.28E+02	11	.....a
2051	1990	9950	4.20E+00	2.41E-01	0.00E+00	1.01E+00	1.20E+00	-1.00E-04	-3.28E+02	11	.....a
2052	1991	9955	4.20E+00	2.41E-01	0.00E+00	1.01E+00	1.20E+00	-1.02E-04	-3.28E+02	11	.....a
2053	1992	9959.2	4.20E+00	2.40E-01	0.00E+00	1.01E+00	1.20E+00	-1.04E-04	-3.28E+02	11	.....a

Appendix A7: Potentiostat Sample Data (Cell #107)

	B	C	D	E	F	G	H	I	J	K	L
59	Pt	T	Vf	Im	Vu	Pwr	Sig	Ach	Temp	IERange	Over
60	#	s	V	A	V	W	V	V	deg C	#	bits
61	0	5	3.37E+00	5.00E-01	0.00E+00	1.69E+00	2.50E+00	-1.68E-04	-3.28E+02	11	.....a
62	1	10	3.38E+00	5.00E-01	0.00E+00	1.69E+00	2.50E+00	-1.67E-04	-3.28E+02	11	.....a
63	2	15	3.39E+00	5.00E-01	0.00E+00	1.70E+00	2.50E+00	-1.63E-04	-3.28E+02	11	.....a
64	3	20	3.40E+00	5.00E-01	0.00E+00	1.70E+00	2.50E+00	-1.65E-04	-3.28E+02	11	.....a
65	4	25	3.41E+00	5.00E-01	0.00E+00	1.70E+00	2.50E+00	-1.65E-04	-3.28E+02	11	.....a
66	5	30	3.42E+00	5.00E-01	0.00E+00	1.71E+00	2.50E+00	-1.65E-04	-3.28E+02	11	.....a
67	6	35	3.42E+00	5.00E-01	0.00E+00	1.71E+00	2.50E+00	-1.72E-04	-3.28E+02	11	.....a
68	7	40	3.43E+00	5.00E-01	0.00E+00	1.71E+00	2.50E+00	-1.75E-04	-3.28E+02	11	.....a
69	8	45	3.44E+00	5.00E-01	0.00E+00	1.72E+00	2.50E+00	-1.79E-04	-3.28E+02	11	.....a
70	9	50	3.44E+00	5.00E-01	0.00E+00	1.72E+00	2.50E+00	-1.76E-04	-3.28E+02	11	.....a
71	10	55	3.45E+00	5.00E-01	0.00E+00	1.72E+00	2.50E+00	-1.77E-04	-3.28E+02	11	.....a
72	11	60	3.45E+00	5.00E-01	0.00E+00	1.73E+00	2.50E+00	-1.76E-04	-3.28E+02	11	.....a
73	12	65	3.46E+00	5.00E-01	0.00E+00	1.73E+00	2.50E+00	-1.75E-04	-3.28E+02	11	.....a
74	13	70	3.46E+00	5.00E-01	0.00E+00	1.73E+00	2.50E+00	-1.73E-04	-3.28E+02	11	.....a
75	14	75	3.47E+00	5.00E-01	0.00E+00	1.73E+00	2.50E+00	-1.69E-04	-3.28E+02	11	.....a
76	15	80	3.47E+00	5.00E-01	0.00E+00	1.74E+00	2.50E+00	-1.71E-04	-3.28E+02	11	.....a
3219	3158	15790	4.20E+00	1.55E-01	0.00E+00	6.51E-01	7.75E-01	-9.70E-05	-3.28E+02	11	.....a
3220	3159	15795	4.20E+00	1.55E-01	0.00E+00	6.50E-01	7.74E-01	-9.89E-05	-3.28E+02	11	.....a
3221	3160	15800	4.20E+00	1.54E-01	0.00E+00	6.49E-01	7.72E-01	-9.71E-05	-3.28E+02	11	.....a
3222	3161	15805	4.20E+00	1.54E-01	0.00E+00	6.48E-01	7.71E-01	-9.74E-05	-3.28E+02	11	.....a
3223	3162	15810	4.20E+00	1.54E-01	0.00E+00	6.47E-01	7.70E-01	-9.53E-05	-3.28E+02	11	.....a
3224	3163	15815	4.20E+00	1.54E-01	0.00E+00	6.46E-01	7.69E-01	-9.71E-05	-3.28E+02	11	.....a
3225	3164	15820	4.20E+00	1.54E-01	0.00E+00	6.45E-01	7.67E-01	-9.64E-05	-3.28E+02	11	.....a
3226	3165	15825	4.20E+00	1.53E-01	0.00E+00	6.44E-01	7.66E-01	-9.69E-05	-3.28E+02	11	.....a
3227	3166	15830	4.20E+00	1.53E-01	0.00E+00	6.43E-01	7.65E-01	-9.73E-05	-3.28E+02	11	.....a
3228	3167	15835	4.20E+00	1.53E-01	0.00E+00	6.42E-01	7.64E-01	-9.81E-05	-3.28E+02	11	.....a
3229	3168	15840	4.20E+00	1.53E-01	0.00E+00	6.41E-01	7.63E-01	-1.02E-04	-3.28E+02	11	.....a
3230	3169	15845	4.20E+00	1.52E-01	0.00E+00	6.40E-01	7.61E-01	-9.92E-05	-3.28E+02	11	.....a
3231	3170	15850	4.20E+00	1.52E-01	0.00E+00	6.39E-01	7.60E-01	-9.71E-05	-3.28E+02	11	.....a
3232	3171	15855	4.20E+00	1.52E-01	0.00E+00	6.37E-01	7.59E-01	-1.00E-04	-3.28E+02	11	.....a
3233	3172	15860	4.20E+00	1.52E-01	0.00E+00	6.37E-01	7.58E-01	-1.02E-04	-3.28E+02	11	.....a
3234	3173	15865	4.20E+00	1.51E-01	0.00E+00	6.36E-01	7.57E-01	-9.61E-05	-3.28E+02	11	.....a
3235	3174	15870	4.20E+00	1.51E-01	0.00E+00	6.35E-01	7.55E-01	-9.60E-05	-3.28E+02	11	.....a
3236	3175	15872.5	4.20E+00	1.51E-01	0.00E+00	6.34E-01	7.54E-01	-9.63E-05	-3.28E+02	11	.....a

Appendix A8: Potentiostat Sample Data (Cell #109)

	B	C	D	E	F	G	H	I	J	K	L
58	TABLE	3193									
59	Pt	T	Vf	Im	Vu	Pwr	Sig	Ach	Temp	IERange	Over
60	#	s	V	A	V	W	V	V	deg C	#	bits
61	0	5	3.37E+00	5.00E-01	0.00E+00	1.69E+00	2.50E+00	-1.41E-04	-3.28E+02	11	.....a
62	1	10	3.38E+00	5.00E-01	0.00E+00	1.69E+00	2.50E+00	-1.47E-04	-3.28E+02	11	.....a
63	2	15	3.39E+00	5.00E-01	0.00E+00	1.70E+00	2.50E+00	-1.48E-04	-3.28E+02	11	.....a
64	3	20	3.40E+00	5.00E-01	0.00E+00	1.70E+00	2.50E+00	-1.49E-04	-3.28E+02	11	.....a
65	4	25	3.41E+00	5.00E-01	0.00E+00	1.70E+00	2.50E+00	-1.52E-04	-3.28E+02	11	.....a
66	5	30	3.42E+00	5.00E-01	0.00E+00	1.71E+00	2.50E+00	-1.52E-04	-3.28E+02	11	.....a
67	6	35	3.42E+00	5.00E-01	0.00E+00	1.71E+00	2.50E+00	-1.55E-04	-3.28E+02	11	.....a
68	7	40	3.43E+00	5.00E-01	0.00E+00	1.71E+00	2.50E+00	-1.58E-04	-3.28E+02	11	.....a
69	8	45	3.44E+00	5.00E-01	0.00E+00	1.72E+00	2.50E+00	-1.58E-04	-3.28E+02	11	.....a
70	9	50	3.44E+00	5.00E-01	0.00E+00	1.72E+00	2.50E+00	-1.52E-04	-3.28E+02	11	.....a
71	10	55	3.45E+00	5.00E-01	0.00E+00	1.72E+00	2.50E+00	-1.53E-04	-3.28E+02	11	.....a
72	11	60	3.45E+00	5.00E-01	0.00E+00	1.73E+00	2.50E+00	-1.53E-04	-3.28E+02	11	.....a
73	12	65	3.46E+00	5.00E-01	0.00E+00	1.73E+00	2.50E+00	-1.54E-04	-3.28E+02	11	.....a
74	13	70	3.46E+00	5.00E-01	0.00E+00	1.73E+00	2.50E+00	-1.54E-04	-3.28E+02	11	.....a
75	14	75	3.47E+00	5.00E-01	0.00E+00	1.73E+00	2.50E+00	-1.47E-04	-3.28E+02	11	.....a
76	15	80	3.47E+00	5.00E-01	0.00E+00	1.74E+00	2.50E+00	-1.51E-04	-3.28E+02	11	.....a
3235	3174	15870	4.20E+00	1.51E-01	0.00E+00	6.33E-01	7.54E-01	-7.21E-05	-3.28E+02	11	.....a
3236	3175	15875	4.20E+00	1.51E-01	0.00E+00	6.32E-01	7.53E-01	-7.21E-05	-3.28E+02	11	.....a
3237	3176	15880	4.20E+00	1.50E-01	0.00E+00	6.31E-01	7.51E-01	-7.18E-05	-3.28E+02	11	.....a
3238	3177	15885	4.20E+00	1.50E-01	0.00E+00	6.30E-01	7.50E-01	-7.11E-05	-3.28E+02	11	.....a
3239	3178	15890	4.20E+00	1.50E-01	0.00E+00	6.29E-01	7.49E-01	-7.48E-05	-3.28E+02	11	.....a
3240	3179	15895	4.20E+00	1.50E-01	0.00E+00	6.28E-01	7.48E-01	-7.11E-05	-3.28E+02	11	.....a
3241	3180	15900	4.20E+00	1.49E-01	0.00E+00	6.27E-01	7.46E-01	-7.17E-05	-3.28E+02	11	.....a
3242	3181	15905	4.20E+00	1.49E-01	0.00E+00	6.26E-01	7.45E-01	-7.28E-05	-3.28E+02	11	.....a
3243	3182	15910	4.20E+00	1.49E-01	0.00E+00	6.25E-01	7.44E-01	-7.21E-05	-3.28E+02	11	.....a
3244	3183	15915	4.20E+00	1.49E-01	0.00E+00	6.24E-01	7.43E-01	-7.69E-05	-3.28E+02	11	.....a
3245	3184	15920	4.20E+00	1.48E-01	0.00E+00	6.23E-01	7.42E-01	-7.51E-05	-3.28E+02	11	.....a
3246	3185	15925	4.20E+00	1.48E-01	0.00E+00	6.22E-01	7.40E-01	-7.31E-05	-3.28E+02	11	.....a
3247	3186	15930	4.20E+00	1.48E-01	0.00E+00	6.21E-01	7.39E-01	-7.46E-05	-3.28E+02	11	.....a
3248	3187	15935	4.20E+00	1.48E-01	0.00E+00	6.20E-01	7.38E-01	-7.31E-05	-3.28E+02	11	.....a
3249	3188	15940	4.20E+00	1.47E-01	0.00E+00	6.19E-01	7.37E-01	-7.56E-05	-3.28E+02	11	.....a
3250	3189	15945	4.20E+00	1.47E-01	0.00E+00	6.18E-01	7.36E-01	-7.40E-05	-3.28E+02	11	.....a
3251	3190	15950	4.20E+00	1.47E-01	0.00E+00	6.17E-01	7.35E-01	-7.32E-05	-3.28E+02	11	.....a
3252	3191	15955	4.20E+00	1.47E-01	0.00E+00	6.16E-01	7.33E-01	-7.22E-05	-3.28E+02	11	.....a
3253	3192	15958	4.20E+00	1.46E-01	0.00E+00	6.15E-01	7.32E-01	-7.23E-05	-3.28E+02	11	.....a

Appendix A9: Potentiostat Sample Data (Cell #110)

	B	C	D	E	F	G	H	I	J	K	L
59	Pt	T	Vf	Im	Vu	Pwr	Sig	Ach	Temp	IERange	Over
60	#	s	V	A	V	W	V	V	deg C	#	bits
61	0	5	3.37E+00	5.00E-01	0.00E+00	1.68E+00	2.50E+00	-1.55E-04	-3.28E+02	11	.....a
62	1	10	3.38E+00	5.00E-01	0.00E+00	1.69E+00	2.50E+00	-1.51E-04	-3.28E+02	11	.....a
63	2	15	3.39E+00	5.00E-01	0.00E+00	1.69E+00	2.50E+00	-1.52E-04	-3.28E+02	11	.....a
64	3	20	3.40E+00	5.00E-01	0.00E+00	1.70E+00	2.50E+00	-1.53E-04	-3.28E+02	11	.....a
65	4	25	3.41E+00	5.00E-01	0.00E+00	1.70E+00	2.50E+00	-1.56E-04	-3.28E+02	11	.....a
66	5	30	3.41E+00	5.00E-01	0.00E+00	1.71E+00	2.50E+00	-1.55E-04	-3.28E+02	11	.....a
67	6	35	3.42E+00	5.00E-01	0.00E+00	1.71E+00	2.50E+00	-1.56E-04	-3.28E+02	11	.....a
68	7	40	3.43E+00	5.00E-01	0.00E+00	1.71E+00	2.50E+00	-1.60E-04	-3.28E+02	11	.....a
69	8	45	3.43E+00	5.00E-01	0.00E+00	1.72E+00	2.50E+00	-1.66E-04	-3.28E+02	11	.....a
70	9	50	3.44E+00	5.00E-01	0.00E+00	1.72E+00	2.50E+00	-1.67E-04	-3.28E+02	11	.....a
71	10	55	3.44E+00	5.00E-01	0.00E+00	1.72E+00	2.50E+00	-1.62E-04	-3.28E+02	11	.....a
72	11	60	3.45E+00	5.00E-01	0.00E+00	1.72E+00	2.50E+00	-1.60E-04	-3.28E+02	11	.....a
73	12	65	3.46E+00	5.00E-01	0.00E+00	1.73E+00	2.50E+00	-1.58E-04	-3.28E+02	11	.....a
74	13	70	3.46E+00	5.00E-01	0.00E+00	1.73E+00	2.50E+00	-1.53E-04	-3.28E+02	11	.....a
75	14	75	3.47E+00	5.00E-01	0.00E+00	1.73E+00	2.50E+00	-1.56E-04	-3.28E+02	11	.....a
76	15	80	3.47E+00	5.00E-01	0.00E+00	1.74E+00	2.50E+00	-1.56E-04	-3.28E+02	11	.....a
3227	3166	15830	4.20E+00	1.55E-01	0.00E+00	6.51E-01	7.75E-01	-8.10E-05	-3.28E+02	11	.....a
3228	3167	15835	4.20E+00	1.55E-01	0.00E+00	6.50E-01	7.73E-01	-8.28E-05	-3.28E+02	11	.....a
3229	3168	15840	4.20E+00	1.54E-01	0.00E+00	6.49E-01	7.72E-01	-8.22E-05	-3.28E+02	11	.....a
3230	3169	15845	4.20E+00	1.54E-01	0.00E+00	6.48E-01	7.71E-01	-8.24E-05	-3.28E+02	11	.....a
3231	3170	15850	4.20E+00	1.54E-01	0.00E+00	6.47E-01	7.70E-01	-7.91E-05	-3.28E+02	11	.....a
3232	3171	15855	4.20E+00	1.54E-01	0.00E+00	6.45E-01	7.68E-01	-8.31E-05	-3.28E+02	11	.....a
3233	3172	15860	4.20E+00	1.53E-01	0.00E+00	6.44E-01	7.67E-01	-8.17E-05	-3.28E+02	11	.....a
3234	3173	15865	4.20E+00	1.53E-01	0.00E+00	6.44E-01	7.66E-01	-8.34E-05	-3.28E+02	11	.....a
3235	3174	15870	4.20E+00	1.53E-01	0.00E+00	6.42E-01	7.65E-01	-8.51E-05	-3.28E+02	11	.....a
3236	3175	15875	4.20E+00	1.53E-01	0.00E+00	6.41E-01	7.64E-01	-8.20E-05	-3.28E+02	11	.....a
3237	3176	15880	4.20E+00	1.52E-01	0.00E+00	6.40E-01	7.62E-01	-7.75E-05	-3.28E+02	11	.....a
3238	3177	15885	4.20E+00	1.52E-01	0.00E+00	6.40E-01	7.61E-01	-7.88E-05	-3.28E+02	11	.....a
3239	3178	15890	4.20E+00	1.52E-01	0.00E+00	6.39E-01	7.60E-01	-7.70E-05	-3.28E+02	11	.....a
3240	3179	15894.5	4.20E+00	1.52E-01	0.00E+00	6.38E-01	7.59E-01	-7.90E-05	-3.28E+02	11	.....a

Appendix B1: Leaching Conditions Calculator

	A	B	C	D	E	F	G	H	I
1	NMC-HCl			NMC-Acid-Mix					
2	Pulp Density	5%		5%					
3	Cathode Mass	5.125	g	5.100	g				
4	Cathode Proportion to Cell	5.7%		5.7%					
5									
6									
7	LCO	% Cathode	Mass (g)	Concentration (g/L)	Dilute 1:10 (g/l) (1 part sample 9 parts HCl)	Dilute 1:30 (g/l) (.5 ml sample 9.5 ml HCl)	PPM	Molar Mass (g/mol)	Conc. (molL-1)
8	Co	17.885	1.018451389	9.936	0.99	0.033	33.12	58.933	0.017
9									
10	NMC	% Cathode	Mass (g)	Concentration (g/L)	Dilute 1:10 (g/l) (1 part sample 9 parts HCl)	Dilute 1:30 (g/l) (.5 ml sample 9.5 ml HCl)	PPM	Molar Mass (g/mol)	Conc. (molL-1)
11	Li	0.076	0.3895	3.800	0.38	0.013	12.67	6.941	0.055
12	Co	0.2048	1.0496	10.240	1.02	0.034	34.13	58.933	0.017
13	Ni	0.1935	0.9916875	9.675	0.97	0.032	32.25	58.693	0.016
14	Mn	0.1947	0.9978375	9.735	0.97	0.032	32.45	54.938	0.018
15									
16	NMC-MIX	% Cathode	Mass (g)	Concentration (g/L)	Dilute 1:10 (g/l) (1 part sample 9 parts Acid-Mix)	Dilute 1:30 (g/l) (.5 ml sample 9.5 ml Acid-Mix)	PPM	Molar Mass (g/mol)	Conc. (molL-1)
17	Li	0.076	0.3895	3.800	0.38	0.013	12.67	6.941	0.055
18	Co	0.2048	1.0496	10.240	1.02	0.034	34.13	58.933	0.017
19	Ni	0.1935	0.9916875	9.675	0.97	0.032	32.25	58.693	0.016
20	Mn	0.1947	0.9978375	9.735	0.97	0.032	32.45	54.938	0.018

Appendix B2: Leaching Dilution Calculator

	A	B	C	D
23	**Dilution Calculator**			
24	Volume HCl	10	ml	Volume Concentrated Acid added
25	Required HCl Concentration	4%	%vol	
26	Initial Concentration	37%	%w/w	Grams of HCl in 100 g
27	Distilled Water	92.5	ml	Distilled Water
28		1.2945694	mol/L	
29				
30	Volume H2O2	12.0	ml	Volume Concentrated Acid added
31	Required H2O2 Concentration	4%	%vol	
32	Initial Concentration	30%	%w/w	Grams of H2O2 in 100 g
33		1.3		Distilled Water
34				
35	**Molarity Calculator**			
36	Density	1.2	g/mL	
37	Weight %	37%	%w/w	Grams of HCl in 100 g
38	Molecular Weight	36.46	g/mol	
39	Concentration	12.2	M	
40				
41	Density	1.8	g/mL	
42	Weight %	4%	%w/w	Grams of H2SO4 in 100 g
43	Molecular Weight	36.46	g/mol	
44	Concentration	2.0	M	
45	Volume	90	ml	

Appendix B3: MP-AES Data (LCO-HCl)

	A	B	C	D	E	F	G	H	I	J	K	L
1	Label	Type	Date Time	Element	Element Label	Flags	Unadjusted Data	Concentration	Unit	Intensity	Concentration SD	Concentration %RSD
2	Blank	BLK	2/10/2020 10:08	Co 340.512	Co		0	0	ppm	0	-	-
3	Standard 1	STD	2/10/2020 10:10	Co 340.512	Co		1	1	ppm	6232.58	-	-
4	Standard 2	STD	2/10/2020 10:12	Co 340.512	Co		1	1	ppm	12404.06	-	-
5	Standard 3	STD	2/10/2020 10:15	Co 340.512	Co		2	2	ppm	25005.37	-	-
6	Standard 4	STD	2/10/2020 10:17	Co 340.512	Co		5	5	ppm	62639.69	-	-
7	Standard 5	STD	2/10/2020 10:19	Co 340.512	Co		10	10	ppm	124055.16	-	-
8	Standard 6	STD	2/10/2020 10:21	Co 340.512	Co		25	25	ppm	313703.16	-	-
9	Standard 7	STD	2/10/2020 10:24	Co 340.512	Co		50	50	ppm	623427.59	-	-
10	5 ppm reference	Sample	2/10/2020 10:26	Co 340.512	Co		5.26	5.26	ppm	65543.82	0.02	0.45
11	2min	Sample	2/10/2020 10:28	Co 340.512	Co		2.650	2.65	ppm	33003.34	0.01	0.31
12	5min	Sample	2/10/2020 10:30	Co 340.512	Co		6.07	6.07	ppm	75691.06	0.07	1.08
13	10min	Sample	2/10/2020 10:33	Co 340.512	Co		13.13	13.13	ppm	163688.9	0.15	1.18
14	15min	Sample	2/10/2020 10:35	Co 340.512	Co		18.33	18.33	ppm	228577.75	0.21	1.13
15	30min	Sample	2/10/2020 10:37	Co 340.512	Co		26.69	26.69	ppm	332685.24	0.18	0.67
16	60min	Sample	2/10/2020 10:39	Co 340.512	Co		31.4	31.4	ppm	391408.83	0.06	0.2
17	120min	Sample	2/10/2020 10:42	Co 340.512	Co		30.7	30.7	ppm	382701.32	0.37	1.2
18	24hr	Sample	2/10/2020 10:45	Co 340.512	Co		33.12	33.12	ppm	398223.64	0.16	1.02

	M	N	O	P	Q	R	S	T	U	V	W	X	Y
1	Intensity SD	Intensity %RSD	Weight	Volume	Dilution	Internal Standard	Replicates	Concentration Replicate 1	Concentration Replicate 2	Concentration Replicate 3	Intensity Replicate 1	Intensity Replicate 2	Intensity Replicate 3
2	18.78	> 100.00	-	-	-	-	3	0.000	0.000	0.000	21	-4	-16
3	17.37	0.28	-	-	-	-	3	0.500	0.500	0.500	6234	6249	6215
4	248.03	2	-	-	-	-	3	1.000	1.000	1.000	12131	12466	12615
5	348.34	1.39	-	-	-	-	3	2.000	2.000	2.000	24643	25036	25337
6	1070.87	1.71	-	-	-	-	3	5.000	5.000	5.000	61410	63139	63370
7	1825.41	1.47	-	-	-	-	3	10.000	10.000	10.000	122024	124585	125557
8	5202.35	1.66	-	-	-	-	3	25.000	25.000	25.000	308245	314258	318606
9	6722.87	1.08	-	-	-	-	3	50.000	50.000	50.000	615931	628921	625431
10	296.72	0.45	1	1	1	-	3	5.240	5.240	5.280	65381	65364	65886
11	103.7	0.31	1	1	1	-	3	2.650	2.640	2.660	32978	32915	33117
12	817.36	1.08	1	1	1	-	3	6.000	6.090	6.130	74783	75924	76367
13	1926.18	1.18	1	1	1	-	3	13.050	13.030	13.310	162690	162468	165909
14	2591.68	1.13	1	1	1	-	3	18.120	18.350	18.530	225890	228781	231062
15	2218.08	0.67	1	1	1	-	3	26.550	26.620	26.890	331021	331832	335203
16	763.99	0.2	1	1	1	-	3	31.370	31.350	31.460	391141	390815	392271
17	4578.76	1.2	1	1	1	-	3	31.040	30.310	30.740	386989	377878	383237
18	905.6	1.02	1	1	1	-	3	33.200	33.230	33.190	398414	396604	399814

Appendix B4: MP-AES Results (LCO-HCl)

	A	B	C	D	E
20	Time (minutes)	Co 340.512 nm (ppm)	Conc. (g/L)	Intensity	% Leach
21	2	2.65	0.795	33003.34	8%
22	5	6.07	1.821	75691.06	18%
23	10	13.13	3.939	163688.9	40%
24	15	18.33	5.499	228577.75	55%
25	30	26.69	8.007	332685.24	81%
26	60	31.4	9.42	391408.83	95%
27	120	30.7	9.21	382701.32	93%
28	24hr	33.12	9.936	398223.64	

Appendix B5: MP-AES Data (NMC-HCl)

	A	B	C	D	E	F	G	H	I	J	K	L
3	Label	Type	Date Time	Element	Element Label	Flags	Unadjusted Data	Concentration	Unit	Intensity	Concentration SD	Concentration %RSD
4	5 ppm reference	Sample	2/10/2020 10:26	Co 340.512	Co		5.22	5.224	ppm	59183.38253	0.01	0.11
5	5 ppm reference	Sample	2/10/2020 10:26	Ni 361.939	Ni		5.12	5.116	ppm	43559.29941	0.05	0.96
6	5 ppm reference	Sample	2/10/2020 10:26	Mn 403.076	Mn		5.11	5.109	ppm	203185.4079	0.08	1.54
7	2min	Sample	2/10/2020 10:46	Co 340.512	Co		1.541	1.541	ppm	18135.14836	0.12	7.59
8	2min	Sample	2/10/2020 10:46	Ni 361.939	Ni		1.25	1.253	ppm	12339.19973	0.10	8.28
9	2min	Sample	2/10/2020 10:46	Mn 403.076	Mn		1.78	1.785	ppm	80876.06117	0.08	4.69
10	5min	Sample	2/10/2020 10:48	Co 340.512	Co		4.04	4.041	ppm	47648.30832	0.62	15.35
11	5min	Sample	2/10/2020 10:48	Ni 361.939	Ni		3.41	3.413	ppm	30682.52265	0.20	5.82
12	5min	Sample	2/10/2020 10:48	Mn 403.076	Mn		3.55	3.551	ppm	152936.6283	0.25	7.02
13	10min	Sample	2/10/2020 10:50	Co 340.512	Co		11.01	11.014	ppm	135434.1602	0.45	4.07
14	10min	Sample	2/10/2020 10:50	Ni 361.939	Ni		8.36	8.362	ppm	75476.08827	0.26	3.09
15	10min	Sample	2/10/2020 10:50	Mn 403.076	Mn		9.46	9.463	ppm	420783.2637	0.44	4.60
16	15min	Sample	2/10/2020 10:52	Co 340.512	Co		17.24	17.235	ppm	218289.9846	0.47	2.75
17	15min	Sample	2/10/2020 10:52	Ni 361.939	Ni		13.21	13.212	ppm	119808.9091	0.49	3.70
18	15min	Sample	2/10/2020 10:52	Mn 403.076	Mn		19.50	19.495	ppm	890288.3518	0.62	3.17
19	30min	Sample	2/10/2020 10:54	Co 340.512	Co		24.25	24.254	ppm	301963.5581	0.47	1.95
20	30min	Sample	2/10/2020 10:54	Ni 361.939	Ni		21.17	21.170	ppm	193685.6575	0.57	2.69
21	30min	Sample	2/10/2020 10:54	Mn 403.076	Mn		25.31	25.312	ppm	1158028.224	0.82	3.23
22	60min	Sample	2/10/2020 10:57	Co 340.512	Co		29.20	29.202	ppm	366210.0076	0.51	1.75
23	60min	Sample	2/10/2020 10:57	Ni 361.939	Ni		28.85	28.849	ppm	265904.258	0.24	0.84
24	60min	Sample	2/10/2020 10:57	Mn 403.076	Mn		26.99	26.990	ppm	1224441.296	0.70	2.60
25	120min	Sample	2/10/2020 10:59	Co 340.512	Co		30.82	30.824	ppm	388563.0252	0.52	1.69
26	120min	Sample	2/10/2020 10:59	Ni 361.939	Ni		29.68	29.675	ppm	274497.1273	0.22	0.73
27	120min	Sample	2/10/2020 10:59	Mn 403.076	Mn		28.01	28.009	ppm	1281273.115	0.28	1.01
28	24hr	Sample	2/10/2020 11:02	Co 340.512	Co		34.14	34.138	ppm	408563.0252	0.73	2.14
29	24hr	Sample	2/10/2020 11:02	Ni 361.939	Ni		32.26	32.259	ppm	294497.1273	0.68	2.11
30	24hr	Sample	2/10/2020 11:02	Mn 403.076	Mn		32.45	32.453	ppm	1331273.115	0.53	1.64

	M	N	O	P	Q	R	S	T	U	V	W	X	Y
3	Intensity SD	Intensity %RSD	Weight	Volume	Dilution	Internal Standard	Replicates	Concentration Replicate 1	Concentration Replicate 2	Concentration Replicate 3	Intensity Replicate 1	Intensity Replicate 2	Intensity Replicate 3
4	92.51	0.16	1	1	1	-	3	5.2309852	5.2172391	5.2241299	59230.05861	59265.88322	59054.20576
5	37.84	0.09	1	1	1	-	3	5.0555744	5.1152278	5.1759437	43610.06612	43548.55753	43519.27459
6	1111.94	0.55	1	1	1	-	3	5.0342157	5.0743697	5.2170831	202748.0197	202095.9972	204712.2068
7	702.71	3.87	1	1	1	-	3	1.4026221	1.5312174	1.6887668	19085.76477	17408.93667	17910.74365
8	44.96	0.36	1	1	1	-	3	1.169455008	1.399153525	1.190436142	12324.93322	12292.67678	12399.9892
9	1283.44	1.59	1	1	1	-	3	1.700814743	1.89904906	1.753920112	82040.35495	81499.78606	79088.0425
10	1567.41	3.29	1	1	1	-	3	3.964868829	4.836529361	3.32295462	47060.2834	46091.41527	49793.22631
11	1003.50	3.27	1	1	1	-	3	3.684972475	3.33749323	3.215898473	29994.58306	32101.46715	29951.51772
12	4161.01	2.72	1	1	1	-	3	3.301598766	3.460346677	3.891739952	149382.2095	150652.3557	158775.3198
13	142.43	0.11	1	1	1	-	3	10.8786135	11.61786714	10.54653199	135428.5542	135262.5859	135611.3406
14	896.87	1.19	1	1	1	-	3	8.271196084	8.100127992	8.714248567	75685.76407	74287.93029	76454.57047
15	6019.21	1.43	1	1	1	-	3	8.854442665	9.849573044	9.685411785	419930.0985	413874.9693	428544.7235
16	800.08	0.37	1	1	1	-	3	17.90558096	16.92780566	16.87164856	217163.3667	218762.5454	218944.0417
17	230.69	0.19	1	1	1	-	3	13.89711893	12.79283018	12.94639681	119664.6394	119627.6352	120134.4528
18	11745.97	1.32	1	1	1	-	3	18.62270142	19.96673682	19.89593857	876299.6524	889524.5555	905040.8476
19	5417.05	1.79	1	1	1	-	3	24.91494242	24.0215904	23.82598349	309602.7306	298642.9541	297644.9898
20	1192.47	0.62	1	1	1	-	3	21.97402146	20.82678824	20.70962164	194957.691	192090.7829	194008.4986
21	39497.18	3.41	1	1	1	-	3	24.15889187	25.946166	25.83204501	1106099.724	1201814.205	1166170.744
22	3692.45	1.01	1	1	1	-	3	29.92077416	28.77888175	28.90643571	369542.8071	368025.074	361062.1417
23	7659.94	2.88	1	1	1	-	3	29.10228727	28.52338181	28.92034905	276725.5722	260061.7758	260925.426
24	10190.04	0.83	1	1	1	-	3	26.50283607	27.98152206	26.48430996	1213698.042	1221494.733	1238131.112
25	3596.03	0.93	1	1	1	-	3	30.25846358	30.70106858	31.51370036	390555.5123	391618.8971	383514.6663
26	3929.06	1.43	1	1	1	-	3	29.83306114	29.82516039	29.36811962	273064.9449	270563.7094	279862.7274
27	3308.90	0.26	1	1	1	-	3	27.88025668	28.40177094	27.74641233	1282600.3	1276723.368	1284495.677
28	10657.01	2.61	1	1	1	-	3	33.30946358	34.02106858	35.08370036	408555.5123	421618.8971	395514.6663
29	9938.77	3.37	1	1	1	-	3	32.38306114	33.02516039	31.36811962	303064.9449	280563.7094	299862.7274
30	6199.67	0.47	1	1	1	-	3	32.88025583	31.70177094	32.77641233	1322600.3	1336723.368	1334495.677

Appendix B6: MP-AES Results (NMC-HCl)

	A	B	C	D	E
33	Time (minutes)	Co (340.512 nm)	Conc. (g/L)	Intensity	% Leach
34	2	1.541	0.46	18135	5%
35	5	4.041	1.21	47648	12%
36	10	11.014	3.30	135434	32%
37	15	17.235	5.17	218290	50%
38	30	24.254	7.28	301964	71%
39	60	29.202	8.76	366210	86%
40	120	30.824	9.25	388563	90%
41	24hr	34.138	10.24	408563	
42					
43		Ni (361.939 nm)	Conc. (g/L)		% Leach
44	2	1.253	0.38	12339	4%
45	5	3.413	1.02	30683	11%
46	10	8.362	2.51	75476	26%
47	15	13.212	3.96	119809	41%
48	30	21.170	6.35	193686	66%
49	60	28.849	8.65	265904	89%
50	120	29.675	8.90	274497	92%
51	24hr	32.26	9.68	294497	
52					
53		Mn (403.076 nm)	Conc. (g/L)		% Leach
54	2	1.78	0.54	80876	5%
55	5	3.55	1.07	152937	11%
56	10	9.463	2.84	420783	29%
57	15	19.495	5.85	890288	60%
58	30	25.312	7.59	1158028	78%
59	60	26.990	8.10	1224441	83%
60	120	28.009	8.40	1281273	86%
61	24hr	32.45	9.74	1331273	

Appendix B7: MP-AES Data (NMC-H2SO4-H2O2)

	A	B	C	D	E	F	G	H	I	J	K	L
3	Label	Type	Date Time	Element	Element Label	Flags	Unadjusted Data	Concentration	Unit	Intensity	Concentration SD	Concentration %RSD
4	5 ppm reference	Sample	2/10/2020 10:26	Co 340.512	Co		5.22	5.224	ppm	59183.38253	0.01	0.11
5	5 ppm reference	Sample	2/10/2020 10:26	Ni 361.939	Ni		5.12	5.116	ppm	43559.29941	0.05	0.96
6	5 ppm reference	Sample	2/10/2020 10:26	Mn 403.076	Mn		5.11	5.109	ppm	203185.4079	0.08	1.54
7	2min	Sample	2/10/2020 11:01	Co 340.512	Co		1.308	1.308	ppm	20150.16485	0.12	7.59
8	2min	Sample	2/10/2020 11:01	Ni 361.939	Ni		1.26	1.263	ppm	13710.22192	0.10	8.28
9	2min	Sample	2/10/2020 11:01	Mn 403.076	Mn		1.70	1.702	ppm	223195.6235	0.08	4.69
10	5min	Sample	2/10/2020 11:03	Co 340.512	Co		4.34	4.341	ppm	53609.23147	0.62	15.35
11	5min	Sample	2/10/2020 11:03	Ni 361.939	Ni		3.65	3.646	ppm	34091.69183	0.20	5.82
12	5min	Sample	2/10/2020 11:03	Mn 403.076	Mn		3.75	3.751	ppm	296596.2537	0.25	7.02
13	10min	Sample	2/10/2020 11:05	Co 340.512	Co		11.58	11.581	ppm	145741.6595	0.45	4.07
14	10min	Sample	2/10/2020 11:05	Ni 361.939	Ni		8.63	8.629	ppm	83121.57956	0.26	3.09
15	10min	Sample	2/10/2020 11:08	Mn 403.076	Mn		9.26	9.263	ppm	547314.7375	0.44	4.60
16	15min	Sample	2/10/2020 11:08	Co 340.512	Co		16.90	16.902	ppm	224396.2792	0.47	2.75
17	15min	Sample	2/10/2020 11:08	Ni 361.939	Ni		14.21	14.212	ppm	128306.1953	0.49	3.70
18	15min	Sample	2/10/2020 11:08	Mn 403.076	Mn		12.50	12.495	ppm	694394.465	0.62	3.17
19	30min	Sample	2/10/2020 11:10	Co 340.512	Co		24.92	24.921	ppm	328107.6572	0.47	1.95
20	30min	Sample	2/10/2020 11:10	Ni 361.939	Ni		21.07	21.070	ppm	202613.6935	0.57	2.69
21	30min	Sample	2/10/2020 11:12	Mn 403.076	Mn		19.98	19.979	ppm	1029549.879	0.82	3.23
22	60min	Sample	2/10/2020 11:12	Co 340.512	Co		30.97	30.965	ppm	418751.8603	0.51	1.64
23	60min	Sample	2/10/2020 11:12	Ni 361.939	Ni		29.92	29.915	ppm	278041.7682	0.24	0.78
24	60min	Sample	2/10/2020 11:12	Mn 403.076	Mn		28.26	28.256	ppm	1394564.402	0.48	1.67
25	120min	Sample	2/10/2020 11:14	Co 340.512	Co		31.82	31.824	ppm	433032.991	0.76	2.33
26	120min	Sample	2/10/2020 11:14	Ni 361.939	Ni		31.01	31.009	ppm	285367.1785	0.22	0.69
27	120min	Sample	2/10/2020 11:14	Mn 403.076	Mn		30.01	30.009	ppm	1466229.387	0.28	0.94

	M	N	O	P	Q	R	S	T	U	V	W	X	Y
3	Intensity SD	Intensity %RSD	Weight	Volume	Dilution	Internal Standard	Replicates	Concentration Replicate 1	Concentration Replicate 2	Concentration Replicate 3	Intensity Replicate 1	Intensity Replicate 2	Intensity Replicate 3
4	92.51	0.16	1	1	1	-	3	5.2309852	5.2172391	5.2241299	59230.05861	59265.88322	59054.20576
5	37.84	0.09	1	1	1	-	3	5.0555744	5.1152278	5.1759437	43610.06612	43548.55753	43519.27459
6	1111.94	0.55	1	1	1	-	3	5.0342157	5.0743697	5.2170831	202748.0197	202095.9972	204712.2068
7	780.79	3.87	1	1	1	-	3	1.3026221	1.2312174	1.3887668	21206.4053	19343.26297	19900.82628
8	49.95	0.36	1	1	1	-	3	1.279455008	1.309153525	1.201043614	13694.37024	13658.52975	13777.76578
9	1426.04	1.59	1	1	1	-	3	1.623814743	1.78904906	1.693920112	231155.9499	220555.3178	217875.6028
10	1741.57	3.29	1	1	1	-	3	4.064868829	4.636529361	4.32295462	52289.20377	53212.68363	55325.80701
11	1115.00	3.27	1	1	1	-	3	3.784972475	3.53749323	3.615898473	33327.31451	35668.29684	33279.46414
12	4623.35	2.72	1	1	1	-	3	3.601598766	3.760346677	3.891739952	295980.2328	297391.5063	296417.022
13	5377.56	3.76	1	1	1	-	3	11.8786135	11.61786714	11.24653199	142365.0602	143180.651	151679.2673
14	1439.70	1.73	1	1	1	-	3	8.571196084	8.600127992	8.714248567	82984.1823	81431.03365	84949.52274
15	6688.01	1.50	1	1	1	-	3	8.954442665	9.449573044	9.385411785	544366.7761	543638.8547	553938.5816
16	4125.74	1.84	1	1	1	-	3	16.90558096	16.92780566	16.87164856	230181.5185	220847.2727	222160.0464
17	4131.82	3.22	1	1	1	-	3	14.89711893	13.79283018	13.94639681	132960.7105	122919.5946	129038.2809
18	25187.96	2.58	1	1	1	-	3	12.62270142	11.96673682	12.89593857	693666.2805	703916.1728	685600.9417
19	5900.89	1.84	1	1	1	-	3	24.91494242	24.0215904	25.82598349	331780.8118	328492.1712	324049.9886
20	1399.05	0.69	1	1	1	-	3	21.97402146	21.32678824	19.90962164	201064.1011	202323.0921	204453.8873
21	45449.52	3.67	1	1	1	-	3	19.15889187	19.946166	20.83204501	1027555.249	1035349.117	1025745.271
22	6285.62	1.50	1	1	1	-	3	30.92077416	30.06788818	31.90643571	427269.7857	416694.5267	412291.2685
23	2012.13	0.70	1	1	1	-	3	28.10228727	30.52338181	31.12034905	275250.6358	278957.5286	279917.1401
24	16742.73	1.17	1	1	1	-	3	27.80283607	28.48152206	28.48430996	1337442.269	1412771.925	1433479.013
25	2270.21	0.52	1	1	1	-	3	31.25846358	31.70106858	32.51370036	431728.347	429132.1079	438238.5181
26	3240.17	1.10	1	1	1	-	3	29.83306114	31.82516039	31.36811962	282294.3833	283959.6772	289847.4749
27	17319.17	1.17	1	1	1	-	3	30.88025668	29.40177094	29.74641233	1458444.778	1476359.298	1463884.086

Appendix B8: MP-AES Results (NMC-H2SO4-H2O2)

	B	C	D	E
33	Co (340.512 nm)	Conc. (g/L)	Intensity	% Leach
34	1.308	0.392260628	20150.165	4%
35	4.341	1.302435281	53609.231	13%
36	11.581	3.474301263	145741.660	34%
37	16.902	5.070503518	224396.279	50%
38	24.921	7.476251632	328107.657	73%
39	30.965	9.289509805	418751.860	91%
40	31.824	9.547323252	433032.991	93%
41				
42	Ni (361.939 nm)	Conc. (g/L)		% Leach
43	1.263	0.378965215	13710.222	4%
44	3.646	1.093836418	34091.692	11%
45	8.629	2.588557264	83121.580	27%
46	14.212	4.263634593	128306.195	44%
47	21.070	6.321043134	202613.693	65%
48	29.915	8.974601813	278041.768	93%
49	31.009	9.302634115	285367.178	96%
50				
51	Mn (403.076 nm)	Conc. (g/L)		% Leach
52	1.70	0.510678391	223195.62	5%
53	3.75	1.12536854	296596.25	12%
54	9.263	2.778942749	547314.737	29%
55	12.495	3.74853768	694394.465	39%
56	19.979	5.993710288	1029549.879	62%
57	28.256	8.476866809	1394564.402	87%
58	30.009	9.002843996	1466229.387	92%

Appendix B9: MP-AES Data (NMC-H2SO4-1M)

	A	B	C	D	E	F	G	H	I	J	K	L
3	Label	Type	Date Time	Element	Element Label	Flags	Unadjusted Data	Concentration	Unit	Intensity	Concentration SD	Concentration %RSD
4	5 ppm reference	Sample	5/10/2020 9:05	Co 340.512	Co		4.53	4.527	ppm	38338.42702	0.012903	0.29
5	5 ppm reference	Sample	5/10/2020 9:05	Ni 361.939	Ni		4.52	4.523	ppm	30396.17571	0.018401	0.41
6	5 ppm reference	Sample	5/10/2020 9:05	Mn 403.076	Mn		4.59	4.588	ppm	141785.094	0.015510	0.34
7	0min	Sample	5/10/2020 9:07	Co 340.512	Co		1.45	1.446	ppm	11460.37055	0.034766	2.40
8	0min	Sample	5/10/2020 9:07	Ni 361.939	Ni		1.47	1.466	ppm	11422.14505	0.010122	0.69
9	0min	Sample	5/10/2020 9:07	Mn 403.076	Mn		1.42	1.418	ppm	89038.75753	0.008717	0.61
10	15min	Sample	5/10/2020 9:09	Co 340.512	Co		5.02	5.020	ppm	48107.62537	0.028134	0.56
11	15min	Sample	5/10/2020 9:09	Ni 361.939	Ni		5.69	5.689	ppm	40759.21482	0.163530	2.87
12	15min	Sample	5/10/2020 9:09	Mn 403.076	Mn		2.15	2.149	ppm	130362.5992	0.075987	3.54
13	30min	Sample	5/10/2020 9:11	Co 340.512	Co		7.24	7.239	ppm	71490.74375	0.040407	0.56
14	30min	Sample	5/10/2020 9:11	Ni 361.939	Ni		8.02	8.021	ppm	56819.65275	0.122512	1.53
15	30min	Sample	5/10/2020 9:11	Mn 403.076	Mn		2.97	2.966	ppm	164877.9591	0.029817	1.01
16	45min	Sample	5/10/2020 9:13	Co 340.512	Co		11.23	11.228	ppm	108198.9121	0.120568	1.07
17	45min	Sample	5/10/2020 9:13	Ni 361.939	Ni		11.63	11.627	ppm	88562.84127	0.189918	1.63
18	45min	Sample	5/10/2020 9:13	Mn 403.076	Mn		8.10	8.103	ppm	410093.2225	0.080465	0.99
19	60min	Sample	5/10/2020 9:15	Co 340.512	Co		11.34	11.343	ppm	105523.5743	0.194114	1.71
20	60min	Sample	5/10/2020 9:15	Ni 361.939	Ni		12.13	12.125	ppm	92390.48848	0.139367	1.15
21	60min	Sample	5/10/2020 9:15	Mn 403.076	Mn		8.09	8.088	ppm	424668.1625	0.133147	1.65

	M	N	O	P	Q	R	S	T	U	V	W	X	Y
3	Intensity SD	Intensity %RSD	Weight	Volume	Dilution	Internal Standard	Replicates	Concentration Replicate 1	Concentration Replicate 2	Concentration Replicate 3	Intensity Replicate 1	Intensity Replicate 2	Intensity Replicate 3
4	235.53	0.61	1	1	1	-	3	4.530	4.510	4.541	38159.5401	38184.5389	38671.2020
5	26.40	0.09	1	1	1	-	3	4.548	4.519	4.503	30431.6013	30388.6799	30368.2459
6	775.93	0.55	1	1	1	-	3	4.580	4.609	4.574	141479.8795	141024.8907	142850.5117
7	391.13	3.41	1	1	1	-	3	1.421	1.423	1.495	11989.4904	11056.1559	11335.4653
8	25.02	0.22	1	1	1	-	3	1.456	1.461	1.480	11414.2042	11396.2500	11455.9809
9	1370.95	1.54	1	1	1	-	3	1.416	1.409	1.430	88472.3962	87716.1058	90927.7706
10	1550.30	3.22	1	1	1	-	3	5.004	5.059	4.996	48964.3817	49426.9956	45931.4988
11	452.14	1.11	1	1	1	-	3	5.554	5.595	5.919	41287.1144	40182.7919	40807.7381
12	295.52	0.23	1	1	1	-	3	2.044	2.220	2.183	130054.0057	130760.9781	130272.8137
13	172.39	0.24	1	1	1	-	3	7.229	7.293	7.195	71317.2679	71725.8352	71429.1282
14	1599.30	2.81	1	1	1	-	3	7.968	8.191	7.905	55232.8046	59008.8188	56217.3349
15	2189.97	1.33	1	1	1	-	3	3.005	2.959	2.933	167955.2468	163036.5388	163642.0917
16	1043.59	0.96	1	1	1	-	3	11.225	11.378	11.083	108860.0320	106725.6338	109011.0704
17	836.95	0.95	1	1	1	-	3	11.567	11.430	11.883	89376.4845	88900.4818	87411.5575
18	4451.15	1.09	1	1	1	-	3	8.178	7.992	8.140	406692.4022	416381.1075	407206.1580
19	2199.16	2.08	1	1	1	-	3	11.110	11.585	11.334	102673.4246	105870.7128	108026.5854
20	700.85	0.76	1	1	1	-	3	12.227	12.221	11.928	91614.2257	92244.9128	93312.3270
21	2087.31	0.49	1	1	1	-	3	7.900	8.174	8.191	423668.9598	427573.2701	422762.2576

Appendix B10: MP-AES Results (NMC-H2SO4-1M)

	A	B	C	D	E
25	Time (minutes)	Co (340.512 nm)	Conc. (g/L)	Intensity	% Leach
26	0	1.446	0.433888665	11460.371	4%
27	15	5.020	1.505964417	48107.625	15%
28	30	7.239	2.171738422	71490.744	21%
29	45	11.228	3.368533103	108198.912	33%
30	60	11.343	3.402823438	105523.574	33%
31					
32		Ni (361.939 nm)	Conc. (g/L)		% Leach
33	0	1.466	0.439722086	11422.145	5%
34	15	5.689	1.706731368	40759.215	18%
35	30	8.021	2.406370909	56819.653	25%
36	45	11.627	3.487983704	88562.841	36%
37	60	12.125	3.637630145	92390.488	38%
38					
39		Mn (403.076 nm)	Conc. (g/L)		% Leach
40	0	1.42	0.42548583	89038.76	4%
41	15	2.15	0.644673359	130362.60	7%
42	30	2.966	0.889721964	164877.959	9%
43	45	8.103	2.430976693	410093.223	25%
44	60	8.088	2.426504576	424668.162	25%

Appendix B11: MP-AES Data (NMC-H2SO4-2M)

	A	B	C	D	E	F	G	H	I	J	K	L
3	Label	Type	Date Time	Element	Element Label	Flags	Unadjusted Data	Concentration	Unit	Intensity	Concentration SD	Concentration %RSD
4	5 ppm reference	Sample	5/10/2020 9:05	Co 340.512	Co		4.53	4.527	ppm	38338.42702	0.012903	0.29
5	5 ppm reference	Sample	5/10/2020 9:05	Ni 361.939	Ni		4.52	4.523	ppm	30396.17571	0.018401	0.41
6	5 ppm reference	Sample	5/10/2020 9:05	Mn 403.076	Mn		4.59	4.588	ppm	141785.094	0.015510	0.34
7	0min	Sample	5/10/2020 9:24	Co 340.512	Co		2.01	2.015	ppm	15964.13674	0.048429	2.40
8	0min	Sample	5/10/2020 9:24	Ni 361.939	Ni		2.04	2.042	ppm	15910.88916	0.014100	0.69
9	0min	Sample	5/10/2020 9:24	Mn 403.076	Mn		1.98	1.976	ppm	124029.7505	0.012143	0.61
10	15min	Sample	5/10/2020 9:26	Co 340.512	Co		6.99	6.993	ppm	67013.25287	0.039190	0.56
11	15min	Sample	5/10/2020 9:26	Ni 361.939	Ni		7.92	7.925	ppm	56777.0192	0.227795	2.87
12	15min	Sample	5/10/2020 9:26	Mn 403.076	Mn		2.99	2.993	ppm	181593.287	0.105849	3.54
13	30min	Sample	5/10/2020 9:28	Co 340.512	Co		10.08	10.084	ppm	99585.61146	0.056287	0.56
14	30min	Sample	5/10/2020 9:28	Ni 361.939	Ni		11.17	11.173	ppm	79148.98581	0.170657	1.53
15	30min	Sample	5/10/2020 9:28	Mn 403.076	Mn		4.13	4.131	ppm	229672.7032	0.041534	1.01
16	45min	Sample	5/10/2020 9:30	Co 340.512	Co		15.64	15.641	ppm	150719.5792	0.167950	1.07
17	45min	Sample	5/10/2020 9:30	Ni 361.939	Ni		16.20	16.196	ppm	123366.8058	0.264553	1.63
18	45min	Sample	5/10/2020 9:30	Mn 403.076	Mn		11.29	11.288	ppm	571254.1538	0.112087	0.99
19	60min	Sample	5/10/2020 9:32	Co 340.512	Co		15.80	15.800	ppm	146992.8709	0.270398	1.71
20	60min	Sample	5/10/2020 9:32	Ni 361.939	Ni		16.89	16.891	ppm	128698.6651	0.194136	1.15
21	60min	Sample	5/10/2020 9:32	Mn 403.076	Mn		11.27	11.267	ppm	591556.8423	0.185471	1.65

	M	N	O	P	Q	R	S	T	U	V	W	X	Y
3	Intensity SD	Intensity %RSD	Weight	Volume	Dilution	Internal Standard	Replicates	Concentration Replicate 1	Concentration Replicate 2	Concentration Replicate 3	Intensity Replicate 1	Intensity Replicate 2	Intensity Replicate 3
4	235.53	0.61	1	1	1	-	3	4.530	4.510	4.541	38159.5401	38184.5389	38671.2020
5	26.40	0.09	1	1	1	-	3	4.548	4.519	4.503	30431.6013	30388.6799	30368.2459
6	775.93	0.55	1	1	1	-	3	4.580	4.609	4.574	141479.8795	141024.8907	142850.5117
7	544.84	3.41	1	1	1	-	3	1.979	1.982	2.083	16701.1934	15401.0714	15790.1454
8	34.86	0.22	1	1	1	-	3	2.028	2.036	2.061	15899.8277	15874.8178	15958.0220
9	1909.72	1.54	1	1	1	-	3	1.973	1.963	1.992	123240.8170	122187.3151	126661.1194
10	2159.55	3.22	1	1	1	-	3	6.971	7.048	6.959	68206.7025	68851.1173	63981.9388
11	629.83	1.11	1	1	1	-	3	7.736	7.793	8.245	57512.3760	55974.0702	56844.6115
12	411.66	0.23	1	1	1	-	3	2.847	3.093	3.040	181163.4206	182148.2234	181468.2171
13	240.14	0.24	1	1	1	-	3	10.070	10.159	10.023	99343.9620	99913.0905	99499.7819
14	2227.81	2.81	1	1	1	-	3	11.099	11.410	11.012	76938.5284	82198.4636	78309.9654
15	3050.60	1.33	1	1	1	-	3	4.186	4.123	4.085	233959.3221	227107.6303	227951.1572
16	1453.70	0.96	1	1	1	-	3	15.636	15.849	15.438	151640.5101	148667.3231	151850.9045
17	1165.86	0.95	1	1	1	-	3	16.112	15.922	16.553	124500.1995	123837.1344	121763.0835
18	6200.39	1.09	1	1	1	-	3	11.392	11.132	11.338	566516.8583	580013.0900	567232.5130
19	3063.40	2.08	1	1	1	-	3	15.475	16.137	15.788	143022.6521	147476.4300	150479.5306
20	976.27	0.76	1	1	1	-	3	17.032	17.023	16.616	127617.3419	128495.8802	129982.7733
21	2907.59	0.49	1	1	1	-	3	11.005	11.386	11.410	590164.9668	595603.6168	588901.9434

Appendix B12: MP-AES Results (NMC-H2SO4-2M)

	A	B	C	D	E
25	Time (minutes)	Co (340.512 nm)	Conc. (g/L)	Intensity	% Leach
26	0	2.015	0.604400874	15964.137	6%
27	15	6.993	2.097787481	67013.253	20%
28	30	10.084	3.025201409	99585.611	30%
29	45	15.641	4.69231975	150719.579	46%
30	60	15.800	4.740085709	146992.871	46%
31					
32		Ni (361.939 nm)	Conc. (g/L)		% Leach
33	0	2.042	0.612526749	15910.889	6%
34	15	7.925	2.377453052	56777.019	25%
35	30	11.173	3.352041199	79148.986	35%
36	45	16.196	4.858712774	123366.806	50%
37	60	16.891	5.067168185	128698.665	52%
38					
39		Mn (403.076 nm)	Conc. (g/L)		% Leach
40	0	1.98	0.592695841	124029.75	6%
41	15	2.99	0.898021021	181593.29	9%
42	30	4.131	1.239370318	229672.703	13%
43	45	11.288	3.386316714	571254.154	35%
44	60	11.267	3.380087116	591556.842	35%

Appendix B13: MP-AES Data (NMC-H2SO4-3M)

	A	B	C	D	E	F	G	H	I	J	K	L
3	Label	Type	Date Time	Element	Element Label	Flags	Unadjusted Data	Concentration	Unit	Intensity	Concentration SD	Concentration %RSD
4	5 ppm reference	Sample	5/10/2020 9:05	Co 340.512	Co		4.53	4.527	ppm	38338.42702	0.012903	0.29
5	5 ppm reference	Sample	5/10/2020 9:05	Ni 361.939	Ni		4.52	4.523	ppm	30396.17571	0.018401	0.41
6	5 ppm reference	Sample	5/10/2020 9:05	Mn 403.076	Mn		4.59	4.588	ppm	141785.094	0.015510	0.34
7	0min	Sample	5/10/2020 13:01	Co 340.512	Co		3.18	3.176	ppm	25165.18133	0.076341	2.40
8	0min	Sample	5/10/2020 13:01	Ni 361.939	Ni		3.22	3.219	ppm	25081.24412	0.022226	0.69
9	0min	Sample	5/10/2020 13:01	Mn 403.076	Mn		3.11	3.114	ppm	195515.1859	0.019142	0.61
10	15min	Sample	5/10/2020 13:03	Co 340.512	Co		11.02	11.023	ppm	105636.8213	0.061777	0.56
11	15min	Sample	5/10/2020 13:03	Ni 361.939	Ni		12.49	12.492	ppm	89500.86101	0.359087	2.87
12	15min	Sample	5/10/2020 13:03	Mn 403.076	Mn		4.72	4.719	ppm	286255.879	0.166855	3.54
13	30min	Sample	5/10/2020 13:05	Co 340.512	Co		15.90	15.896	ppm	156982.4921	0.088728	0.56
14	30min	Sample	5/10/2020 13:05	Ni 361.939	Ni		17.61	17.613	ppm	124767.0709	0.269016	1.53
15	30min	Sample	5/10/2020 13:08	Mn 403.076	Mn		6.51	6.512	ppm	362046.2112	0.065473	1.01
16	45min	Sample	5/10/2020 13:08	Co 340.512	Co		24.66	24.656	ppm	237587.8886	0.264749	1.07
17	45min	Sample	5/10/2020 13:08	Ni 361.939	Ni		25.53	25.530	ppm	194470.1482	0.417030	1.63
18	45min	Sample	5/10/2020 13:08	Mn 403.076	Mn		17.79	17.793	ppm	900500.5782	0.176689	0.99
19	60min	Sample	5/10/2020 13:10	Co 340.512	Co		24.91	24.907	ppm	231713.2652	0.426244	1.71
20	60min	Sample	5/10/2020 13:10	Ni 361.939	Ni		26.63	26.626	ppm	202875.0628	0.306028	1.15
21	60min	Sample	5/10/2020 13:12	Mn 403.076	Mn		17.76	17.761	ppm	932504.8668	0.292369	1.65

	M	N	O	P	Q	R	S	T	U	V	W	X	Y
3	Intensity SD	Intensity %RSD	Weight	Volume	Dilution	Internal Standard	Replicates	Concentration Replicate 1	Concentration Replicate 2	Concentration Replicate 3	Intensity Replicate 1	Intensity Replicate 2	Intensity Replicate 3
4	235.53	0.61	1	1	1	-	3	4.530	4.510	4.541	38159.5401	38184.5389	38671.2020
5	26.40	0.09	1	1	1	-	3	4.548	4.519	4.503	30431.6013	30388.6799	30368.2459
6	775.93	0.55	1	1	1	-	3	4.580	4.609	4.574	141479.8795	141024.8907	142850.5117
7	858.87	3.41	1	1	1	-	3	3.120	3.124	3.284	26327.0458	24277.5893	24890.9089
8	54.95	0.22	1	1	1	-	3	3.197	3.209	3.249	25063.8073	25024.3827	25155.5424
9	3010.40	1.54	1	1	1	-	3	3.109	3.094	3.140	194271.5449	192610.8496	199663.1631
10	3404.22	3.22	1	1	1	-	3	10.989	11.110	10.970	107518.1242	108533.9520	100858.3877
11	992.83	1.11	1	1	1	-	3	12.195	12.285	12.998	90660.0460	88235.1265	89607.4105
12	648.92	0.23	1	1	1	-	3	4.488	4.876	4.793	285578.2560	287130.6569	286058.7242
13	378.55	0.24	1	1	1	-	3	15.874	16.014	15.800	156601.5662	157498.7161	156847.1941
14	3511.82	2.81	1	1	1	-	3	17.496	17.985	17.359	121282.6005	129574.1370	123444.4750
15	4808.83	1.33	1	1	1	-	3	6.598	6.499	6.440	368803.4537	358002.7402	359332.4398
16	2291.56	0.96	1	1	1	-	3	24.648	24.984	24.335	239039.6045	234352.8000	239371.2612
17	1837.82	0.95	1	1	1	-	3	25.398	25.098	26.094	196256.7815	195211.5541	191942.1090
18	9774.03	1.09	1	1	1	-	3	17.958	17.548	17.873	893032.9085	914307.7901	894161.0359
19	4829.01	2.08	1	1	1	-	3	24.395	25.438	24.887	225454.7823	232475.5271	237209.4862
20	1538.95	0.76	1	1	1	-	3	26.849	26.835	26.193	201170.5112	202555.4013	204899.2760
21	4583.40	0.49	1	1	1	-	3	17.348	17.948	17.986	930310.7738	938884.0287	928319.7978

Appendix B14: MP-AES Results (NMC-H2SO4-3M)

	A	B	C	D	E
25	Time (minutes)	Co (340.512 nm)	Conc. (g/L)	Intensity	% Leach
26	0	3.176	0.952751649	25165.181	9%
27	15	11.023	3.306862326	105636.821	32%
28	30	15.896	4.768797916	156982.492	47%
29	45	24.656	7.396771857	237587.889	72%
30	60	24.907	7.472068069	231713.265	73%
31					
32		Ni (361.939 nm)	Conc. (g/L)		% Leach
33	0	3.219	0.965560929	25081.244	10%
34	15	12.492	3.747715152	89500.861	39%
35	30	17.613	5.28401416	124767.071	55%
36	45	25.530	7.659066693	194470.148	79%
37	60	26.626	7.987666874	202875.063	83%
38					
39		Mn (403.076 nm)	Conc. (g/L)		% Leach
40	0	3.11	0.934300336	195515.19	10%
41	15	4.72	1.41560187	286255.88	15%
42	30	6.512	1.95369028	362046.211	20%
43	45	17.793	5.338044614	900500.578	55%
44	60	17.761	5.328224543	932504.867	55%

Appendix B15: MP-AES Data (NMC-H2SO4-4M)

	A	B	C	D	E	F	G	H	I	J	K	L
3	Label	Type	Date Time	Element	Element Label	Flags	Unadjusted Data	Concentration	Unit	Intensity	Concentration SD	Concentration %RSD
4	5 ppm reference	Sample	5/10/2020 9:05	Co 340.512	Co		4.53	4.527	ppm	38338.42702	0.012903	0.29
5	5 ppm reference	Sample	5/10/2020 9:05	Ni 361.939	Ni		4.52	4.523	ppm	30396.17571	0.018401	0.41
6	5 ppm reference	Sample	5/10/2020 9:05	Mn 403.076	Mn		4.59	4.588	ppm	141785.094	0.015510	0.34
7	0min	Sample	5/10/2020 13:15	Co 340.512	Co		3.56	3.564	ppm	28244.01544	0.085681	2.40
8	0min	Sample	5/10/2020 13:15	Ni 361.939	Ni		3.61	3.612	ppm	28149.80893	0.024945	0.69
9	0min	Sample	5/10/2020 13:15	Mn 403.076	Mn		3.50	3.495	ppm	219435.4913	0.021483	0.61
10	15min	Sample	5/10/2020 13:17	Co 340.512	Co		12.37	12.371	ppm	118560.9582	0.069335	0.56
11	15min	Sample	5/10/2020 13:17	Ni 361.939	Ni		14.02	14.021	ppm	100450.8439	0.403019	2.87
12	15min	Sample	5/10/2020 13:17	Mn 403.076	Mn		5.30	5.296	ppm	321277.8546	0.187269	3.54
13	30min	Sample	5/10/2020 13:19	Co 340.512	Co		17.84	17.841	ppm	176188.5151	0.099584	0.56
14	30min	Sample	5/10/2020 13:19	Ni 361.939	Ni		19.77	19.768	ppm	140031.6981	0.301929	1.53
15	30min	Sample	5/10/2020 13:19	Mn 403.076	Mn		7.31	7.309	ppm	406340.7549	0.073483	1.01
16	45min	Sample	5/10/2020 13:21	Co 340.512	Co		27.67	27.672	ppm	266655.5788	0.297140	1.07
17	45min	Sample	5/10/2020 13:21	Ni 361.939	Ni		28.65	28.654	ppm	218262.5985	0.468051	1.63
18	45min	Sample	5/10/2020 13:21	Mn 403.076	Mn		19.97	19.970	ppm	1010672.321	0.198305	0.99
19	60min	Sample	5/10/2020 13:23	Co 340.512	Co		27.95	27.954	ppm	260062.2246	0.478392	1.71
20	60min	Sample	5/10/2020 13:23	Ni 361.939	Ni		29.88	29.883	ppm	227695.8124	0.343469	1.15
21	60min	Sample	5/10/2020 13:23	Mn 403.076	Mn		19.93	19.934	ppm	1046592.175	0.328139	1.65

	M	N	O	P	Q	R	S	T	U	V	W	X	Y
3	Intensity SD	Intensity %RSD	Weight	Volume	Dilution	Internal Standard	Replicates	Concentration Replicate 1	Concentration Replicate 2	Concentration Replicate 3	Intensity Replicate 1	Intensity Replicate 2	Intensity Replicate 3
4	235.53	0.61	1	1	1	-	3	4.530	4.510	4.541	38159.5401	38184.5389	38671.2020
5	26.40	0.09	1	1	1	-	3	4.548	4.519	4.503	30431.6013	30388.6799	30368.2459
6	775.93	0.55	1	1	1	-	3	4.580	4.609	4.574	141479.8795	141024.8907	142850.5117
7	963.95	3.41	1	1	1	-	3	3.502	3.506	3.686	29548.0283	27247.8309	27936.1872
8	61.67	0.22	1	1	1	-	3	3.589	3.601	3.647	28130.2388	28085.9908	28233.1972
9	3378.71	1.54	1	1	1	-	3	3.490	3.472	3.524	218039.6971	216175.8240	224090.9527
10	3820.71	3.22	1	1	1	-	3	12.333	12.469	12.312	120672.4291	121812.5384	113197.9072
11	1114.30	1.11	1	1	1	-	3	13.687	13.788	14.588	101751.8493	99030.2531	100570.4292
12	728.31	0.23	1	1	1	-	3	5.037	5.472	5.379	320517.3278	322259.6571	321056.5788
13	424.86	0.24	1	1	1	-	3	17.817	17.973	17.733	175760.9848	176767.8965	176036.6640
14	3941.48	2.81	1	1	1	-	3	19.636	20.186	19.483	136120.9203	145426.8848	138547.2893
15	5397.17	1.33	1	1	1	-	3	7.406	7.294	7.228	413924.7123	401802.5854	403294.9671
16	2571.92	0.96	1	1	1	-	3	27.664	28.041	27.313	268284.9049	263024.6933	268657.1382
17	2062.67	0.95	1	1	1	-	3	28.506	28.169	29.286	220267.8174	219094.7117	215425.2664
18	10969.83	1.09	1	1	1	-	3	20.156	19.695	20.060	1002291.0197	1026168.7766	1003557.1678
19	5419.82	2.08	1	1	1	-	3	27.379	28.551	27.932	253038.0476	260917.7455	266230.8808
20	1727.23	0.76	1	1	1	-	3	30.134	30.118	29.397	225782.7174	227337.0419	229967.6780
21	5144.15	0.49	1	1	1	-	3	19.470	20.144	20.186	1044129.6455	1053751.7952	1041895.0834

Appendix B16: MP-AES Results (NMC-H2SO4-4M)

	A	B	C	D	E
25	Time (minutes)	Co (340.512 nm)	Conc. (g/L)	Intensity	% Leach
26	0	3.564	1.069316049	28244.015	10%
27	15	12.371	3.711440397	118560.958	36%
28	30	17.841	5.352236497	176188.515	52%
29	45	27.672	8.30172991	266655.579	81%
30	60	27.954	8.386238237	260062.225	82%
31					
32		Ni (361.939 nm)	Conc. (g/L)		% Leach
33	0	3.612	1.083692481	28149.809	11%
34	15	14.021	4.206229362	100450.844	43%
35	30	19.768	5.930486872	140031.698	61%
36	45	28.654	8.596115208	218262.598	89%
37	60	29.883	8.964917978	227695.812	93%
38					
39		Mn (403.076 nm)	Conc. (g/L)		% Leach
40	0	3.50	1.048607311	219435.49	11%
41	15	5.30	1.588793681	321277.85	16%
42	30	7.309	2.192714517	406340.755	23%
43	45	19.970	5.991127683	1010672.321	62%
44	60	19.934	5.980106175	1046592.175	61%

Appendix B17: MP-AES Data (NMC-H2SO4-5M)

	A	B	C	D	E	F	G	H	I	J	K	L
3	Label	Type	Date Time	Element	Element Label	Flags	Unadjusted Data	Concentration	Unit	Intensity	Concentration SD	Concentration %RSD
4	5 ppm reference	Sample	5/10/2020 9:05	Co 340.512	Co		4.53	4.527	ppm	38338.42702	0.012903	0.29
5	5 ppm reference	Sample	5/10/2020 9:05	Ni 361.939	Ni		4.52	4.523	ppm	30396.17571	0.018401	0.41
6	5 ppm reference	Sample	5/10/2020 9:05	Mn 403.076	Mn		4.59	4.588	ppm	141785.094	0.015510	0.34
7	0min	Sample	5/10/2020 13:25	Co 340.512	Co		3.72	3.719	ppm	29468.17179	0.089395	2.40
8	0min	Sample	5/10/2020 13:25	Ni 361.939	Ni		3.77	3.769	ppm	29369.88216	0.026026	0.69
9	0min	Sample	5/10/2020 13:25	Mn 403.076	Mn		3.65	3.647	ppm	228946.2972	0.022415	0.61
10	15min	Sample	5/10/2020 13:27	Co 340.512	Co		12.91	12.908	ppm	123699.645	0.072340	0.56
11	15min	Sample	5/10/2020 13:27	Ni 361.939	Ni		14.63	14.628	ppm	104804.5994	0.420487	2.87
12	15min	Sample	5/10/2020 13:27	Mn 403.076	Mn		5.53	5.526	ppm	335202.7274	0.195386	3.54
13	30min	Sample	5/10/2020 13:29	Co 340.512	Co		18.61	18.614	ppm	183824.9041	0.103900	0.56
14	30min	Sample	5/10/2020 13:29	Ni 361.939	Ni		20.63	20.625	ppm	146100.973	0.315015	1.53
15	30min	Sample	5/10/2020 13:29	Mn 403.076	Mn		7.63	7.626	ppm	423952.4368	0.076668	1.01
16	45min	Sample	5/10/2020 13:31	Co 340.512	Co		28.87	28.872	ppm	278213.0048	0.310019	1.07
17	45min	Sample	5/10/2020 13:31	Ni 361.939	Ni		29.90	29.896	ppm	227722.5687	0.488337	1.63
18	45min	Sample	5/10/2020 13:31	Mn 403.076	Mn		20.84	20.836	ppm	1054477.032	0.206900	0.99
19	60min	Sample	5/10/2020 13:33	Co 340.512	Co		29.17	29.166	ppm	271333.8805	0.499127	1.71
20	60min	Sample	5/10/2020 13:33	Ni 361.939	Ni		30.51	30.512	ppm	237564.6384	0.113315	0.37
21	60min	Sample	5/10/2020 13:33	Mn 403.076	Mn		20.80	20.798	ppm	1091953.729	0.342361	1.65

	M	N	O	P	Q	R	S	T	U	V	W	X	Y
3	Intensity SD	Intensity %RSD	Weight	Volume	Dilution	Internal Standard	Replicates	Concentration Replicate 1	Concentration Replicate 2	Concentration Replicate 3	Intensity Replicate 1	Intensity Replicate 2	Intensity Replicate 3
4	235.53	0.61	1	1	1	-	3	4.530	4.510	4.541	38159.5401	38184.5389	38671.2020
5	26.40	0.09	1	1	1	-	3	4.548	4.519	4.503	30431.6013	30388.6799	30368.2459
6	775.93	0.55	1	1	1	-	3	4.580	4.609	4.574	141479.8795	141024.8907	142850.5117
7	1005.73	3.41	1	1	1	-	3	3.653	3.658	3.845	30828.7033	28428.8105	29147.0016
8	64.34	0.22	1	1	1	-	3	3.744	3.758	3.805	29349.4638	29303.2981	29456.8846
9	3525.15	1.54	1	1	1	-	3	3.641	3.623	3.677	227490.0063	225545.3489	233803.5364
10	3986.30	3.22	1	1	1	-	3	12.868	13.009	12.846	125902.6315	127092.1556	118104.1478
11	1162.60	1.11	1	1	1	-	3	14.280	14.385	15.220	106161.9932	103322.4371	104929.3678
12	759.88	0.23	1	1	1	-	3	5.255	5.709	5.612	334409.2378	336227.0834	334971.8611
13	443.28	0.24	1	1	1	-	3	18.589	18.752	18.501	183378.8437	184429.3971	183666.4715
14	4112.31	2.81	1	1	1	-	3	20.488	21.061	20.327	142020.6936	151729.9986	144552.2267
15	5631.09	1.33	1	1	1	-	3	7.727	7.610	7.541	431865.0991	419217.5733	420774.6380
16	2683.39	0.96	1	1	1	-	3	28.863	29.256	28.497	279912.9494	274424.7489	280301.3161
17	2152.07	0.95	1	1	1	-	3	29.741	29.390	30.556	229814.6982	228590.7475	224762.2605
18	11445.29	1.09	1	1	1	-	3	21.029	20.549	20.930	1045732.4671	1070645.1374	1047053.4928
19	5654.73	2.08	1	1	1	-	3	28.566	29.788	29.143	264005.2606	272226.4815	277769.8995
20	1802.10	0.76	1	1	1	-	3	30.440	30.423	30.672	235568.6257	237190.3180	239934.9715
21	5367.11	0.49	1	1	1	-	3	20.314	21.017	21.061	1089384.4689	1099423.6632	1087053.0561

Appendix B18: MP-AES Results (NMC-H2SO4-5M)

	A	B	C	D	E
25	Time (minutes)	Co (340.512 nm)	Conc. (g/L)	Intensity	% Leach
26	0	3.719	1.115662506	29468.172	11%
27	15	12.908	3.872302203	123699.645	38%
28	30	18.614	5.584213932	183824.904	55%
29	45	28.872	8.66154473	278213.005	85%
30	60	29.166	8.74971583	271333.881	85%
31					
32		Ni (361.939 nm)	Conc. (g/L)		% Leach
33	0	3.769	1.130662043	29369.882	12%
34	15	14.628	4.388536384	104804.599	45%
35	30	20.625	6.187526922	146100.973	64%
36	45	29.896	8.96868932	227722.569	93%
37	60	30.512	9.153476795	237564.638	95%
38					
39		Mn (403.076 nm)	Conc. (g/L)		% Leach
40	0	3.65	1.094056206	228946.30	11%
41	15	5.53	1.657655414	335202.73	17%
42	30	7.626	2.287751478	423952.437	23%
43	45	20.836	6.250796036	1054477.032	64%
44	60	20.798	6.239296832	1091953.729	64%

Appendix B19: Reaction Kinetics Calculations

	A	B	C	D	E	F	G	H
5	LCO-HCL	t	x(Co)		x(Ni)		x(Mn)	
6		2	0.08	0.027				
7		5	0.18	0.065				
8		10	0.40	0.155				
9		15	0.55	0.236				
10		30	0.81	0.421				
11		60	0.95	0.627				
12		120	0.93	0.582				
13								
14	NMC-HCL							
15		2	0.05	0.015	0.04	0.013	0.05	0.019
16		5	0.12	0.041	0.11	0.037	0.11	0.038
17		10	0.32	0.122	0.26	0.095	0.29	0.109
18		15	0.50	0.209	0.41	0.161	0.60	0.264
19		30	0.71	0.338	0.66	0.299	0.78	0.396
20		60	0.86	0.475	0.89	0.527	0.83	0.448
21		120	0.90	0.540	0.92	0.569	0.86	0.485
22								
23	NMC-H2SO4Mix	2	0.04	0.013	0.04	0.013	0.05	0.018
24		5	0.13	0.044	0.11	0.039	0.12	0.040
25		10	0.34	0.129	0.27	0.099	0.29	0.106
26		15	0.50	0.204	0.44	0.176	0.39	0.150
27		30	0.73	0.354	0.65	0.297	0.62	0.273
28		60	0.91	0.547	0.93	0.583	0.87	0.494
29		120	0.93	0.592	0.96	0.662	0.92	0.578

Appendix B20: Diffusion Kinetics Calculations

	A	B	C	D	E	F	G	H
5	LCO-HCL	t	x(Co)		x(Ni)		x(Mn)	
6		2	0.08	0.002				
7		5	0.18	0.012				
8		10	0.40	0.065				
9		15	0.55	0.140				
10		30	0.81	0.382				
11		60	0.95	0.686				
12		120	0.93	0.622				
13								
14	NMC-HCL							
15		2	0.05	0.001	0.04	0.001	0.05	0.001
16		5	0.12	0.005	0.11	0.004	0.11	0.004
17		10	0.32	0.041	0.26	0.025	0.29	0.033
18		15	0.50	0.113	0.41	0.069	0.60	0.172
19		30	0.71	0.266	0.66	0.215	0.78	0.347
20		60	0.86	0.463	0.89	0.541	0.83	0.422
21		120	0.90	0.561	0.92	0.603	0.86	0.477
22								
23	NMC-H2SO4-Mix	2	0.04	0.000	0.04	0.001	0.05	0.001
24		5	0.13	0.006	0.11	0.004	0.12	0.005
25		10	0.34	0.046	0.27	0.027	0.29	0.031
26		15	0.50	0.108	0.44	0.082	0.39	0.060
27		30	0.73	0.287	0.65	0.213	0.62	0.183
28		60	0.91	0.570	0.93	0.623	0.87	0.491
29		120	0.93	0.637	0.96	0.734	0.92	0.616
30								
31		Conc (M)						
32	NMC-H2SO4	1	0.09		0.10		0.10	
33		2	0.32		0.39		0.15	
34		3	0.47		0.55		0.20	
35		4	0.72		0.79		0.55	
36		5	0.73		0.83		0.55	

Appendix B21: Reaction Model Calculations

	B	C	D	E	F	G	H	I
2			Co	Rxn	Ni	Rxn	Mn	Rxn
3	1M	0	0.04	0.014	0.05	0.015	0.04	0.015
4		15	0.15	0.052	0.18	0.063	0.07	0.023
5		30	0.21	0.076	0.25	0.091	0.09	0.031
6		45	0.33	0.124	0.36	0.138	0.25	0.091
7		60	0.33	0.126	0.38	0.145	0.25	0.091
8	2M	0	0.06	0.020	0.06	0.022	0.06	0.021
9		15	0.20	0.074	0.25	0.090	0.09	0.032
10		30	0.30	0.110	0.35	0.132	0.13	0.044
11		45	0.46	0.185	0.50	0.207	0.35	0.133
12		60	0.46	0.187	0.52	0.219	0.35	0.133
13	3M	0	0.09	0.032	0.10	0.034	0.10	0.033
14		15	0.32	0.122	0.39	0.151	0.15	0.051
15		30	0.47	0.189	0.55	0.231	0.20	0.072
16		45	0.72	0.348	0.79	0.407	0.55	0.233
17		60	0.73	0.353	0.83	0.441	0.55	0.232
18	4M	0	0.10	0.036	0.11	0.039	0.11	0.037
19		15	0.36	0.139	0.43	0.173	0.16	0.058
20		30	0.52	0.218	0.61	0.271	0.23	0.082
21		45	0.81	0.426	0.89	0.518	0.62	0.273
22		60	0.82	0.434	0.93	0.581	0.61	0.272
23	5M	0	0.11	0.038	0.12	0.041	0.11	0.039
24		15	0.38	0.146	0.45	0.182	0.17	0.060
25		30	0.55	0.231	0.64	0.288	0.23	0.085
26		45	0.85	0.464	0.93	0.582	0.64	0.290
27		60	0.85	0.474	0.95	0.622	0.64	0.289
28								
29								
30	kvalue							
31			Co		Ni		Mn	
32	1.00	0.00	0.00200	-6.21	0.00220	-6.12	0.00150	-6.50
33	2.00	0.69	0.00300	-5.81	0.00340	-5.68	0.00220	-6.12
34	3.00	1.10	0.00580	-5.15	0.00710	-4.95	0.00390	-5.55
35	4.00	1.39	0.00720	-4.93	0.00950	-4.66	0.00460	-5.38
36	5.00	1.61	0.00790	-4.84	0.01040	-4.57	0.00490	-5.32
37								
38		Co	Ni	Mn				
39	Mvalue	0.921	1.0462	0.7959				
40	Nvalue	-6.272	-6.1965	-6.5358				

Appendix B22: Diffusion Model Calculations

	B	C	D	E	F	G	H	I
2			Co	Diff	Ni	Diff	Mn	Diff
3	1M	0	0.04	0.001	0.05	0.001	0.04	0.001
4		15	0.15	0.008	0.18	0.011	0.07	0.002
5		30	0.21	0.017	0.25	0.023	0.09	0.003
6		45	0.33	0.043	0.36	0.052	0.25	0.023
7		60	0.33	0.044	0.38	0.057	0.25	0.023
8	2M	0	0.06	0.001	0.06	0.001	0.06	0.001
9		15	0.20	0.015	0.25	0.023	0.09	0.003
10		30	0.30	0.034	0.35	0.048	0.13	0.006
11		45	0.46	0.090	0.50	0.111	0.35	0.048
12		60	0.46	0.092	0.52	0.123	0.35	0.048
13	3M	0	0.09	0.003	0.10	0.003	0.10	0.003
14		15	0.32	0.041	0.39	0.061	0.15	0.008
15		30	0.47	0.093	0.55	0.136	0.20	0.015
16		45	0.72	0.278	0.79	0.362	0.55	0.137
17		60	0.73	0.286	0.83	0.412	0.55	0.137
18	4M	0	0.10	0.004	0.11	0.004	0.11	0.004
19		15	0.36	0.053	0.43	0.080	0.16	0.010
20		30	0.52	0.122	0.61	0.181	0.23	0.019
21		45	0.81	0.389	0.89	0.527	0.62	0.183
22		60	0.82	0.402	0.93	0.620	0.61	0.182
23	5M	0	0.11	0.004	0.12	0.005	0.11	0.004
24		15	0.38	0.058	0.45	0.088	0.17	0.010
25		30	0.55	0.135	0.64	0.201	0.23	0.021
26		45	0.85	0.446	0.93	0.621	0.64	0.203
27		60	0.85	0.461	0.95	0.679	0.64	0.203
28								
29								
30	kvalue							
31			Co		Ni		Mn	
32	1.00	0.00	0.00080	-7.13	0.00100	-6.91	0.00040	-7.82
33	2.00	0.69	0.00170	-6.38	0.00220	-6.12	0.00090	-7.01
34	3.00	1.10	0.00540	-5.22	0.00750	-4.89	0.00260	-5.95
35	4.00	1.39	0.00760	-4.88	0.01120	-4.49	0.00350	-5.65
36	5.00	1.61	0.00870	-4.74	0.01250	-4.38	0.00390	-5.55
37								
38		Co	Ni	Mn				
39	Mvalue	1.6041	1.7075	1.5255				
40	Nvalue	-7.2066	-6.9937	-7.8589				

Appendix B23: Activation Energy Calculations

	A	B	C	D	E	F	G	H	I
2	Reaction Model		lnk			Ea			
3							Co	Ni	Mn
4		Co	Ni	Mn			-31.591537	-36.024562	-27.111954
5	1	-6.21	-6.12	-6.50					
6	2	-5.81	-5.68	-6.12					
7	3	-5.15	-4.95	-5.55					
8	4	-4.93	-4.66	-5.38					
9	5	-4.84	-4.57	-5.32					
10									
11									
12									
13	Diffusion Model					Ea			
14	1	-7.13	-6.91	-7.82			Co	Ni	Mn
15	2	-6.38	-6.12	-7.01			-54.732725	-58.296937	-51.674004
16	3	-5.22	-4.89	-5.95					
17	4	-4.88	-4.49	-5.65					
18	5	-4.74	-4.38	-5.55					
19									
20									
21									
22									
23		T(K)							
24		303.15	0.0032987	3.29869701					
25		313.15	0.00319336	3.19335782					
26		323.15	0.00309454	3.09453814					
27		333.15	0.00300165	3.00165091					
28		343.15	0.00291418	2.91417747					

Appendix B24: Reaction Rate Coefficient

	A	B	C	D
2	Diffusion Model			
3		Co	Ni	Mn
4	C	3	3	3
5	M	1.60	1.71	1.53
6	S/L	50	50	50
7	N	-7.21	-6.99	-7.86
8	Ea	-54.732725	-58.296937	-51.674004
9	R	8.314	8.314	8.314
10	T	323.14	323.14	323.14
11	k	0.0054	0.0075	0.0026
12				
13	k0	1.59E+09	8.57E+08	1.07E+10
14				
15	Reaction Model			
16		Co	Ni	Mn
17	C	3	3	3
18	M	0.921	1.0462	0.7959
19	S/L	50	50	50
20	N	-6.2715	-6.1965	-6.5358
21	Ea	-31.591537	-36.024562	-27.111954
22	R	8.314	8.314	8.314
23	T	323.14	323.14	323.14
24	k	0.0058	0.0071	0.0039
25				
26	k0	9.42E+07	7.48E+07	2.05E+08

Appendix C1: Mass Balance Data

	A	B	C	D	E	F	G	H	I	J	K	L
6	Company/Source	Region	Year	Value	Unit	Link						
7	Unison	Hawkes Bay	2019	3.9	tons batteries (Hawkes Bay)/year	https://www.baybuzz.co.nz/2019/12/01/batteries-face-serious-charges/						
8	Vector	NZ	2019	17026	Evs	https://blob-static.vector.co.nz/blob/vector/media/vector/vector_new_energy_futures_paper						
9	Vector	NZ	2020	997	Battery Packs	https://blob-static.vector.co.nz/blob/vector/media/vector/vector_new_energy_futures_paper						
10	Vector	NZ	2030	83807	Battery Packs	https://blob-static.vector.co.nz/blob/vector/media/vector/vector_new_energy_futures_paper						
11				150852.6								
12	WasteMINZ	NZ		600 - 800	tons (small handheld)	Email Correspondance						
13	WasteMINZ	NZ		480 - 640	tons (small handheld LiBs)	Email Correspondance						
14	IFRI	World	2016	80%	Market Share (small batteries)	https://www.ifri.org/sites/default/files/atoms/files/danino_recycling_batteries_2020.pdf						
15	IFRI	World	2016	8%	Market Share (small batteries inc. Lead Acid)	https://www.ifri.org/sites/default/files/atoms/files/danino_recycling_batteries_2020.pdf						
16	IFRI	Europe	2016	74906	tons LiBs Brought to Market	https://www.ifri.org/sites/default/files/atoms/files/danino_recycling_batteries_2020.pdf						
17	ProSUM	Europe	2015	85000	tons LiBs Brought to Market	https://www.ifri.org/sites/default/files/atoms/files/danino_recycling_batteries_2020.pdf						

Appendix C2: Electric Vehicle Data

	A	B	C	D	E	F	G	H	I	J
5	Model		Year	Cells	Source	Unit	Battery Pack Weight (kg)	Source	Cell Weight (g)	Source
6	BMW	-	2018	96	https://www	Cells in 33 kWh BMW I3	230	https://www.b		
7	Nissan	-	2018	192	https://www	Cells in 30 kWh Nissan Leaf	270	https://www.n	799	http://www.el
8	Tesla	-	2018	7104	https://www	Cells in 85 kWh Model S	544	https://www.te	45	https://cleante
9	Tesla	-	2017	4416	https://www	Cells in 75 kWh Model 3	478	https://www.te	45	https://cleante
10	Tesla	-	2017	8000	Estimated	Cells in 100 kWh Model X	771	https://www.te	45	https://cleante
11	Tesla	-	2017	7200	Estimated	Cells in 90 kWh Model X	544	https://www.te	45	https://cleante
12	Golf	-	2019	264	https://www	Cells in 35.8 kWh Model E-golf	330	https://www.g		
13	Nissan		2020	192	https://www	Cells in 40 kWh ENV200	290	https://www.n	799	http://www.el
14	Hyundai	-	2019	176	https://www	Cells in 28 kWh Ioniq	271.8	https://www.h		
15	Hyundai	-	2019	180	https://www	Cells in 39.2 kWh Kona	380.52	Estimated		
16										
17	Transport NZ	NZ	2020	20916	Evs inc. PHEV	https://www.transport.govt.nz/n				

Appendix C3: Transport NZ Data

	A	B	C	D	E	F	G	H	I	J	K	L	M	N	O	P	Q	R	S	T	U	V	W	X	Y	Z	AA	AB	AC	AD	AE	AF
7				**2015**	**2015**	**2015**	**2015**	**2015**	**2016**	**2016**	**2016**	**2016**	**2016**	**2017**	**2017**	**2017**	**2017**	**2017**	**2018**	**2018**	**2018**	**2018**	**2018**	**2019**	**2019**	**2019**	**2019**	**2019**	**2020**	**2020**	**2020**	**Grand Total**
8	**New**	Ev Type	Vehicle Make Model	15Q1	15Q2	15Q3	15Q4	Total	16Q1	16Q2	16Q3	16Q4	Total	17Q1	17Q2	17Q3	17Q4	Total	18Q1	18Q2	18Q3	18Q4	Total	19Q1	19Q2	19Q3	19Q4	Total	20Q1	20Q2	Total	Total
9	**Heavy EV**	Pure electric	Alexander Dennis Enviro 200																2				2		3	5		8				10
10	**Heavy EV**	Pure electric	Byd K9ra											1				1														1
11	**Heavy EV**	Pure electric	Factory Built C12rfdd																		1		1									1
12	**Heavy EV**	Pure electric	Factory Built Ev10														1	1		1			1		1			1	1		1	4
13	**Heavy EV**	Pure electric	Factory Built Golden Dragon																								1	1				1
14	**Heavy EV**	Pure electric	Factory Built Sea Electric																		2	1	3				2	2				5
15	**Heavy EV**	Pure electric	Factory Built Teg Hunan																2	1	7	1	11									11
16	**Heavy EV**	Pure electric	Factory Built Yutong																					1				1				1
17	**Heavy EV**	Pure electric	Fuso Ecanter																							1		1				1
18	**Heavy EV**	Pure electric	Hino 500							1			1		1	1	1	3														4
19	**Heavy EV**	Pure electric	Hino Gh																								1	1				1
20	**Heavy EV**	Pure electric	Isuzu F Series						1		1		2				1	1							1	2	4	7	4		4	14
21	**Heavy EV**	Pure electric	Isuzu Fsr																								1	1				1
22	**Heavy EV**	Pure electric	Isuzu N Series																							3		3				3
23	**Heavy EV**	Pure electric	Iveco Acco																								2	2				2
24	**Heavy EV**	Pure electric	Ldv Ev80																1		10	17	28	6	1	6	6	19	1	2	3	50
25	**Heavy EV**	Pure electric	Xcmg E300																		1		1									1
144	**Used light**	Pure electric	Tesla Model S 70 D												1			1														1
145	**Used light**	Pure electric	Tesla Model X			2		2													1		1				1	1				4
146	**Used light**	Pure electric	Toyota Alphard																	1			1									1
147	**Used light**	Pure electric	Toyota Aqua																	2		1	3									3
148	**Used light**	Pure electric	Toyota Camry																								1	1				1
149	**Used light**	Pure electric	Toyota Corolla												1			1														1
150	**Used light**	Pure electric	Volkswagen E-golf											2		1		3							1		1	2				5
151	**Used light**	Pure electric	Volkswagen E-Golf								2		2	2	1			3						1		1	3	5	2		2	12
152	**Used light**	Pure electric	Volkswagen E-Up												1			1														1
153	**Used light**	Pure electric	Total	33	34	49	81	197	104	157	197	244	702	340	474	628	790	2,232	619	943	984	1,057	3,603	856	913	941	789	3,499	764	384	1,148	11,381
154	**Grand Total**	Total	Total	129	113	123	140	505	172	377	396	573	1,518	646	780	970	1,295	3,691	1,047	1,466	1,563	1,514	5,590	1,457	1,700	2,182	1,679	7,018	1,624	810	2,434	20,756

Appendix C4: Transport NZ EV Registrations Data

	A	B	C	D	E	F	G	H	I	J	K	L	M	N
1	Light EV fleet size_crosstab													
2	**Year of Period**	**Electric Hybrid**	**Jan**	**Feb**	**Mar**	**Apr**	**May**	**Jun**	**Jul**	**Aug**	**Sep**	**Oct**	**Nov**	**Dec**
3	**2013**	New light plug-in hybrid	5	5	6	6	6	7	7	7	8	11	11	11
4	**2013**	New light pure electric	90	90	97	97	97	97	96	97	98	99	99	99
5	**2013**	Used light pure electric	33	33	33	33	34	36	38	39	40	44	49	53
6	**2013**	Total	128	128	136	136	137	140	141	143	146	154	159	163
7	**2014**	New light plug-in hybrid	13	24	54	91	115	135	146	156	175	192	207	224
8	**2014**	New light pure electric	99	98	99	102	110	113	123	128	131	133	136	138
9	**2014**	Used light plug-in hybrid	1	1	1	1	2	2	2	2	2	2	2	2
10	**2014**	Used light pure electric	55	56	65	68	74	75	81	90	93	101	116	124
11	**2014**	Total	168	179	219	262	301	325	352	376	401	428	461	488
12	**2015**	New light plug-in hybrid	248	261	307	321	335	355	370	386	410	424	441	451
13	**2015**	New light pure electric	144	150	150	160	162	178	183	188	192	194	198	205
14	**2015**	Used light plug-in hybrid	2	2	3	3	4	6	10	11	11	12	14	15
15	**2015**	Used light pure electric	135	146	157	166	178	191	215	223	239	262	284	320
16	**2015**	Total	529	559	617	650	679	730	778	808	852	892	937	991
17	**2016**	New light plug-in hybrid	463	476	505	542	566	610	643	670	695	738	766	779
18	**2016**	New light pure electric	210	211	213	220	224	315	348	368	381	394	498	581
19	**2016**	Used light plug-in hybrid	17	18	19	22	25	29	39	56	74	91	102	116
20	**2016**	Used light pure electric	361	382	422	467	522	577	653	713	771	862	941	1,012
21	**2016**	Total	1,051	1,087	1,159	1,251	1,337	1,531	1,683	1,807	1,921	2,085	2,307	2,488
22	**2017**	New light plug-in hybrid	801	826	867	894	933	995	1,026	1,068	1,107	1,138	1,174	1,199
23	**2017**	New light pure electric	641	718	743	757	822	869	904	949	998	1,102	1,199	1,262
24	**2017**	Used light plug-in hybrid	133	146	168	183	202	218	246	278	312	345	398	456
25	**2017**	Used light pure electric	1,116	1,228	1,347	1,475	1,635	1,818	2,012	2,228	2,439	2,707	2,998	3,227
26	**2017**	Total	2,691	2,918	3,125	3,309	3,592	3,900	4,188	4,523	4,856	5,292	5,769	6,144
27	**2018**	New light plug-in hybrid	1,231	1,294	1,351	1,407	1,488	1,542	1,617	1,680	1,760	1,820	1,901	1,939
28	**2018**	New light pure electric	1,327	1,357	1,424	1,476	1,551	1,634	1,678	1,753	1,835	1,906	1,962	2,002
29	**2018**	Used light plug-in hybrid	493	514	560	582	635	675	739	782	808	849	875	897
30	**2018**	Used light pure electric	3,507	3,679	3,844	4,090	4,449	4,779	5,129	5,447	5,753	6,214	6,541	6,799
31	**2018**	Total	6,558	6,844	7,179	7,555	8,123	8,630	9,163	9,662	10,156	10,789	11,279	11,637
32	**2019**	New light plug-in hybrid	1,989	2,106	2,176	2,240	2,338	2,408	2,468	2,553	2,659	2,762	2,844	2,879
33	**2019**	New light pure electric	2,066	2,145	2,220	2,315	2,410	2,616	2,701	2,891	3,393	3,541	3,687	3,859
34	**2019**	Used light plug-in hybrid	940	984	1,027	1,072	1,123	1,178	1,246	1,295	1,366	1,422	1,490	1,544
35	**2019**	Used light pure electric	7,087	7,372	7,643	7,914	8,238	8,541	8,877	9,152	9,462	9,751	10,005	10,241
36	**2019**	Total	12,082	12,607	13,066	13,541	14,109	14,743	15,292	15,891	16,880	17,476	18,026	18,523
37	**2020**	New light plug-in hybrid	2,969	3,081	3,139	3,141	3,194	3,247						
38	**2020**	New light pure electric	3,998	4,116	4,260	4,275	4,332	4,463						
39	**2020**	Used light plug-in hybrid	1,618	1,677	1,729	1,731	1,779	1,834						
40	**2020**	Used light pure electric	10,532	10,785	10,998	11,009	11,155	11,372						
41	**2020**	Total	19,117	19,659	20,126	20,156	20,460	20,916						

Appendix D1: Preliminary Economic Analysis

	A	B	C	D	E	F	G	H	I	J	K
15		% Cathode	% Recovery	% Overall	Metal Recovered (g)	Revenue (NZD/kg LiB)		Cost (NZD)	Unit (g)	Supplier	
16	Li_2CO_3	7.6%	10.3%	0.2%	2.1	$ 2.16		$ 102.00	100	https://www.sigmaaldrich.	
17	$CoSO_4$	20.5%	20.5%	1.1%	11.4	$ 215.80		$ 190.00	10	https://www.sigmaaldrich.	
18	$NiSO_4$	19.4%	20.3%	1.1%	10.6	$ 117.55		$ 111.00	10	https://www.sigmaaldrich.	
19	MnO_2	19.5%	62.4%	3.3%	32.8	$ 31.08		$ 94.80	100	https://www.sigmaaldrich.	
20	Non Metals	33.1%									
21											
22		% Case	% Recovery		Metal Recovered (kg)	Revenue (NZD/kg LiB)		Cost (NZD)	Unit (kg)		
23	Fe	25%	90%	23%	0.2	$ 54.23		$ 241.00	1	https://www.sigmaaldrich.	
24											
25		% Foils	% Recovery		Metal Recovered (kg)	Revenue (NZD/kg LiB)		Cost (NZD)	Unit (kg)		
26	Al	7%	90%	6%	0.1	$ 31.01		$ 265.00	0.500	https://www.sigmaaldrich.	
27	Cu	7%	90%	6%	0.1	$ 17.55		$ 300.00	1	https://www.sigmaaldrich.	
28											
29		% Electrolyte	% Recovery		Electrolyte Recovered (g)	Revenue (NZD/kg LiB)		Cost (NZD)	Unit (ml)		
30	$LiPF_6$ in EC/DMC	10%	90%	9%	90.0	$ 162.90		$ 905.00	500	https://www.sigmaaldrich.	
31											
32	**Total**					$ 632.26	per	1	kg	Influent Lithium-ion Batteri	
33											
34											
35	Li_2CO_3	$ 2.16	0.2%	2							
36	Cu	$ 17.55	5.9%	59							
37	Al	$ 31.01	5.9%	59							
38	MnO_2	$ 31.08	3.3%	33							
39	Fe	$ 54.23	23%	225							
40	$NiSO_4$	$ 117.55	1.1%	11							
41	$LiPF_6$	$ 162.90	9%	90							
42	$CoSO_4$	$ 215.80	1.1%	11							
43				511							

Appendix E1: Battery Pack Design Calculations

	A	B	C	D	E
1	Battery Sizing Calculations				
2	Zain Kader				
3	3/07/2020				
4		Changeable inputs			
5					
6					
7	**Description**	**Value**	**Unit**	**Formula**	**Notes**
8					
9	**18650 Cell**				
10	Capacity (Typical)	3180	mAh		
11	Voltage (Nominal)	3.6	V		
12	Max Continuous Discharge Rate	10	A		
13	DR	3.1	C	=(B12/(B10/1000))	
14					
15	**Pack**				
16	Series	7	Cells	=ROUNDUP((B25/B11), 0)	
17	Parallel	15	Cells	=ROUND(B30/(B10/1000),0)	
18	Voltage	25.2	V	=B11*B16	
19	Capacity	47.70	Ah	=B17*B10/1000	
20	Power	1.20	kWh	=B19*B18/1000	
21	Cells	105		=B35*B36	
22	Current	150	A	=B12*B17	Max discharge current (Capacity))
23					
24	**Inverter**				
25	Output Voltage Requirement	24	V		
26	Output Current Requirement	25	A		
27	Output Power Requirement	600	W		
28	Run Time	2	hours/day		
29	Output Energy Requirment	1200	Wh	=B27*B28	
30	Capacity Requirement	48	Ah	=B29/B18	
31					
32	**BMS Requirement**				
33	Current	150	A	=B22	Max discharge current (Capacity)
34	Voltage	25.2	V	=B18	
35	Sizing	7	s	=B16	
36		15	p	=B17	
37	Separate				Charge/Discharge
38					
39	**Solar**				
40	Time to charge	7.5	hours	=(B20*1000)/Components!B30	Could use more solar panels, but $$$
41					
42	**Solar Controller**				
43	Current	6.3	A	=Components!B30/'Battery Design'!B18	Use higher rated controller for solar upgrade in the future (factor of 2)
44					
45					
46	**Cost**				
47	BMS	$138.00		=IF(B33<=Components!B6,Components!B7,IF('Battery Design'!B33<=Components	
48	Cell	$331.58		=B35*B36*Components!B18	
49	Case	$13.65		=B35*B36*Components!B21	Using single cell holder
50	Inverter	$94.90		=Components!B26	
51	Solar Panel	$239.00		=Components!B31	160W unit
52	Solar Controller	$50.26		=Components!B35	10 A
53	Kapton Tape	$35.00			
54	Connectors	$50.00			
55					
56					
57	**Total**	**$952.39**			

Appendix E2: Battery Pack Component Calculations

	A	B	C	D	E	F
3	Description	Value	Unit	Formula	Supplier	Notes
4						
5	**BMS #1**					
6	Current	70	A			Separate
7	Cost	$40			https://www.aliexpress.c	
8						
9	**BMS #2**					
10	Current	150	A			Separate
11	Cost	$138.0			https://www.aliexpress.c	
12						
13	**BMS #3**					
14	Current	220	A			Common
15	Cost	$190			https://www.aliexpress.c	
16						
17	**Cell**					
18	Cost	$3.16	per Cell	=600/190	GearShop	
19						
20	**Cell Cases**					
21	Cost	$0.13	per cell		https://www.aliexpress.c	
22		$0.49	Per 3 Cells		https://www.aliexpress.c	
23		$0.58	per 4 Cells		https://www.aliexpress.c	
24						
25	**Inverter**					
26	Cost	$94.90			https://www.jaycar.co.n	(1500 W surge)
27						
28	**Solar Panel**					
29	Voltage	12	V			
30	Power	160	W			
31	Cost	$239.00			https://www.jaycar.co.n	
32						
33	**Solar Controller**					
34	Current	10	A			
35	Cost	$50.26			https://www.aliexpress.c	

Appendix F1: Battery Survey

	A	B	C	D	E	F	G	H	I	J
2	**Cell #**	**Voltage**	**Manufacturer**	**Model**	**Capacity (mAh)**	**Max Discharge (A)**	**Max Charge (A)**	**Chemistry**	**Image**	**Data Sheet**
3	1	0	Sanyo/Panasonic	UR18650FK	2400 (2.5V)	4.6	2.3	ICR / LCO (LiCoO2)		Data Sheet
4	2	0	Sanyo/Panasonic	UR18650FK	2400 (2.5V)	4.6	2.3	ICR / LCO (LiCoO2)		Data Sheet
5	3	0	Sanyo/Panasonic	UR18650FK	2400 (2.5V)	4.6	2.3	ICR / LCO (LiCoO2)		Data Sheet
6	4	0	Sanyo/Panasonic	UR18650FK	2400 (2.5V)	4.6	2.3	ICR / LCO (LiCoO2)		Data Sheet
7	5	0	Sanyo/Panasonic	UR18650FK	2400 (2.5V)	4.6	2.3	ICR / LCO (LiCoO2)		Data Sheet
8	6	0	Sanyo/Panasonic	UR18650FK	2400 (2.5V)	4.6	2.3	ICR / LCO (LiCoO2)		Data Sheet
9	7	0	Samsung	ICR18650-22E	2200 (2.75V)	4.4	1.1 (2.2)	INR / NMC (LiNiMnCoO2)		Data Sheet
10	8	0.02	Sony	US18650VTC3	1600 (2.5V)	10 (30)	1.5 (3)	INR / NMC (LiNiMnCoO2)		Data Sheet

	A	B	C	D	E	F	G	H	I	J
11	9	0.02	Sony	US18650VTC3	1600 (2.5V)	10 (30)	1.5 (3)	INR / NMC (LiNiMnCoO2)		Data Sheet
12	10	0.04	Sony	US18650VTC6	3120 (2V)	15 (30)	2 (5)	INR / NMC (LiNiMnCoO2)		Data Sheet
13	11	0.05	Sony	US18650VTC3	1600 (2.5V)	10 (30)	1.5 (3)	INR / NMC (LiNiMnCoO2)		Data Sheet
14	12	0.05	Sony	US18650VTC3	1600 (2.5V)	10 (30)	1.5 (3)	INR / NMC (LiNiMnCoO2)		Data Sheet
15	13	0.1	Sony	US18650VTC6	3120 (2V)	15 (30)	2 (5)	INR / NMC (LiNiMnCoO2)		Data Sheet
16	14	0.11	Sony	US18650VTC6	3120 (2V)	15 (30)	2 (5)	INR / NMC (LiNiMnCoO2)		Data Sheet
17	15	0.12	Sony	US18650VTC6	3120 (2V)	15 (30)	2 (5)	INR / NMC (LiNiMnCoO2)		Data Sheet
18	16	0.12	LG	LGDAS31865 / ICR18650S3	2200	3.2	1.075	INR / NMC (LiNiMnCoO2)		Data Sheet
19	17	0.14	LG	LGDAS31865 / ICR18650S3	2200	3.2	1.075	INR / NMC (LiNiMnCoO2)		Data Sheet
20	18	0.15	Panasonic	CGR18650E	2550 (3V)	4.9	1.715	ICR / LCO (LiCoO2)		Data Sheet

	A	B	C	D	E	F	G	H	I	J
21	19	0.15	Panasonic	CGR18650E	2550 (3V)	4.9	1.715	ICR / LCO (LiCoO2)		Data Sheet
22	20	0.15	Panasonic	CGR18650E	2550 (3V)	4.9	1.715	ICR / LCO (LiCoO2)		Data Sheet
23	21	0.15	Panasonic	CGR18650E	2550 (3V)	4.9	1.715	ICR / LCO (LiCoO2)		Data Sheet
24	22	0.68	Sony	US18650VTC3	1600 (2.5V)	10 (30)	1.5 (3)	INR / NMC (LiNiMnCoO2)		Data Sheet
25	23	0.75	Sony	US18650VTC3	1600 (2.5V)	10 (30)	1.5 (3)	INR / NMC (LiNiMnCoO2)		Data Sheet
26	24	0.77	BAK	C18650CC	2600 (3V)	5.2	2.6	ICR / LCO (LiCoO2)		
27	25	0.78	Sony	US18650VTC3	1600 (2.5V)	10 (30)	1.5 (3)	INR / NMC (LiNiMnCoO2)		Data Sheet
28	26	1.26	LG	LGDAS31865 / ICR18650S3	2200	3.2	1.075	INR / NMC (LiNiMnCoO2)		Data Sheet
29	27	1.28	LG	LGDAS31865 / ICR18650S3	2200	3.2	1.075	INR / NMC (LiNiMnCoO2)		Data Sheet
30	28	1.31	LG	LGABE11865 / ICR18650E1	3200 (2.5V)	1.55 (4.6)	1.55	NCA (LiNiCoAlO2)	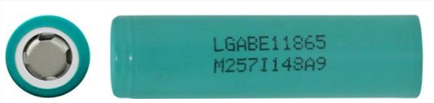	Data Sheet

	A	B	C	D	E	F	G	H	I	J
31	29	1.57	Samsung	ICR18650-22E	2200 (2.75V)	4.4	1.1 (2.2)	INR / NMC (LiNiMnCoO2)		Data Sheet
32	30	1.59	Panasonic	NCR18650BD	3200 (2.5V)	10	1.5	NCA (LiNiCoAlO2)		Data Sheet
33	31	1.6	Samsung	ICR18650-22E	2200 (2.75V)	4.4	1.1 (2.2)	INR / NMC (LiNiMnCoO2)		Data Sheet
34	32	1.6	Samsung	ICR18650-22E	2200 (2.75V)	4.4	1.1 (2.2)	INR / NMC (LiNiMnCoO2)		Data Sheet
35	33	1.6	Panasonic	NCR18650BD	3200 (2.5V)	10	1.5	NCA (LiNiCoAlO2)		Data Sheet
36	34	1.6	Samsung	ICR18650-22F	2200 (2.75V)	4.4	1.1 (2.2)	NCA (LiNiCoAlO2)		Data Sheet
37	35	1.62	Samsung	ICR18650-20C	2000 (? 2.75V)	2 (? 4)	?	ICR / LCO (LiCoO2)		Data Sheet
38	36	1.62	Samsung	ICR18650-20C	2000 (? 2.75V)	2 (? 4)	?	ICR / LCO (LiCoO2)		Data Sheet
39	37	1.62	Samsung	ICR18650-22E	2200 (2.75V)	4.4	1.1 (2.2)	INR / NMC (LiNiMnCoO2)		Data Sheet
40	38	1.72	Samsung	ICR18650-22E	2200 (2.75V)	4.4	1.1 (2.2)	INR / NMC (LiNiMnCoO2)		Data Sheet

	A	B	C	D	E	F	G	H	I	J
41	39	1.81	Samsung	ICR18650-22E	2200 (2.75V)	4.4	1.1 (2.2)	INR / NMC (LiNiMnCoO2)		Data Sheet
42	40	1.83	LG	LGDAS31865 / ICR18650S3	2200	3.2	1.075	INR / NMC (LiNiMnCoO2)		Data Sheet
43	41	1.83	Samsung	ICR18650-22E	2200 (2.75V)	4.4	1.1 (2.2)	INR / NMC (LiNiMnCoO2)		Data Sheet
44	42	1.83	LG	LGDAS31865 / ICR18650S3	2200	3.2	1.075	INR / NMC (LiNiMnCoO2)		Data Sheet
45	43	2.14	LG	LGABB41865 / ICR18650B4	2600	1.25 (5)	1.25 (2.5)	ICR / LCO (LiCoO2)		Data Sheet
46	44	2.14	LG	LGABB41865 / ICR18650B4	2600	1.25 (5)	1.25 (2.5)	ICR / LCO (LiCoO2)		Data Sheet
47	45	2.17	LG	LGABB41865 / ICR18650B4	2600	1.25 (5)	1.25 (2.5)	ICR / LCO (LiCoO2)		Data Sheet
48	46	2.17	LG	LGABB41865 / ICR18650B4	2600	1.25 (5)	1.25 (2.5)	ICR / LCO (LiCoO2)		Data Sheet
49	47	2.31	LG	LGABB41865 / ICR18650B4	2600	1.25 (5)	1.25 (2.5)	ICR / LCO (LiCoO2)		Data Sheet
50	48	2.31	LG	LGABB41865 / ICR18650B4	2600	1.25 (5)	1.25 (2.5)	ICR / LCO (LiCoO2)		Data Sheet

	A	B	C	D	E	F	G	H	I	J
51	49	2.34	LG	LGDAS31865 / ICR18650S3	2200	3.2	1.075	INR / NMC (LiNiMnCoO2)		Data Sheet
52	50	2.34	LG	LGDAS31865 / ICR18650S3	2200	3.2	1.075	INR / NMC (LiNiMnCoO2)		Data Sheet
53	51	2.35	LG	LGDAS31865 / ICR18650S3	2200	3.2	1.075	INR / NMC (LiNiMnCoO2)		Data Sheet
54	52	2.36	LG	LGDAS31865 / ICR18650S3	2200	3.2	1.075	INR / NMC (LiNiMnCoO2)		Data Sheet
55	53	2.41	Samsung	ICR18650-22F	2200 (2.75V)	4.4	1.1 (2.2)	NCA (LiNiCoAlO2)		Data Sheet
56	54	2.41	Samsung	ICR18650-22F	2200 (2.75V)	4.4	1.1 (2.2)	NCA (LiNiCoAlO2)		Data Sheet
57	55	2.54	Panasonic	NCR18650B	3350 (2.5V)	4.875 (6.5)	1.625	NCA (LiNiCoAlO2)		Data Sheet
58	56	2.54	Panasonic	NCR18650B	3350 (2.5V)	4.875 (6.5)	1.625	NCA (LiNiCoAlO2)		Data Sheet
59	57	2.6	Samsung	ICR18650-28A	2800 (2.75V)	5.6	1.4 (2.8)	ICR / LCO (LiCoO2)		Data Sheet
60	58	2.6	Samsung	ICR18650-28A	2800 (2.75V)	5.6	1.4 (2.8)	ICR / LCO (LiCoO2)		Data Sheet

	A	B	C	D	E	F	G	H	I	J
61	59	2.63	Panasonic	NCR18650B	3350 (2.5V)	4.875 (6.5)	1.625	NCA (LiNiCoAlO2)		Data Sheet
62	60	2.63	Panasonic	NCR18650B	3350 (2.5V)	4.875 (6.5)	1.625	NCA (LiNiCoAlO2)		Data Sheet
63	61	2.63	Panasonic	NCR18650B	3350 (2.5V)	4.875 (6.5)	1.625	NCA (LiNiCoAlO2)		Data Sheet
64	62	2.64	Panasonic	NCR18650B	3350 (2.5V)	4.875 (6.5)	1.625	NCA (LiNiCoAlO2)		Data Sheet
65	63	2.85	Samsung	ICR18650-28A	2800 (2.75V)	5.6	1.4 (2.8)	ICR / LCO (LiCoO2)		Data Sheet
66	64	2.85	Samsung	ICR18650-28A	2800 (2.75V)	5.6	1.4 (2.8)	ICR / LCO (LiCoO2)		Data Sheet
67	65	2.93	Sanyo/Panasonic	UR18650FK	2400 (2.5V)	4.6	2.3	ICR / LCO (LiCoO2)		
68	66	2.93	Sanyo/Panasonic	UR18650FK	2400 (2.5V)	4.6	2.3	ICR / LCO (LiCoO2)		
69	67	2.98	Samsung	ICR18650-20C	2000 (? 2.75V)	2 (? 4)	?	ICR / LCO (LiCoO2)		Data Sheet
70	68	2.99	Samsung	ICR18650-20C	2000 (? 2.75V)	2 (? 4)	?	ICR / LCO (LiCoO2)		Data Sheet

	A	B	C	D	E	F	G	H	I	J
71	69	3	Samsung	ICR18650-20C	2000 (? 2.75V)	2 (? 4)	?	ICR / LCO (LiCoO2)		Data Sheet
72	70	3	Samsung	ICR18650-20C	2000 (? 2.75V)	2 (? 4)	?	ICR / LCO (LiCoO2)		Data Sheet
73	71	3.08	Sanyo/Panasonic	UR18650FK	2400 (2.5V)	4.6	2.3	ICR / LCO (LiCoO2)		Data Sheet
74	72	3.08	Sanyo/Panasonic	UR18650FK	2400 (2.5V)	4.6	2.3	ICR / LCO (LiCoO2)		Data Sheet
75	73	3.1	Samsung	ICR18650-22F	2200 (2.75V)	4.4	1.1 (2.2)	NCA (LiNiCoAlO2)		Data Sheet
76	74	3.11	Panasonic	NCR18650BD	3200 (2.5V)	10	1.5	NCA (LiNiCoAlO2)		Data Sheet
77	75	3.12	Panasonic	NCR18650BD	3200 (2.5V)	10	1.5	NCA (LiNiCoAlO2)		Data Sheet
78	76	3.12	Panasonic	NCR18650BD	3200 (2.5V)	10	1.5	NCA (LiNiCoAlO2)		Data Sheet
79	77	2.12	Panasonic	NCR18650BD	3200 (2.5V)	10	1.5	NCA (LiNiCoAlO2)		Data Sheet
80	78	3.13	Panasonic	NCR18650BD	3200 (2.5V)	10	1.5	NCA (LiNiCoAlO2)		Data Sheet

	A	B	C	D	E	F	G	H	I	J
81	79	3.13	Panasonic	NCR18650BD	3200 (2.5V)	10	1.5	NCA (LiNiCoAlO2)		Data Sheet
82	80	3.14	Sanyo/Panasonic	UR18650FK	2400 (2.5V)	4.6	2.3	ICR / LCO (LiCoO2)		Data Sheet
83	81	3.14	Sanyo/Panasonic	UR18650FK	2400 (2.5V)	4.6	2.3	ICR / LCO (LiCoO2)		Data Sheet
84	82	3.18	Samsung	ICR18650-28A	2800 (2.75V)	5.6	1.4 (2.8)	ICR / LCO (LiCoO2)		Data Sheet
85	83	3.18	Samsung	ICR18650-28A	2800 (2.75V)	5.6	1.4 (2.8)	ICR / LCO (LiCoO2)		Data Sheet
86	84	3.25	LG	LGDAS31865 / ICR18650S3	2200	3.2	1.075	INR / NMC (LiNiMnCoO2)		Data Sheet
87	85	3.25	LG	LGDAS31865 / ICR18650S3	2200	3.2	1.075	INR / NMC (LiNiMnCoO2)		Data Sheet
88	86	3.32	Samsung	ICR18650-22E	2200 (2.75V)	4.4	1.1 (2.2)	INR / NMC (LiNiMnCoO2)		Data Sheet
89	87	3.53	Panasonic	NCR18650B	3350 (2.5V)	4.875 (6.5)	1.625	NCA (LiNiCoAlO2)		Data Sheet
90	88	3.54	Panasonic	NCR18650B	3350 (2.5V)	4.875 (6.5)	1.625	NCA (LiNiCoAlO2)		Data Sheet

	A	B	C	D	E	F	G	H	I	J
91	89	3.54	Panasonic	NCR18650B	3350 (2.5V)	4.875 (6.5)	1.625	NCA (LiNiCoAlO2)		Data Sheet
92	90	3.54	Panasonic	NCR18650B	3350 (2.5V)	4.875 (6.5)	1.625	NCA (LiNiCoAlO2)		Data Sheet
93	91	3.59	Samsung	ICR18650-22F	2200 (2.75V)	4.4	1.1 (2.2)	NCA (LiNiCoAlO2)		Data Sheet
94	92	3.59	Samsung	ICR18650-22F	2200 (2.75V)	4.4	1.1 (2.2)	NCA (LiNiCoAlO2)		Data Sheet
95	93	3.59	Samsung	ICR18650-22F	2200 (2.75V)	4.4	1.1 (2.2)	NCA (LiNiCoAlO2)		Data Sheet
96	94	3.59	Samsung	ICR18650-22F	2200 (2.75V)	4.4	1.1 (2.2)	NCA (LiNiCoAlO2)		Data Sheet
97	95	3.58	Samsung	ICR18650-22F	2200 (2.75V)	4.4	1.1 (2.2)	NCA (LiNiCoAlO2)		Data Sheet
98	96	3.6	Samsung	ICR18650-22F	2200 (2.75V)	4.4	1.1 (2.2)	NCA (LiNiCoAlO2)		Data Sheet
99	97	3.63	Samsung	ICR18650-22F	2200 (2.75V)	4.4	1.1 (2.2)	NCA (LiNiCoAlO2)		Data Sheet
100	98	3.63	Samsung	ICR18650-22F	2200 (2.75V)	4.4	1.1 (2.2)	NCA (LiNiCoAlO2)		Data Sheet

	A	B	C	D	E	F	G	H	I	J
101	99	3.66	Panasonic	NCR18650BD	3200 (2.5V)	10	1.5	NCA (LiNiCoAlO2)		Data Sheet
102	100	3.68	Panasonic	NCR18650BD	3200 (2.5V)	10	1.5	NCA (LiNiCoAlO2)		Data Sheet
103	101	3.69	LG	LGDAS31865 / ICR18650S3	2200	3.2	1.075	INR / NMC (LiNiMnCoO2)		Data Sheet
104	102	3.69	LG	LGDAS31865 / ICR18650S3	2200	3.2	1.075	INR / NMC (LiNiMnCoO2)		Data Sheet
105	103	3.72	Sanyo/Panasonic	UR18650RX	2000	22	1.37	IMR / LMO (LiMn2O4)		Data Sheet
106	104	3.73	Sanyo/Panasonic	UR18650RX	2000	22	1.37	IMR / LMO (LiMn2O4)		Data Sheet
107	105	3.73	Sanyo/Panasonic	UR18650RX	2000	22	1.37	IMR / LMO (LiMn2O4)		Data Sheet
108	106	3.73	Sanyo/Panasonic	UR18650RX	2000	22	1.37	IMR / LMO (LiMn2O4)		Data Sheet
109	107	3.73	Sanyo/Panasonic	UR18650RX	2000	22	1.37	IMR / LMO (LiMn2O4)		Data Sheet
110	108	3.73	Sanyo/Panasonic	UR18650RX	2000	22	1.37	IMR / LMO (LiMn2O4)		Data Sheet

	A	B	C	D	E	F	G	H	I	J
111	109	3.8	Samsung	INR18650-25R	2500 (2.5V)	10 (20, 100 Pulse)	1.25 (4)	INR / NMC (LiNiMnCoO2)		Data Sheet
112	110	3.8	Samsung	INR18650-25R	2500 (2.5V)	10 (20, 100 Pulse)	1.25 (4)	INR / NMC (LiNiMnCoO2)		Data Sheet
113	111	4.01	LG	LGABE11865 / ICR18650E1	3200 (2.5V)	1.55 (4.6)	1.55	NCA (LiNiCoAlO2)	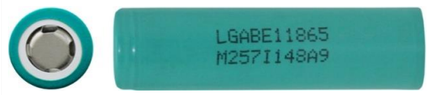	Data Sheet
114	112	4.02	LG	LGABE11865 / ICR18650E1	3200 (2.5V)	1.55 (4.6)	1.55	NCA (LiNiCoAlO2)	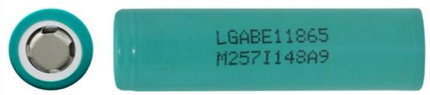	Data Sheet
115	113	4.05	LG	LGABE11865 / ICR18650E1	3200 (2.5V)	1.55 (4.6)	1.55	NCA (LiNiCoAlO2)	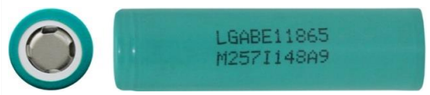	Data Sheet

References

Aaltonen, M., Peng, C., Wilson, B., & Lundström, M. (2017, 10/31). Leaching of Metals from Spent Lithium-Ion Batteries. *Recycling, 2*, 20.

Agrawal, K. K., Jain, S., Jain, A. K., & Dahiya, S. (2014). Assessment of greenhouse gas emissions from coal and natural gas thermal power plants using life cycle approach. *International Journal of Environmental Science and Technology, 11*(4), 1157-1164.

Amarakoon, S., Smith, J., & Segal, B. (2013). *Application of life-cycle assessment to nanoscale technology: Lithium-ion batteries for electric vehicles*.EPA.

Aravindan, V., Gnanaraj, J., Madhavi, S., & Liu, H. K. (2011). Lithium ‐ ion conducting electrolyte salts for lithium batteries. *Chemistry–A European Journal, 17*(51), 14326-14346.

Archuleta, M. M. (1995). Toxicity of materials used in the manufacture of lithium batteries. *Journal of Power Sources, 54*(1), 138-142.

Bahaloo-Horeh, N., & Mousavi, S. M. (2017). Enhanced recovery of valuable metals from spent lithium-ion batteries through optimization of organic acids produced by Aspergillus niger. *Waste management, 60*, 666-679.

Bahgat, M., Farghaly, F., Basir, S. A., & Fouad, O. (2007). Synthesis, characterization and magnetic properties of microcrystalline lithium cobalt ferrite from spent lithium-ion batteries. *Journal of materials processing technology, 183*(1), 117-121.

Barik, S., Prabaharan, G., & Kumar, L. (2017). Leaching and separation of Co and Mn from electrode materials of spent lithium-ion batteries using hydrochloric acid: Laboratory and pilot scale study. *Journal of cleaner production, 147*, 37-43.

Bernhardt, D., & Reilly, I. (2019). mineral commodity summaries 2019. *US Geological Survey, Reston, USA*, 42-43.

Bertuol, D. A., Toniasso, C., Jiménez, B. M., Meili, L., Dotto, G. L., Tanabe, E. H., & Aguiar, M. L. (2015). Application of spouted bed elutriation in the recycling of lithium ion batteries. *Journal of Power Sources, 275*, 627-632.

Buchmann, I. (2020). Battery University. Retrieved from https://batteryuniversity.com/learn/article/bu_808c_coulombic_and_energy_efficiency_with_the_battery

Castillo, S., Ansart, F., Laberty-Robert, C., & Portal, J. (2002). Advances in the recovering of spent lithium battery compounds. *Journal of Power Sources, 112*(1), 247-254.

Chagnes, A., & Pospiech, B. (2013). A brief review on hydrometallurgical technologies for recycling spent lithium‐ion batteries. *Journal of Chemical Technology & Biotechnology, 88*(7), 1191-1199.

Chen, M., Zheng, Z., Wang, Q., Zhang, Y., Ma, X., Shen, C., . . . Gionet, P. (2019). Closed loop recycling of electric vehicle batteries to enable ultra-high quality cathode powder. *Scientific reports, 9*(1), 1-9.

Chen, X., Fan, B., Xu, L., Zhou, T., & Kong, J. (2016). An atom-economic process for the recovery of high value-added metals from spent lithium-ion batteries. *Journal of cleaner production, 112*, 3562-3570.

Chen, X., Xu, B., Zhou, T., Liu, D., Hu, H., & Fan, S. (2015). Separation and recovery of metal values from leaching liquor of mixed-type of spent lithium-ion batteries. *Separation and Purification Technology, 144*, 197-205.

Ciez, R. E., & Whitacre, J. (2019). Examining different recycling processes for lithium-ion batteries. *Nature Sustainability, 2*(2), 148-156.

Contestabile, M., Panero, S., & Scrosati, B. (2001). A laboratory-scale lithium-ion battery recycling process. *Journal of Power Sources, 92*(1-2), 65-69.

Dahllöf, L., Romare, M., & Wu, A. (2019). *Mapping of lithium-ion batteries for vehicles: A study of their fate in the Nordic countries*: Nordic Council of Ministers.

Danino-Perraud, R. l. (2020). *The Recycling of Lithium-Ion Batteries: A Strategic Pillar for the European Battery Alliance*). Retrieved from https://www.ifri.org/sites/default/files/atoms/files/danino_recycling_batteries_2020.pdf

De las Casas, C., & Li, W. (2012). A review of application of carbon nanotubes for lithium ion battery anode material. *Journal of Power Sources, 208*, 74-85.

Dhiman, S., & Gupta, B. (2019). Partition studies on cobalt and recycling of valuable metals from waste Li-ion batteries via solvent extraction and chemical precipitation. *Journal of cleaner production, 225*, 820-832.

Dorella, G., & Mansur, M. B. (2007). A study of the separation of cobalt from spent Li-ion battery residues. *Journal of Power Sources, 170*(1), 210-215.

Fan, E., Li, L., Wang, Z., Lin, J., Huang, Y., Yao, Y., . . . Wu, F. (2020). Sustainable Recycling Technology for Li-Ion Batteries and Beyond: Challenges and Future Prospects. *Chemical Reviews*.

Friedrich, B., Peters, L., & Diaz, F. (2017). *State of research on Li-Ion battery recycling*.

Gaines, L. (2018). Lithium-ion battery recycling processes: Research towards a sustainable course. *Sustainable Materials and Technologies, 17*, e00068.

Gaines, L., Richa, K., & Spangenberger, J. (2018). Key issues for Li-ion battery recycling. *MRS Energy & Sustainability, 5*.

Gaines, L., Sullivan, J., Burnham, A., & Belharouak, I. (2012). *Life-cycle analysis for lithium-ion battery production and recycling.* Paper presented at the Transportation Research Board 90th Annual Meeting, Washington, DC.

Gao, W., Song, J., Cao, H., Lin, X., Zhang, X., Zheng, X., . . . Sun, Z. (2018). Selective recovery of valuable metals from spent lithium-ion batteries–process development and kinetics evaluation. *Journal of cleaner production, 178*, 833-845.

Garcia, E., Santos, J., Pereira, E., & Freitas, M. (2008). Electrodeposition of cobalt from spent Li-ion battery cathodes by the electrochemistry quartz crystal microbalance technique. *Journal of Power Sources, 185*(1), 549-553.

Granata, G., Moscardini, E., Pagnanelli, F., Trabucco, F., & Toro, L. (2012). Product recovery from Li-ion battery wastes coming from an industrial pre-treatment plant: Lab scale tests and process simulations. *Journal of Power Sources, 206*, 393-401.

Grützke, M., Mönnighoff, X., Horsthemke, F., Kraft, V., Winter, M., & Nowak, S. (2015). Extraction of lithium-ion battery electrolytes with liquid and supercritical carbon dioxide and additional solvents. *RSC Advances, 5*(54), 43209-43217.

Guan, J., Li, Y., Guo, Y., Su, R., Gao, G., Song, H., . . . Guo, Z. (2017). Mechanochemical process enhanced cobalt and lithium recycling from wasted lithium-ion batteries. *ACS Sustainable Chemistry & Engineering, 5*(1), 1026-1032.

Harper, G., Sommerville, R., Kendrick, E., Driscoll, L., Slater, P., Stolkin, R., . . . Lambert, S. (2019). Recycling lithium-ion batteries from electric vehicles. *Nature, 575*(7781), 75-86.

He, K., Zhang, Z.-Y., Alai, L., & Zhang, F.-S. (2019). A green process for exfoliating electrode materials and simultaneously extracting electrolyte from spent lithium-ion batteries. *Journal of hazardous materials, 375*, 43-51.

He, L.-P., Sun, S.-Y., Mu, Y.-Y., Song, X.-F., & Yu, J.-G. (2017). Recovery of lithium, nickel, cobalt, and manganese from spent lithium-ion batteries using L-tartaric acid as a leachant. *ACS Sustainable Chemistry & Engineering, 5*(1), 714-721.

He, Y., Zhang, T., Wang, F., Zhang, G., Zhang, W., & Wang, J. (2017). Recovery of LiCoO2 and graphite from spent lithium-ion batteries by Fenton reagent-assisted flotation. *Journal of cleaner production, 143*, 319-325.

Heelan, J., Gratz, E., Zheng, Z., Wang, Q., Chen, M., Apelian, D., & Wang, Y. (2016, 2016/10/01). Current and Prospective Li-Ion Battery Recycling and Recovery Processes. *JOM, 68*(10), 2632-2638. https://doi.org/10.1007/s11837-016-1994-y.

Herrmann, C., Raatz, A., Mennenga, M., Schmitt, J., & Andrew, S. (2012). Assessment of automation potentials for the disassembly of automotive lithium ion battery systems. In *Leveraging Technology for a Sustainable World* (pp. 149-154): Springer

Heymans, C., Walker, S. B., Young, S. B., & Fowler, M. (2014). Economic analysis of second use electric vehicle batteries for residential energy storage and load-levelling. *Energy Policy, 71*, 22-30.

Horn, D., Zimmermann, J., Gassmann, A., Stauber, R., & Gutfleisch, O. (2019). Battery Recycling: Focus on Li-ion Batteries. *Modern Battery Engineering: A Comprehensive Introduction*, 223.

Hu, Y., Yu, Y., Huang, K., & Wang, L. (2020). Development tendency and future response about the recycling methods of spent lithium-ion batteries based on bibliometrics analysis. *Journal of Energy Storage, 27*, 101111.

IEA. (2020). Global EV Outlook. Retrieved 21/08/2020, 2020, from https://www.iea.org/reports/global-ev-outlook-2020

Joulié, M., Laucournet, R., & Billy, E. (2014). Hydrometallurgical process for the recovery of high value metals from spent lithium nickel cobalt aluminum oxide based lithium-ion batteries. *Journal of Power Sources, 247*, 551-555.

Kang, J., Senanayake, G., Sohn, J., & Shin, S. M. (2010). Recovery of cobalt sulfate from spent lithium ion batteries by reductive leaching and solvent extraction with Cyanex 272. *Hydrometallurgy, 100*(3-4), 168-171.

Lee, C. K., & Rhee, K.-I. (2002). Preparation of LiCoO2 from spent lithium-ion batteries. *Journal of Power Sources, 109*(1), 17-21.

Li, J., Li, X., Hu, Q., Wang, Z., Zheng, J., Wu, L., & Zhang, L. (2009). Study of extraction and purification of Ni, Co and Mn from spent battery material. *Hydrometallurgy, 99*(1-2), 7-12.

Li, L., Bian, Y., Zhang, X., Guan, Y., Fan, E., Wu, F., & Chen, R. (2018). Process for recycling mixed-cathode materials from spent lithium-ion batteries and kinetics of leaching. *Waste management, 71*, 362-371.

Li, L., Chen, R., Sun, F., Wu, F., & Liu, J. (2011). Preparation of LiCoO2 films from spent lithium-ion batteries by a combined recycling process. *Hydrometallurgy, 108*(3-4), 220-225.

Li, L., Fan, E., Guan, Y., Zhang, X., Xue, Q., Wei, L., . . . Chen, R. (2017). Sustainable recovery of cathode materials from spent lithium-ion batteries using lactic acid leaching system. *ACS Sustainable Chemistry & Engineering, 5*(6), 5224-5233.

Li, L., Ge, J., Chen, R., Wu, F., Chen, S., & Zhang, X. (2010). Environmental friendly leaching reagent for cobalt and lithium recovery from spent lithium-ion batteries. *Waste management, 30*(12), 2615-2621.

Liu, P., Xiao, L., Chen, Y., Tang, Y., Wu, J., & Chen, H. (2019). Recovering valuable metals from LiNixCoyMn1-x-yO2 cathode materials of spent lithium ion batteries via a combination of reduction roasting and stepwise leaching. *Journal of Alloys and Compounds, 783*, 743-752.

Lv, W., Wang, Z., Cao, H., Zheng, X., Jin, W., Zhang, Y., & Sun, Z. (2018). A sustainable process for metal recycling from spent lithium-ion batteries using ammonium chloride. *Waste management, 79*, 545-553.

Mann, M. K., & Spath, P. L. (2000). *A comparison of the environmental consequences of power from biomass, coal, and natural gas.* Paper presented at the First World Conference and Exhibition on Biomass for Energy and Industry.

Mantuano, D. P., Dorella, G., Elias, R. C. A., & Mansur, M. B. (2006). Analysis of a hydrometallurgical route to recover base metals from spent rechargeable batteries by liquid–liquid extraction with Cyanex 272. *Journal of Power Sources, 159*(2), 1510-1518.

Marshall, J., Gastol, D., Sommerville, R., Middleton, B., Goodship, V., & Kendrick, E. (2020). Disassembly of Li Ion Cells—Characterization and Safety Considerations of a Recycling Scheme. *Metals, 10*(6), 773.

Martinez-Laserna, E., Gandiaga, I., Sarasketa-Zabala, E., Badeda, J., Stroe, D.-I., Swierczynski, M., & Goikoetxea, A. (2018). Battery second life: Hype, hope or reality? A critical review of the state of the art. *Renewable and Sustainable Energy Reviews, 93*, 701-718.

MBIE. (2020). *Energy in New Zealand 2020*.

Meshram, P., Pandey, B., & Mankhand, T. (2015). Hydrometallurgical processing of spent lithium ion batteries (LIBs) in the presence of a reducing agent with emphasis on kinetics of leaching. *Chemical Engineering Journal, 281*, 418-427.

MFE. (2020). Legal Frame Work for Waste. Retrieved 12/08/2020, 2020, from https://www.mfe.govt.nz/waste/waste-strategy-and-legislation/legal-framework-waste

Mishra, D., Kim, D.-J., Ralph, D., Ahn, J.-G., & Rhee, Y.-H. (2008). Bioleaching of metals from spent lithium ion secondary batteries using Acidithiobacillus ferrooxidans. *Waste management, 28*(2), 333-338.

Moradi, B., & Botte, G. G. (2016). Recycling of graphite anodes for the next generation of lithium ion batteries. *Journal of Applied Electrochemistry, 46*(2), 123-148.

Musariri, B., Akdogan, G., Dorfling, C., & Bradshaw, S. (2019). Evaluating organic acids as alternative leaching reagents for metal recovery from lithium ion batteries. *Minerals Engineering, 137*, 108-117.

Myoung, J., Jung, Y., Lee, J., & Tak, Y. (2002). Cobalt oxide preparation from waste LiCoO2 by electrochemical–hydrothermal method. *Journal of Power Sources, 112*(2), 639-642.

Nan, J., Han, D., Yang, M., Cui, M., & Hou, X. (2006). Recovery of metal values from a mixture of spent lithium-ion batteries and nickel-metal hydride batteries. *Hydrometallurgy, 84*(1-2), 75-80.

Nan, J., Han, D., & Zuo, X. (2005). Recovery of metal values from spent lithium-ion batteries with chemical deposition and solvent extraction. *Journal of Power Sources, 152*, 278-284.

Nayl, A., Hamed, M. M., & Rizk, S. (2015). Selective extraction and separation of metal values from leach liquor of mixed spent Li-ion batteries. *Journal of the Taiwan Institute of Chemical Engineers, 55*, 119-125.

Nowak, S., & Winter, M. (2017). The role of sub-and supercritical CO2 as "Processing Solvent" for the recycling and sample preparation of lithium ion battery electrolytes. *Molecules, 22*(3), 403.

Oberle, B., Bringezu, S., Hatfield-Dodds, S., Hellweg, S., Schandl, H., Clement, J., . . . Droz-Georget, H. (2019). Global resources outlook 2019: natural resources for the future we want.

Ojanen, S., Lundström, M., Santasalo-Aarnio, A., & Serna-Guerrero, R. (2018). Challenging the concept of electrochemical discharge using salt solutions for lithium-ion batteries recycling. *Waste management, 76*, 242-249.

Or, T., Gourley, S. W., Kaliyappan, K., Yu, A., & Chen, Z. (2020). Recycling of mixed cathode lithium‐ion batteries for electric vehicles: Current status and future outlook. *Carbon Energy*.

Ordoñez, J., Gago, E., & Girard, A. (2016). Processes and technologies for the recycling and recovery of spent lithium-ion batteries. *Renewable and Sustainable Energy Reviews, 60*, 195-205.

Paulino, J. F., Busnardo, N. G., & Afonso, J. C. (2008). Recovery of valuable elements from spent Li-batteries. *Journal of hazardous materials, 150*(3), 843-849.

Peng, C., Liu, F., Wang, Z., Wilson, B. P., & Lundström, M. (2019). Selective extraction of lithium (Li) and preparation of battery grade lithium carbonate (Li2CO3) from spent Li-ion batteries in nitrate system. *Journal of Power Sources, 415*, 179-188.

Peters, J. F., Baumann, M., Zimmermann, B., Braun, J., & Weil, M. (2017). The environmental impact of Li-Ion batteries and the role of key parameters–A review. *Renewable and Sustainable Energy Reviews, 67*, 491-506.

Pinegar, H., & Smith, Y. R. (2019). Recycling of end-of-life lithium ion batteries, Part I: Commercial processes. *Journal of Sustainable Metallurgy*, 1-15.

Pinegar, H., & Smith, Y. R. (2020). Recycling of End-of-Life Lithium-Ion Batteries, Part II: Laboratory-Scale Research Developments in Mechanical, Thermal, and Leaching Treatments. *Journal of Sustainable Metallurgy*, 1-19.

Pinna, E. G., Ruiz, M. C., Ojeda, M. W., & Rodriguez, M. H. (2017). Cathodes of spent Li-ion batteries: Dissolution with phosphoric acid and recovery of lithium and cobalt from leach liquors. *Hydrometallurgy, 167*, 66-71.

Pistoia, G., & Liaw, B. (2018). *Behaviour of Lithium-Ion Batteries in Electric Vehicles: Battery Health, Performance, Safety, and Cost*: Springer.

Ramoni, M. O., & Zhang, H.-C. (2013). End-of-life (EOL) issues and options for electric vehicle batteries. *Clean Technologies and Environmental Policy, 15*(6), 881-891.

Rath, M., Behera, L. P., Dash, B., Sheik, A. R., & Sanjay, K. (2018). Recovery of dimethylglyoxime (DMG) from Ni-DMG complexes. *Hydrometallurgy, 176*, 229-234.

Ribière, P., Grugeon, S., Morcrette, M., Boyanov, S., Laruelle, S., & Marlair, G. (2012). Investigation on the fire-induced hazards of Li-ion battery cells by fire calorimetry. *Energy & Environmental Science, 5*(1), 5271-5280.

Richa, K., Babbitt, C. W., & Gabrielle, G. (2016). Sustainable management of lithium-ion batteries after use in electric vehicles.

Sattar, R., Ilyas, S., Bhatti, H. N., & Ghaffar, A. (2019). Resource recovery of critically-rare metals by hydrometallurgical recycling of spent lithium ion batteries. *Separation and Purification Technology, 209*, 725-733.

Schulz, W., & Bray, L. (1987). Solvent extraction recovery of byproduct 137Cs and 90Sr from HNO3 solutions—a technology review and assessment. *Separation Science and Technology, 22*(2-3), 191-214.

Sethurajan, M., van Hullebusch, E. D., Fontana, D., Akcil, A., Deveci, H., Batinic, B., . . . Chmielarz, A. (2019, 2019/02/01). Recent advances on hydrometallurgical recovery of critical and precious elements from end of life electronic wastes - a review. *Critical Reviews in Environmental Science and Technology, 49*(3), 212-275. https://doi.org/10.1080/10643389.2018.1540760.

Shi, Y., Chen, G., & Chen, Z. (2018). Effective regeneration of LiCoO 2 from spent lithium-ion batteries: a direct approach towards high-performance active particles. *Green chemistry, 20*(4), 851-862.

Shin, S. M., Kim, N. H., Sohn, J. S., Yang, D. H., & Kim, Y. H. (2005). Development of a metal recovery process from Li-ion battery wastes. *Hydrometallurgy, 79*(3-4), 172-181.

Sonoc, A., Jeswiet, J., & Soo, V. K. (2015). Opportunities to improve recycling of automotive lithium ion batteries. *Procedia cIRP, 29*(January), 752-757.

Sun, L., & Qiu, K. (2011). Vacuum pyrolysis and hydrometallurgical process for the recovery of valuable metals from spent lithium-ion batteries. *Journal of hazardous materials, 194*, 378-384.

Swain, B., Jeong, J., Lee, J.-c., Lee, G.-H., & Sohn, J.-S. (2007). Hydrometallurgical process for recovery of cobalt from waste cathodic active material generated during manufacturing of lithium ion batteries. *Journal of Power Sources, 167*(2), 536-544.

Thackeray, M. M., Johnson, C. S., Vaughey, J. T., Li, N., & Hackney, S. A. (2005). Advances in manganese-oxide 'composite'electrodes for lithium-ion batteries. *Journal of Materials Chemistry, 15*(23), 2257-2267.

Transport NZ. (2020). Vehicle Fleet Statistics. Retrieved2020, from https://www.transport.govt.nz/mot-resources/vehicle-fleet-statistics/monthly-electric-and-hybrid-light-vehicle-registrations-2/

Vector. (2018). Lithium battery recycling in Australia

Vector. (2019). New Energy Futures Paper: Batteries Technical Addendum.

Virolainen, S., Fini, M. F., Laitinen, A., & Sainio, T. (2017). Solvent extraction fractionation of Li-ion battery leachate containing Li, Ni, and Co. *Separation and Purification Technology, 179*, 274-282.

Wang, Lin, Y.-C., & Wu, S.-H. (2009). A novel recovery process of metal values from the cathode active materials of the lithium-ion secondary batteries. *Hydrometallurgy, 99*(3-4), 194-201.

Wang, F., Zhang, T., He, Y., Zhao, Y., Wang, S., Zhang, G., . . . Feng, Y. (2018). Recovery of valuable materials from spent lithium-ion batteries by mechanical separation and thermal treatment. *Journal of cleaner production, 185*, 646-652.

Wang, H., & Friedrich, B. (2015). Development of a highly efficient hydrometallurgical recycling process for automotive Li–Ion batteries. *Journal of Sustainable Metallurgy, 1*(2), 168-178.

Wang, X., Gaustad, G., & Babbitt, C. W. (2016). Targeting high value metals in lithium-ion battery recycling via shredding and size-based separation. *Waste management, 51*, 204-213.

Personal Communication (2020) Lithium-ion Battery Data, S. Pritchett, WasteMINZ

Weiguang, I., Wang, Z., Cao, H., Sun, Y., Zhang, Y., & Sun, Z. (2018). A critical review and analysis on the recycling of spent lithium-ion batteries. *ACS Sustainable Chemistry & Engineering, 6*(2), 1504-1521.

Whittingham, M. S. (2004). Lithium batteries and cathode materials. *Chemical Reviews, 104*(10), 4271-4302.

Winslow, K. M., Laux, S. J., & Townsend, T. G. (2018). A review on the growing concern and potential management strategies of waste lithium-ion batteries. *Resources, Conservation and Recycling, 129*, 263-277.

Xiao, J., Guo, J., Zhan, L., & Xu, Z. (2020, 2020/05/10/). A cleaner approach to the discharge process of spent lithium ion batteries in different solutions. *Journal of cleaner production, 255*, 120064. http://www.sciencedirect.com/science/article/pii/S0959652620301116.

Xin, B., Zhang, D., Zhang, X., Xia, Y., Wu, F., Chen, S., & Li, L. (2009). Bioleaching mechanism of Co and Li from spent lithium-ion battery by the mixed culture of acidophilic sulfur-oxidizing and iron-oxidizing bacteria. *Bioresource Technology, 100*(24), 6163-6169.

Xin, Y., Guo, X., Chen, S., Wang, J., Wu, F., & Xin, B. (2016). Bioleaching of valuable metals Li, Co, Ni and Mn from spent electric vehicle Li-ion batteries for the purpose of recovery. *Journal of cleaner production, 116*, 249-258.

Xu, J., Thomas, H., Francis, R. W., Lum, K. R., Wang, J., & Liang, B. (2008). A review of processes and technologies for the recycling of lithium-ion secondary batteries. *Journal of Power Sources, 177*(2), 512-527.

Yang, Y., Xu, S., & He, Y. (2017). Lithium recycling and cathode material regeneration from acid leach liquor of spent lithium-ion battery via facile co-extraction and co-precipitation processes. *Waste management, 64*, 219-227.

Yu, J., He, Y., Ge, Z., Li, H., Xie, W., & Wang, S. (2018). A promising physical method for recovery of LiCoO2 and graphite from spent lithium-ion batteries: Grinding flotation. *Separation and Purification Technology, 190*, 45-52.

Zeng, X., Li, J., & Shen, B. (2015). Novel approach to recover cobalt and lithium from spent lithium-ion battery using oxalic acid. *Journal of hazardous materials, 295*, 112-118.

Zhang, J., Hu, J., Zhang, W., Chen, Y., & Wang, C. (2018). Efficient and economical recovery of lithium, cobalt, nickel, manganese from cathode scrap of spent lithium-ion batteries. *Journal of cleaner production, 204*, 437-446.

Zhang, P., Yokoyama, T., Itabashi, O., Suzuki, T. M., & Inoue, K. (1998). Hydrometallurgical process for recovery of metal values from spent lithium-ion secondary batteries. *Hydrometallurgy, 47*(2-3), 259-271.

Zhang, X., Li, L., Fan, E., Xue, Q., Bian, Y., Wu, F., & Chen, R. (2018). Toward sustainable and systematic recycling of spent rechargeable batteries. *Chemical Society Reviews, 47*(19), 7239-7302.

Zheng, X., Gao, W., Zhang, X., He, M., Lin, X., Cao, H., . . . Sun, Z. (2017). Spent lithium-ion battery recycling–Reductive ammonia leaching of metals from cathode scrap by sodium sulphite. *Waste management, 60*, 680-688.

Zheng, X., Zhu, Z., Lin, X., Zhang, Y., He, Y., Cao, H., & Sun, Z. (2018). A mini-review on metal recycling from spent lithium ion batteries. *Engineering, 4*(3), 361-370.

Zhou, X., He, W.-z., Li, G.-m., Zhang, X.-j., Zhu, S.-g., & Huang, J.-w. (2010). *Recycling of electrode materials from spent lithium-ion batteries.* Paper presented at the 2010 4th International Conference on Bioinformatics and Biomedical Engineering.

Zhu, S.-g., He, W.-Z., Li, G.-M., Xu, Z., ZHANG, X.-j., & Huang, J.-W. (2012). Recovery of Co and Li from spent lithium-ion batteries by combination method of acid leaching and chemical precipitation. *Transactions of Nonferrous Metals Society of China, 22*(9), 2274-2281.

Zhuang, L., Sun, C., Zhou, T., Li, H., & Dai, A. (2019). Recovery of valuable metals from LiNi0. 5Co0. 2Mn0. 3O2 cathode materials of spent Li-ion batteries using mild mixed acid as leachant. *Waste management, 85*, 175-185.